# UNIVERSITÀ DEGLI STUDI DI ROMA "TOR VERGATA"

FACOLTÀ DI INGEGNERIA

DOTTORATO DI RICERCA IN INGEGNERIA DEI MATERIALI

CICLO XXI

# Dielectric and EM properties of carbon filled epoxy resin

Paolo Travaglia

A.A. 2008/2009

Docente Guida/Tutor: Ing. Francesca Nanni

Coordinatore: Prof. Roberto Montanari

# Index

# Introduction

This thesis deals with the dielectric and absorbing properties at microwaves (x-band) of epoxy resin filled nanocomposites. Three different carbonaceous nanofillers were used in the experimental: carbon black (CB), carbon nanofibers (CNF) and carbon nanotubes (CNT). Moreover, various dispersion processes of nanofiller in the resin were tried, in order to analyze the effect of filler distribution on the dielectric properties of the resulting composites. Permittivity was measured using a vector network analyzer in x-band (8,2-12,4 GHz) using the waveguide method. Samples morphology was studied by FEG-SEM. Using the equivalent circuit analogy, a link between samples morphology and permittivity was attempted. The suitability of these materials as electromagnetic microwaves absorbers was finally assessed.

In carbon black samples, realized using fillers with different specific surface areas, the filler distribution within the resin is very different, producing small short branched clusters when using high surface areas filler, and long thick and meandering aggregates in the other case. In both samples the clusters are close to cylindrical shape and may be seen as parallel cylinders capacitors in the resin. As a consequence, high surface area samples present lower values of real permittivity (that takes into account capacity of the system), due to the smaller length of capacitor plates, but higher imaginary permittivity (linked to conductivity and dissipations effects) because, as noted above, the clusters are closely spaced, permitting the activation of hopping and tunnelling conduction modes. CB samples showed good performances as EM absorbers, reaching a peak of -38 dB using a sample 4 mm thick.

In samples loaded with high aspect ratio (CNF and CNT) the key parameter is their dispersion in the resin. In CNF experimentation, despite the use of different methodologies, an unsatisfying dispersion was achieved, with the resulting microstructure made of aggregates. The EM measurements highlighted that the higher the number and the smaller the dimension of the aggregates, the higher are ε’ and ε”,for the same reason found in the case of CB. With CNT, instead, very good dispersions were achieved, by means of the aid of surfactants and of a more powerful sonicator. The results demonstrate again that permittivity is linked to microstructure, with the same trend established with the other type of nanofillers. Nevertheless, in this case, a new evidence was found highlighting that there is an optimum level of dispersion, above which the CNT do not interact each other, resulting in very high ε’ and very low ε”, since dissipation through Joule effect is limited.

The absorbing performance of CNF and CNT demonstrate that too much filler, or too much dispersion of it (i.e. Low ε”), bring to a mostly reflective medium, with low absorbing performance.

An optimum formulation needs, therefore, to be found for every system as a compromise among material composition, microstructure and thickness.

Part of the experimental work (most of chapter 6 ) was carried out during the author secondment to Monash University (Clayton, Victoria Australia) under the supervision of Prof. George Simon.

# 1 Conducting polymer composites

Loading a non conductive polymer with conductive filler, either particles or fibres, produces different grades of conducting polymers composites (CPC). The benefit of coupling the ease of manufacturing, flexibility of shapes and application, low density and low cost with electric conductivity make them very attractive in several applications from antistatic coatings [1] to smart materials applications, to emi shielding and absorbing materials. CPC have found relevance in electronic devices manufacturing, where they are employed as conductive adhesive and circuit elements. Their usefulness has been boosted by the introduction of the Restriction of Hazardous Substances Directive (RoHS) in Europe, and similar laws in the USA, that ban the use of lead from electronic devices since the first of July 2006. Commonly, these adhesives consist on silver powder dispersed into a variety of polymers (DC electrical conductivity inside CPCs is caused by the formation of a network of conductive particles inside the matrix, as better explained in the following §1.1), like silicone polyurethane, polyamide and epoxy, depending on the adhesive required performance in terms of heat resistance, flexibility, mechanical resistance, etc. usually such materials possess low electrical resistivity and high thermal conductivity [2, 3].

CPC are also employed to produce regulators or sensors and also in electronic devices as fault current limiters in circuit protection [4, 5], exploiting their positive temperature coefficient of resistance. [6, 7]. When the CPC is heated above the design specification by the passage of a current, it swells resulting in the separation of conducting particles with a consequent increase of its electrical resistance. The regulator therefore shows two different electrical behaviours, as a function of the current: when the electrical current is close to the design parameter, the regulator shows low resistivity, when it increases above a certain level, the current flow is limited by the increase of the regulator resistivity. Commonly these devices are made of polyethylene matrix filled with carbon black. This kind of device can be found in pc or batteries against short circuit discharges.

In civil engineering self-diagnosis materials, showing both reinforcement and sensor performance in concrete structures, use the same principle. The sensor/reinforcement, in fact, shows an increase of electrical resistance as a consequence of increasing stress and/or strain. Under these conditions, in fact, in self-diagnosis components made of carbonaceous nanofiller in thermosetting resin, the increasing of matrix strain yields to carbon particles separation, resulting in enhanced macroscopic electrical resistance. this, in turn, can be direclty correlated to the level of stress bored by concrete structure . such behaviour was proven in self-monitoring composites tested both outside and inside concrete [8, 9].

Chemical sensors use the variation of resistivity caused by the swelling of the matrix after a certain time of exposure, when it adsorbs organic chemicals. A good sensor is the one that can give different electrical conductivity for different vapours [10-12].

Electromagnetic interferences (EMI) Shielding, electrostatic discharge (ESD) protection and microwave absorbing materials (MAM) are the major applications for conductive polymer composites. The first and latter of them are involved in electronic devices and environments protection and antenna decoupling. Shielding usually performs by reflecting the incident waves, sending them back in the medium from which they came from. To reflect the incident radiation, the shield must have mobile charge carriers (electron or holes) which interact with the electromagnetic fields in the radiation. Materials employed as shields need therefore to be somehow electrically conducting, even if a volume resistivity of 1 Ωcm is typically sufficient. EMI shields can therefore be made of either conductive materials, i.e. metals, or CPC, that can be employed even below percolation . EMI shielding is mostly employed to house electronic equipment, either to provide an electronic-noise-free environment, or shield other electronic components or workers from the noise and radiations generated [13-17].

ESD requirements are less stringent, and they required lower surface resistivity. ESD is employed where there is a constant built up of static electricity, and thus a need to disperse it, as in airplane fuselages [1] and tires, conveyor belts and weaving machines, wherever a relative motion between dissimilar materials occurs [18, 19].

Fig. 1-1 illustrates the typical ranges of surface resistivity of CPC and of their most common applications.

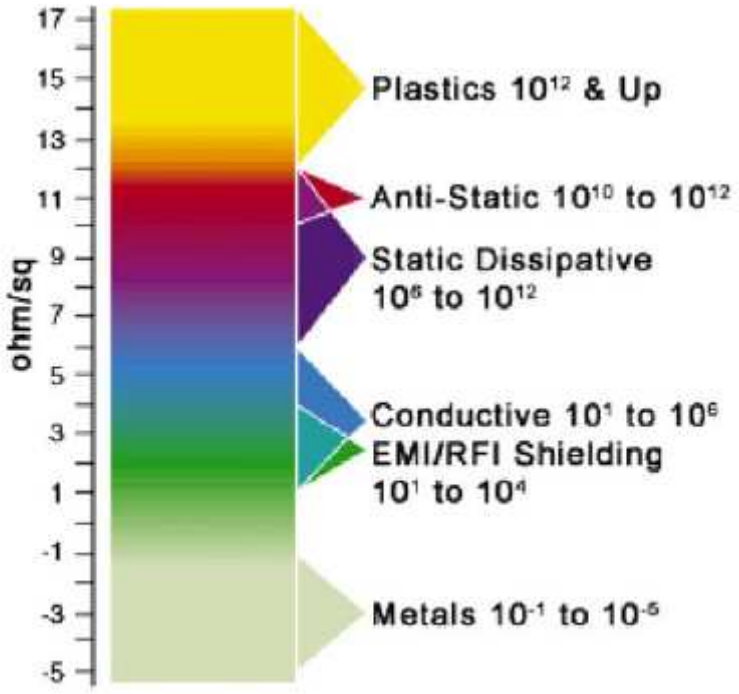


**Fig. 1-1 Surface resistivity of conducting polymer composites and their most common applications. (Available f rom: http://www.rtpcompany.com/products/ conductive/index.htm.)**

Microwave absorbing materials, finally, provide a more efficient electromagnetic wave protection, since they do not reflect incident waves, but dissipate them through the material with virtually no scattering.


**Fig. 1-2 On the left shielding, on the right absorbing**

The mechanism of absorption is much more complex because it involves both the instrinic porperties of the component as well as its extrinsic characteristics, as geometrical shape and dimensions. from the material point of view, the dissipation of the energy associated to the incident waves requires the presence of electric or magentic dipoles able to interact with the electromagnetic fields. These dipoles are responsible for different polarization mechanisms, which occur in the material at difference frequencies (cfr. §2.1.1). CPC are ideal candidate materials to realize absorbing structures, thank to their versatility and possibility to insert dipoles by adding pure conductive, dielectric or magnetic fillers within the insulating matrix [20, 21]. barium titanate, for instance, was used as filler in polyurethane and polyaniline as matrix to produce 2,5 mm thick em

absorbing composites in [22]. peaks of 25 dB absorption at 11,2 GHz were obtained. More than 40 db of attenuation at 8 GHz were obtained by[20] using abs as matrix and 30% vol of barium titanate. In [23] it is reported that 8% vol of in epoxy  in samples 6 mm thick yields 20 dB attenuation at 13 GHz. Hexaferrites were proposed as magnetic fillers: $Co_2Y$-type hexaferrite ($Ba_2Cu_xCo_{2-x}Fe_{12}O_{22}$, x=0,1) were employed as filler of rubber matrix leading to 35 dB attenuation in 3 mm thick samples[24]. the contemporarily use of a conductive and magnetic filler was proposed to [25]: a mix of magnetite, Co-Ti substituted hexaferrite and graphite gives a peak of 22 db attenuation with 2 mm thick samples,.

## 1.1 Distribution of filler into the matrix and its consequence on electric properties

A very important parameter when dealing with EM properties of CPC is the distribution of filler or nanofiller within the matrix. Historically this feature has been investigated in the theory of percolation, i.e. the formation of a continuous network of conductive filler leading to dc conductivity.

Dishovsky and Grigorova in [26] noted that CB concentration influences the EM properties of a filled polymer and that the best values of absorption are obtained just before the onset of percolation. One of the ways to explain the electrical properties of conductive particles filled polymers is percolation theory. Percolation started as a lattice model to study the statistical probability of fluid flowing through a static medium, it was then used to model the conductive behaviour against filler concentration [27]. Percolative behaviour can be recognised when, while increasing the filler content, there is a sharp decrease, in composite resistivity, (several orders of magnitude). The percolation threshold is then identified by the filler volume percent at the resistivity abrupt decrease. The abrupt change in electrical properties is caused by the formation of the so called “infinite cluster”, a network-like conductive pattern inside the composite that encompass the whole volume (Fig. 1-3).

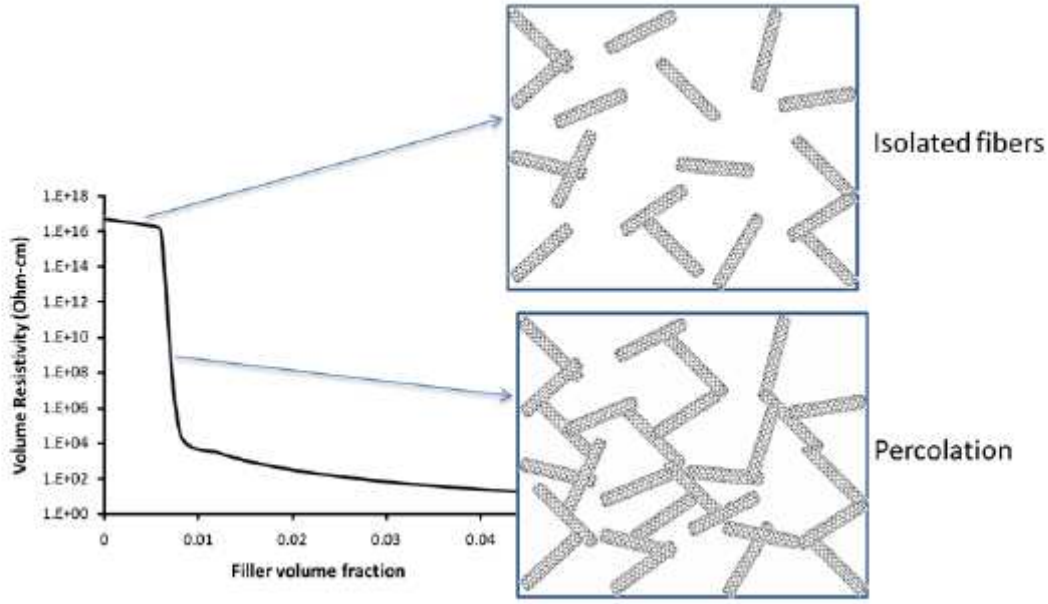


**Fig. 1-3 Percolation threshold and formation of infinitive cluster [19]**

Increasing the filler content above the percolation threshold produces just a slight variation in composite resistivity. If resistivity keeps decreasing after the percolation threshold in a significant way, it means that the three-dimensional conductive-network has not formed yet and conductivity is prevalently caused by tunnelling between close, but not in contact, filler particles. Tunnelling happens when particles are approximately 10 nm or closer [18, 28]. The relationship between current and voltage gives an indication of the type of mechanism active inside the composite [29, 30]. If conductive filler inside the matrix touch each other the relationship will be Ohmic linear, instead when tunnelling is the prevalent mechanism, the relationship between current and voltage is best matched by a power law [30, 31].

Ways to lower the filler content need to be studied when designing EMI shielding materials since the best use of the filler means higher dielectric properties at constant filler ratio (cfr. §1.1.2) or less filler to achieve the desired values of permittivity.

Percolation threshold, electrical and most important for EM application dielectric properties below the percolation threshold, depends on numerous factors including filler aspect ratio [32], conductivity, morphology [28], dispersion and distribution, affinity with the matrix [33], polymer matrix cristallinity [34] and surface tension, manufacturing, and eventual additives [34-37]. In the following some of these parameters will be shortly discussed.

### *1.1.1 Influence of filler shape*

Percolation theory reports that above percolation a power law fits resistivity vs filler loading

$$\rho = \rho_0 (v - v_c)^{-t} \text{ (eq. 1.1)}$$

Where $\rho$ is the composite electrical resistivity (Ω cm) $\rho_0$ is a scaling factor (Ω cm, the scaling factor is needed since percolation theory is valid only assuming the matrix has zero conductance or the filler zero resistance), $v$ is the filler volume fraction and $v_c$ is volume fraction at percolation.

The critical exponent $t$ is related to the lattice dimension (i.e. if a 2D or 3D lattice developed/was studied), and varies between 1,65 and 2 for three-dimensional lattices [27, 38]. If the filler used is fibrous instead of spherical (i.e. CNF, CNT) the exponent is higher than 2 and in particular as reported in [39], close to 3. According to percolation theory, using spherical filling factors, a random packing in three dimensions, yields $v_c$ around 16% volume fraction [28], fibrous fillers or high structure CB[1] show $v_c$ of only several percent or even less than one percent. Fig. 1-4 show the filler aspect ratio needed to achieve percolation by a certain volume fraction

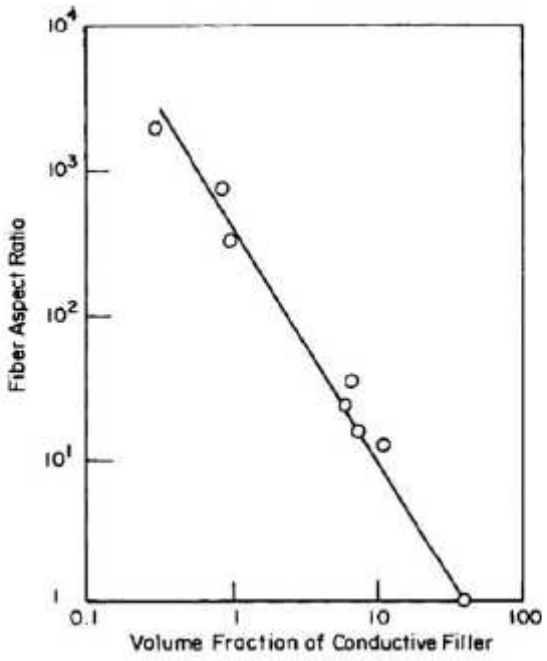


**Fig. 1-4 percolation volume fraction vs filler aspect ratio [40]**

Percolation, as stated and shown in Fig. 1-4, can be drastically reduced using fillers with an aspect ratio >1. Fig. 1-5 shows graphically the consequences: 10% surface fraction of filler is randomly dispersed on a same surface plane, the effect of aspect ratio is substantial, while 10% volume is NOT enough to provide a percolating network of spherical particles, it is more than enough when a

[1] The higher a CB structure the more complex and branched the shape of the complex agglomerate cfr §XX

fibrous filler is used. On a same filler basis, in fact, the high aspect ratio filler provides more occasions of contact among particles compared to the case of close to round fillers (aspect ratio close to 1).

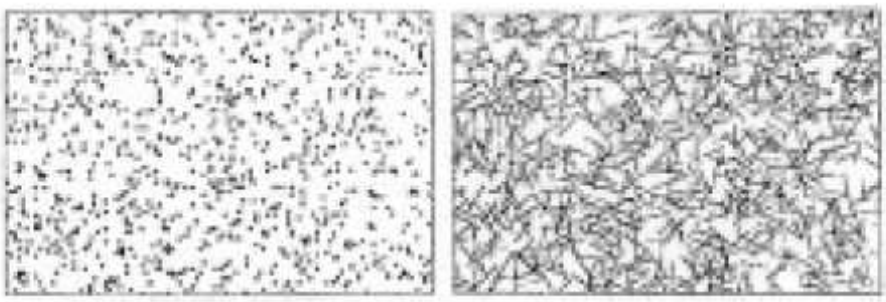

**Fig. 1-5 10% surface of filler fraction , spherical particles (left) fibrous filler (right)**

### *1.1.2 Influence of resin, additives and manufacturing method*

Before dealing with the influence of manufacturing methods on the shape and performance of the conductive paths, it is useful to devote some words to the effect of resin on the resulting properties, of the CPC. Kato and Miyashita [34] determined that polymer cristallinity has a very high influence. CB is present only in the amorphous regions, thus increasing the local filler content easing the formation of a percolative network. On the same paper a remark about the influence of polar resins states that polar matrixes have better wetting properties and so give more conductive composites for the same filler weight. Cheah et al. [33] agrees with the previous mentioned paper about polar polymers, but they state that what matters, instead of taking just the absolute value of matrix polarity, is matrix-filler difference in polarity. Cheah also shows that to achieve good percolation values a good dispersion (the particles are not grouped together in big bundles) is needed but not a good distribution (the particles are evenly distributed inside the matrix). Moreover, quite surprising, it was found that an optimal distribution of filler inside the matrix may lead to worse electric properties. Grunlan et al. [37] tried the use of an additive to promote filer dispersion, but they found that the presence of smaller aggregates provide lower electrical conductivity at a higher percolation threshold. Schueler et al in [35] went further adding $CuCl_2$ to lower the energy barrier that prevents the formation of bigger agglomerates that, from their point of view, help conductivity. Schueler also documented that high shear forces are enough to disperse CB inside a matrix and reach conductivity. In a later paper [41] even CNT were dispersed using just an energetic stirring. Instead of additives that help dispersion Yoon and co-workers [36] used additives that help conduction, via increasing hopping phenomena, γ-aminopropyltrimethoxysilane (APS)

and trimethoxy-npropylsilane (TPS) were tried. The former was proved to lower significantly the percolation limit.

Another important aspect related to the nature of filler, which arises when dealing with fibrous fillers is their very strong agglomeration. Before insertion in the resin it is therefore necessary to disagglomerate the fibres. Many different methodologies were tried, among which there is the sonication method, which was chosen by the author for in this experimental work. Dispersion can be carried out via sonication directly in resin or previously in solvent. Song [42] produced two series of CNT/epoxy samples; in the former CNT were sonicated in resin, while in the latter a solvent was used to sonicate CNT and the resin was added later. The results from mechanical tests were controversial, while electrical conductivity showed important improvements by achieving good filler dispersion with solvent use. The nature of solvent, though, is important since it has an influence on the resulting properties of the composite, as in the case of functional groups formed in the cured epoxy [43]. Sonication can lead to the possibility of fibres cutting if not carefully performed in terms of time and power of sonication; to limit this bad evenience it was suggested that nanofibres doping may provide a better way to preserve the aspect ratio and integrity of fillers [44]. It is also important to remember that, when dealing with almost mono-dimensional fillers as in the case of CNF and CNT, there may be an orientation effect if the composite is extruded before curing.

This very short overview evidences how many aspects and parameters must be taking in count when preparing nanofilled composites for electromagnetic applications. In the following paragraphs the main characteristic of any nanofiller used in this thesis, i.e. CB, CNF and CNT, will be briefly discussed.

## *1.2 Main types of nanofillers*

### *1.2.1 Carbon Black*

Carbon black (CB) is widely used as a filler in several industrial process, such as a reinforcing filler, to improve dimensional stability, conductive filler, ultraviolet light stabilizer, antioxidant to prolong the lifetime of rubber, and pigment or colorant. CB is an amorphous form of carbon with a structure similar to disordered graphite: “When aromatic hydrocarbons are subjected to incomplete combustion at high temperature their molecules will dissociate through the rupture of C-H bonds. Subsequently, carbon atoms and aromatic radicals react to form layer structures composed of hexagonal carbon rings, which tend to stack in three to four layers, forming crystallographic structures” [45]. CB has a turbostratic structure, where the graphite layers are rotated or shifted horizontally [46] Fig. 1-6.

**Fig. 1-6 CB graph planes [47]**

CB essentially consist of elemental carbon in the form of near spherical particle of colloidal size coalesced into particle aggregates and agglomerates. A CB particle is a small spheroidal non-discrete component of a CB aggregate, particle diameters can range from less than 20 nm in some furnace grades to few hundred nm in thermal blacks. Several CB particles form a CB aggregate, a discrete, rigid, colloidal entity of coalesced particles, it is the smallest dispersible unit of carbon black, aggregates dimensions can range from as small as 100 nm to a few micrometers Fig. 1-7.

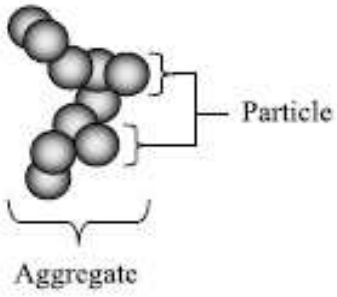


**Fig. 1-7 Schematic showing the distinction between carbon black particles and aggregate.**

Among several characteristics of CB, two influence the microstructure of the resulting CPC most: structure and specific surface area. Structure describe the complexity of the shape of the CB aggregates, they vary quite widely in morphology, from the large individual spheres found in some thermal black to small highly complicated, branched aggregates in high structure{Balberg, 2002 #35}, high surface area CB [48]. The complex and varied shapes of the CB aggregates lead to the creation of voids between the aggregates in any sample of CB that are greater than the voids that would be created if the aggregates were simple spheres of equivalent size. It is this fact that has lead to the commonly used techniques of measuring internal void volumes as a means of indirectly assessing the shape, or “structure” or aggregates within a carbon black sample. In general the greater the measured internal void volume, the more complex, open, and branched the aggregates within a sample are and the greater the structure. The measurements are made using either

volumetric measurement under specific pressures or, more commonly, oil absorption measurements. In either case it is clear that this is a parameter of CB that has a significant influence on the compound in which the CB is dispersed. Increasing only the structure of CB used in a rubber compound will typically increase the compound's hardness, viscosity, stress at high strain and wear resistance. The specific surface area is by definition the available surface area in square meters per unit mass of CB in grams, it also is a measure of porosity.

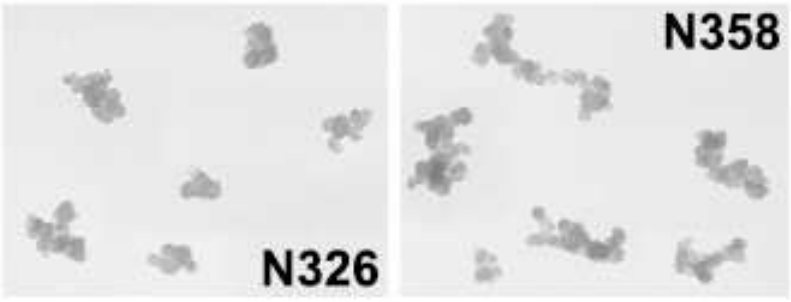


**Fig. 1-8 TEM micrography of low structure (N326) and high structure (N358) CB**

It is several years CB is used in EM application. A 35 dB shielding efficiency was reported in 1996 [49] with a polypropylene sample loaded with 40%w CB at 10 GHz (sample thickness not reported). Another paper from 2000 [50] reports a SE of 20 dB in X-band as its best result when CB and ethylene-vinyl acetate were used, sample thickness was 3,5 mm. Absorbing materials were mostly studied to be used in military applications and as a consequence most of the research was classified, it is now finding their way into mainstream applications on mobile phones and other wireless gadgets. CB was the first filler used in such applications, such as [51, 52] that report respectively a 25 dB peak at 10,5 GHz with samples loaded with 10% CB and –30 dB at various frequencies depending on the thickness. Barba [52] also provides a graphical way to understand how absorbing properties of a composite are not just influenced by filler loading but also from frequency and thickness Fig. 1-9.

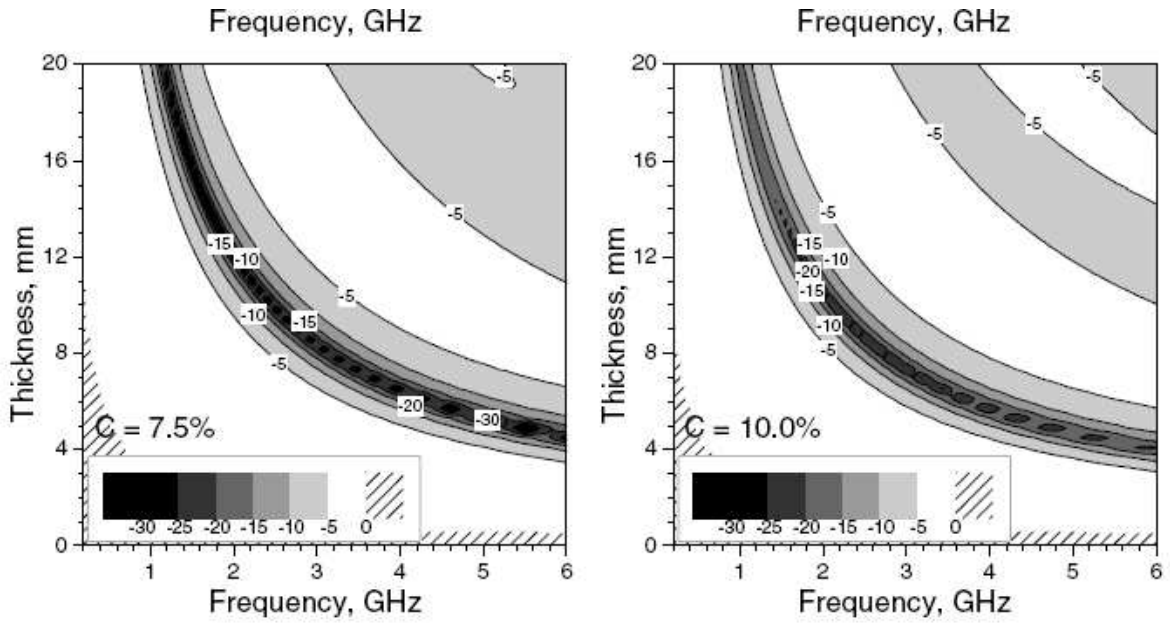


**Fig. 1-9 Influence of frequency and thickness on the absorbing properties of two different CB filled polymers [52]**

Wen et al. [53] used paraffin as a binder to test the absorbing properties of CB and catalysed CB and they achieved more than 20 dB attenuation at 16 GHz with a thickness of 6 mm.

A paper that deals with RAS is [54] by Chin and Lee, they manufactured a single layer absorber that 2,93 mm thickness and loaded with 0,02%w of CB it achieves 55dB attenuation at 10,1 GHz.,

### *1.2.2 Carbon nanofibers*

Carbon nanofibers (CNF) and carbon nanotubes (CNT), are high aspect ratio conductive carbon nanofilles. It is possible to think of them as one-dimensional fillers, due to their high aspect ratio. CNF are much cheaper than CNT, have comparable electrical properties, less microstructural defects and lower density, they also are somewhat easier to disentangle but their diameter is bigger (CNF diameter ranges from tents to hundreds of nm) and often have lower aspect ratio [19, 55], which sometimes make them performance less efficient that those of CNT.

#### *1.2.2.1 CNF structure and properties*

As produced CNF have varying dimension, structure, mechanical, thermal and, most important for conductive polymers, electrical properties [56] Before post treatment CNFs are covered by a layer of amorphous carbon that render them less conductive: “Because the filaments tend to clog the rear of the reactor tube, eventually spending many seconds within the decomposing methane atmosphere, a layer of vapour-deposited carbon both thickens the individual fibres and cements them together in large clumps. The exterior layer of vapour-deposited carbon is not as graphitic as

the interior cylinder, and has graphene planes which are primarily longitudinally oriented" [57] (Fig. 1-10).

CNF structure common features are a hollow core and graphite planes rolled parallel or at an angle around their axis [58, 59] (Fig. 1-10), the stacked planes are nested within each other. CNF are produced with different structures including bamboo-like, parallel and cup-stacked, the d-spacing of the graphene sheets was reported as 0.34 nm (the same as that in MWNTs and graphite platelets) [58, 60]. Single and double layer CNF morphology were identified by Uchida and al. [59], Fig. 1-11 shows a double layer one where, a truncated cone inner layer structure is enveloped by an outer layer of planes of graphite parallel to the axis.

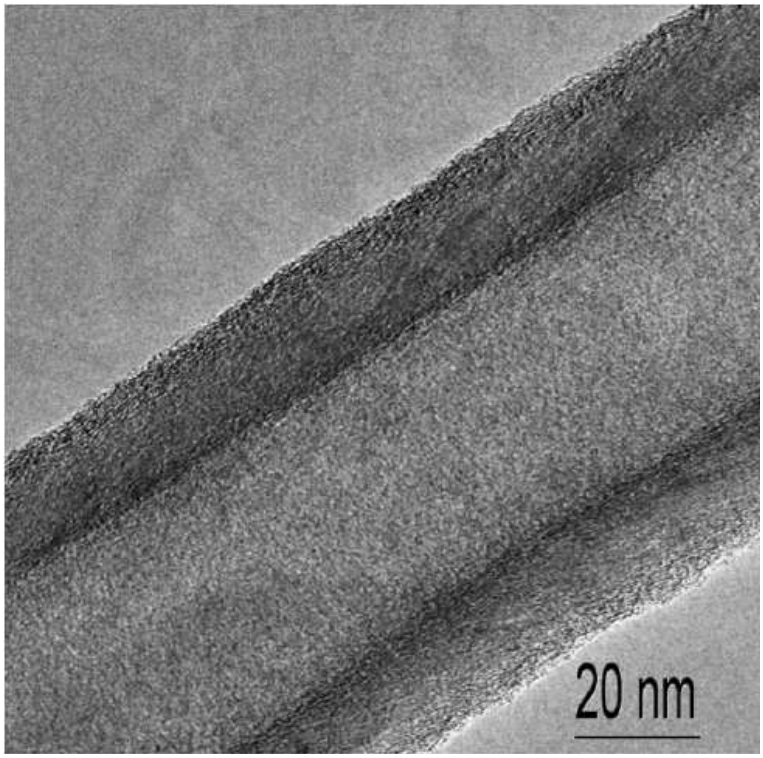


**Fig. 1-10TEM image of a Pyrograf CNF [57].**

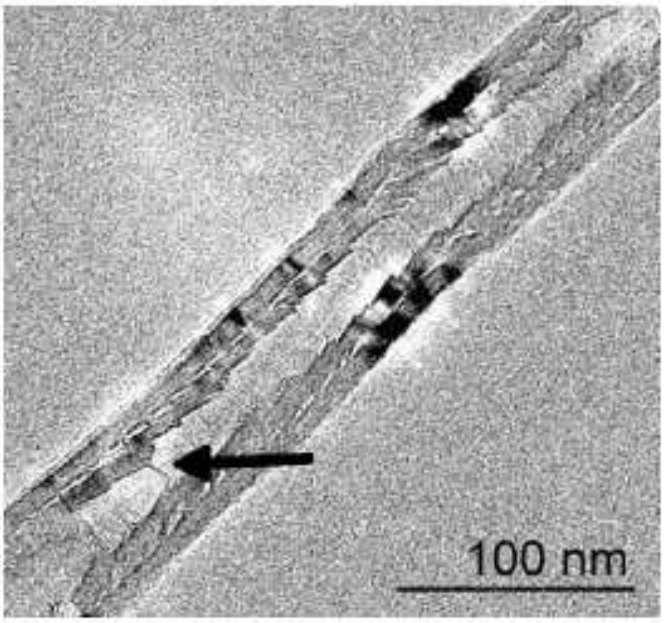


**Fig. 1-11 TEM image of a double layer CNF [58].**

Fig. 1-12 shows a high resolution transmission electron microscopy (HRTEM) image of a side-wall of a CNF (the inset is a schematic illustrating the structure of cup-stacked VGCNF). The nanofiber is clearly seen to have a hollow core surrounded by concentric cup-stacked planes.

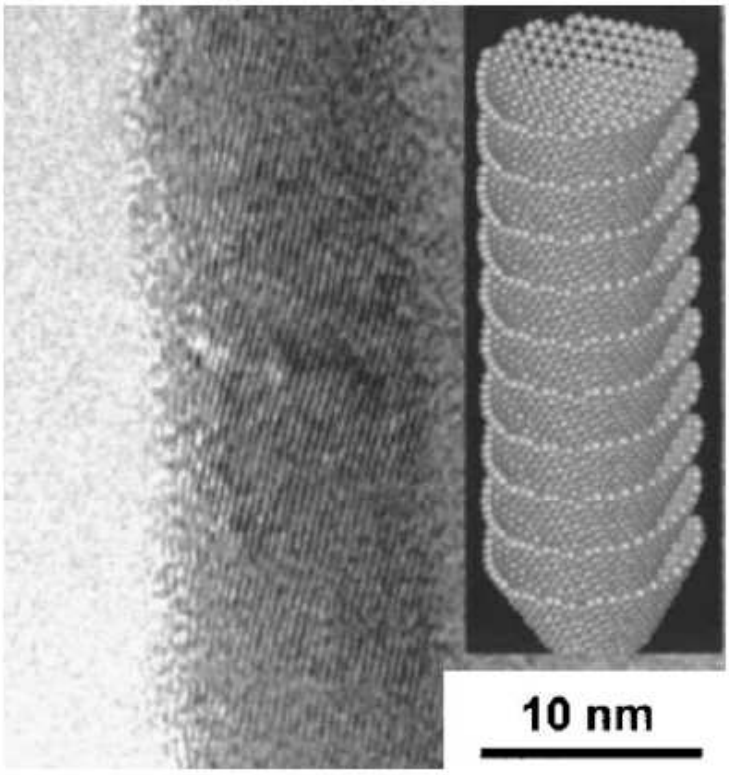


**Fig. 1-12 HRTEM micrografy of cup stacked CNF [61]**

Staked cups structure has a large number of reactive edges both inside and outside the nanofiber [61]. The way graphite sheets (about 3-5) fold at the end of the stacked cones structure is depicted in Fig. 1-13. Fig. 1-13a shows the structure of single layer CNF while Fig. 1-13b depicts a double layer one, HRTEM inset shows the graphite folds [19].

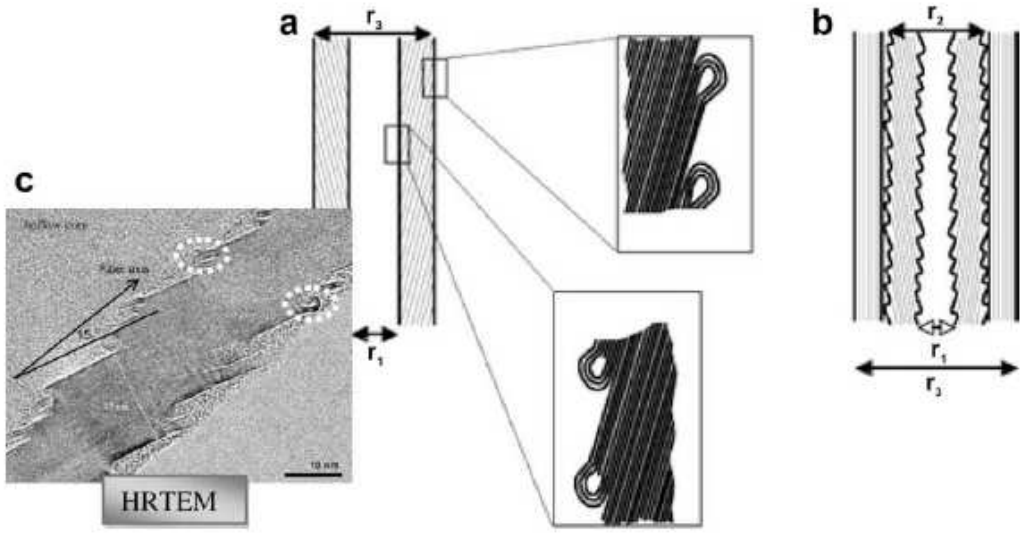


**Fig. 1-13 HRTEM and schematics of graphene loops that folds at the end of the angled graphene planes [19].**

Recently CNF have been proposed for EM applications. Yang et al. [62] found a shielding effectiveness (SE) of 26 dB at 200 MHz with a 1,45 mm sample LCP loaded with 15%w of filler. Zhang [63] studied SE of polyesterpolyol loaded with CNF in K, Q, V bands, and obtained 35 dB at 26 GHz and 60 dB at 75 GHz hinting at absorption contribution since increasing the thickness of the samples produced an increase in shielding. Lee [64] tried 40%w CNF filled PVA of just 30 μm thickness and compared it with a composite filled with the same quantity of CB: It was found that before thermal treating the CNF composite behaved worse than CB filled PVA, while after thermal treatment the SE of CNF was better than CB. Yang et al. [65] compared SE of CNF and MWCNT filled polymer in X band and found that SE of MWCNT was considerable higher than of CNF samples being the se of 5%w loaded samples at 10 GHz, of respectively 7,5 and 24 dB for CNF and CNT specimens. In a subsequent paper the same authors reached 21,9 dB SE in Ku-band, with a filler content in polystyrene of respectively 10%w CNF and 3%w CNT.

### *1.2.3 Carbon nanotubes*

In the very last years, CNT had been a subject on the forefront of scientific research, with many researchers scrambling to find ways to get the most from their properties (electric, thermal and mechanic) that were predicted to be very high. as reported in [66], “CNT can be visualized as a sheet graphite that has been rolled into a tube. Unlike diamond, where a 3-D diamond cubic crystal

structure formed with each carbon atom having four nearest neighbours arranged in a tetrahedron, graphite is formed as a 2-D sheet of carbon atoms arranged in a hexagonal array. In this case, each carbon atom has three nearest neighbours. 'Rolling' sheets of graphite into cylinders forms CNT. The properties of CNT depend on atomic arrangement (how the sheets of graphite are 'rolled'), the diameter and length of the tubes, and the morphology, or nanostructure. Nanotubes exist as either single-walled or multi-walled structures, and multi-walled carbon nanotubes (MWCNT) are simply composed of concentric single-walled carbon nanotubes (SWCNT)" (Fig. 1-14)

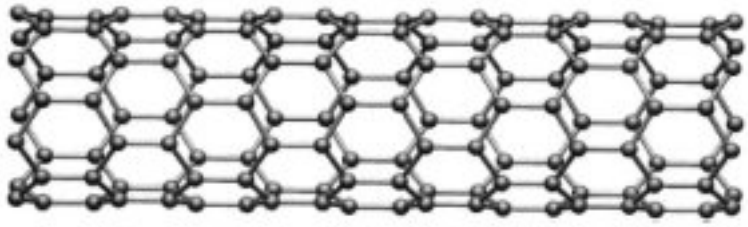

**Fig. 1-14 Sketch of a single wall nanotube**

Multi-walled CNT are composed of a number of concentric single walled CNT held together with relatively weak van der Walls forces. The multi-layered structure of these CNT further complicates the modelling of their properties.

The low density of CNT (between 1,3 and 1,75 g/cm$^2$ [67]) high aspect ratio and extraordinary mechanical properties (tensile strength 50-500 GPa and modulus of 1500 GPa when SWCNT are considered, and 10-60 and 1000 GPa when testing MWCNT [68]) make them particularly attractive for reinforcement in composite materials. In general, the tensile modulus and strength of polymer-rich CNT composites are found to increase with CNT loading, dispersion, and alignment in the matrix. However, the results at low CNT concentrations typically remain far behind the idealized theoretical predictions The gap between the predictions and experimental results arises from imperfect dispersion and poor load transfer. When the interfacial adhesion between the phases is weak, the CNT behave as holes or nanostructured flaws. Moreover, even modest CNT agglomeration impacts the diameter and length distributions of the filler and overall is likely to decrease the aspect ratio (a parameter in the models). In addition, CNT agglomeration reduces the modulus of the filler (another parameter in the models) relative to that of isolated CNT because there are only weak dispersive forces between CNT.

The potential of CNT as conducting fillers in multifunctional polymer composites has been successfully realized. Several orders of magnitude enhancement in electrical conductivity, σ, has been achieved [69] with a very small loading, below 0.1 %w of nanotubes in the polymer matrices, while maintaining the other performance such as mechanical properties, low melt flow viscosities,

etc. A variety of applications are being pursued using these conductive composites: electrostatic dissipation [70], electrostatic painting [71], electromagnetic interference (EMI) shielding [72], and transparent conductive coating [73] The percolation threshold for the electrical conductivity in CNT/polymer composites is influenced by several CNT characteristics most important among them aspect ratio, surface area and dispersion [42, 74], some authors suggest that shorter CNT and some agglomeration permits a lower percolation threshold [41].

As noted above for CNF, disagglomeration and dispersion of CNT inside the matrix is a key issue in any field of application [60]. Different methods of manufacturing can be used to produce filled polymers and disperse CNT such as the ones described in [19, 43, 68, 75]. Permittivity in X-band highlights the effect of CNT type, manufacturing and filler dispersion on the dielectric properties of the resulting composite. For instance Wu et al. [76] reports a relative real permittivity of less than 6 when an epoxy sample is loaded with 4,7%w, while Huang and co-workers [72] report a value of 25 with a loading of 5%w of SWCNT.

CNT have been used in shielding and absorbing applications, obtaining good results. 25 dB attenuation using epoxy filled with 15%w of long SWCNT at a thickness of 2 mm [72] and 16 dB when a polyurethane film loaded with 20%w is considered [77]. Umishita et al. [78] has measured the absorbing and shielding properties of MWCNT, their results are of about 20 dB attenuation for 0,22%w at 5,8GHz, increasing the filler content they obtained 45 dB shielding with PEEK as a matrix and a thickness of 4 mm. Absorbing application are less frequently published since their interest lays mostly in military application and as such most of the results are classified, but what is published is very promising such as more than 30 dB attenuation of CNT dispersed in silicon oil at a concentration of 0,25%w [79]. A peak attenuation of 22 dB at 11,4 GHz using a sample 1 mm thick is reported in [80] , but they Do not report how much filler was used. An absorption peak of 12 dB of attenuation on a sample 1,80 mm thick at 14 GHz is reported in [81] using polyester as matrix, but even in this case, the amount of filler used is not revealed. Multilayer absorbers and radar absorber structures (RAS) in form of composite sandwiches were also produced. RAS originate from the idea to reach valuable absorbing performance by exploiting wave interference. Such structures derive from specific electromagnetic design, that usually define a stacking sequence of layers, each one of which preset peculiar dielectric and/or magnetic properties and thickness. In [82] epoxy-glass fibres face sheets were loaded with CB and the polyurethane core was loaded with CNT, with the result that an attenuation of about 30 db were achieved. another example of RAS is the topic of [83], where a genetic algorithm is used to optimize the layers of MWCNT filled epoxy/glass fibres with a remarkable broadband absorption of more than 10 db over the whole X-band and a peak of -30 dB at 9,5 GHz with an overall thickness of 3,4 mm. Another multilayer

absorbers RAS sandwich produced, in this case epoxy-glass fibres face sheets loaded with CB and the polyurethane core loaded with CNT, got an attenuation of around 30 dB [82].

## 1.3 Equivalent circuit analogy

As outlined in §1.1 most of the research involving CPC was focused on lowering the percolation threshold, and scant attention was given till recently to other EM properties that are equally, if not more, affected by the morphology of filler networks inside the matrix. Nakamura [84] had shown that if a CPC is interpreted as an electrical equivalent circuit an increase in filler content increases its capacity and decrease its resistivity. In a successive paper [85] he suggested that dead branches of CB aggregates in the resin may act as capacitors and may be the cause of dielectric relaxation at high frequency. Further along these lines, Farfán et al. [86] showed that CPC with various filler content below percolation show frequency dependent resistance, which is a typical capacitor behaviour. In its 2006 paper Saib et al.[32] found that conductivity is frequency dependent and there is a high capacitive coupling between filler particles. In this work three different filler types were tested, some of them were also used in different ways, producing a range of different network morphology. Dielectric results were then linked with the morphology as obtained by SEM analysis using an equivalent circuit analogy. The circuit analogy as outlined above interpret the CPC as a circuit composed of capacitors and resistances, $\varepsilon_r'$ represent the ability of the material of store energy, it is then a measurement of the increase of equivalent capacitors inside the sample. These capacitors are produced by dead branches as suggested by Nakamura, but also by close spaced filler, in fact the value of capacitance is proportional to the surface of the conducting filler and inversely proportional to the distance among them. It is then safe to assume that the capacitance of the system increases when the surface area of the particles increases and when filler is better dispersed, since it creates new interface surfaces and so new capacitors, those capacitors will also have close spaced plates contributing even more to the increase in capacitance. The decrease in resistivity as the filler increases is indicated by $\varepsilon_r''$ and is influenced by the formation of more contacts between filler particles allowing a rapid dispersion of the charge by Joule effect. The author hopes to have provided compelling proof in the following chapter to prove that the equivalent circuit analogy is a useful way to link the sample microstructure with the dielectric properties.

## 1.4 References

[1] Kupke M, Wentzel HP, Schulte K. Electrically conductive glass fibre reinforced epoxy resin. Materials Research Innovations. 1998;2(3):164-9.

[2] Kraass KH. Electrically conducting rubber-a new material for electronics. Telecommunications and Radio Engineering, Part 2 (Radio Engineering). 1976;31(3):117.
[3] Ouyang J, Yang Y. Conducting polymer as transparent electric glue. Advanced Materials. 2006;18(16):2141-4.
[4] Duggal AR. An upper limit for high power switching with a polymer current limiter device. IEEE Transactions on Components and Packaging Technologies. 2000;23(3):490-6.
[5] Owen F. Protect your circuits. Sensors. 2001;18(3):62-3.
[6] Horibe H, Kamimura T, Yoshida K. Electrical conductivity of polymer composites filled with metal. Japanese Journal of Applied Physics, Part 1 (Regular Papers, Short Notes & Review Papers). 2005;44(6A):4171-5.
[7] Horibe H, Kamimura T, Yoshida K. Electrical conductivity of polymer composites filled with carbon black. Japanese Journal of Applied Physics, Part 1 (Regular Papers, Short Notes & Review Papers). 2005;44(4A):2025-9.
[8] Nanni F, Auricchio F, Sarchi F, Forte G, Gusmano G. Self-sensing CF-GFRP rods as mechanical reinforcement and sensors of concrete beams. Smart Materials and Structures. 2006;15(1):182-6.
[9] Nanni F, Ruscito G, Forte G, Gusmano G. Design, manufacture and testing of self-sensing carbon fibre-glass fibre reinforced polymer rods. Smart Materials and Structures. 2007;16(6):2368-74.
[10] Bin Z, Xianming D, Wei S, Dingcai W, Ruowen F, Bin Z, et al. Electrical response and adsorption performance of novel composites from polystyrene filled with carbon aerogel in organic vapors. Sensors & Actuators: B Chemical. 2008;132(1):60-6.
[11] Dong XM, Fu RW, Zhang MQ, Zhang B, Rong MZ. Electrical resistance response of carbon black filled amorphous polymer composite sensors to organic vapors at low vapor concentrations. Carbon. 2004;42(12-13):2551-9.
[12] Arshak K, Adley C, Moore E, Cunniffe C, Campion M, Harris J. Characterisation of polymer nanocomposite sensors for quantification of bacterial cultures. Sensors & Actuators: B Chemical. 2007;126(1):226-31.
[13] Yi H, Ning L, Yanfeng M, Feng D, Feifei L, Xiaobo H, et al. The influence of single-walled carbon nanotube structure on the electromagnetic interference shielding efficiency of its epoxy composites. Carbon. 2007;45(8):1614-21.
[14] Awerkamp DR. Shielding effectiveness of filled composites and coated plastics. 1981; New York, NY, USA: IEEE; 1981. p. 277-80.
[15] Heiser JA, King JA, Konell JP, Sutter LL. Shielding effectiveness of carbon-filled nylon 6,6. Polymer Composites. 2004;25(4):407-16.
[16] Simon RM. EMI shielding with aluminium flake filled polymer composites. 1984; New York, NY, USA: IEEE; 1984. p. 732-5.
[17] Yang Y, Gupta MC, Dudley KL. Studies on electromagnetic interference shielding characteristics of metal nanoparticle- and carbon nanostructure-filled polymer composites in the Ku-band frequency. Micro & Nano Letters. 2007;2(4):85-9.
[18] Strumpler R, Glatz-Reichenbach J. Conducting polymer composites. Journal of Electroceramics. 1999;3(4):329-46.
[19] Al-Saleh MH, Sundararaj U. A review of vapor grown carbon nanofiber/polymer conductive composites. Carbon. 2009;47(1):2-22.
[20] Moulart A, Marrett C, Colton J. Polymeric composites for use in electronic and microwave devices. Polymer Engineering and Science. 2004;44(3):588-97.
[21] Folgueras LDC, Alves MA, Rezende MC. Development, characterization and optimization of dielectric radar absorbent materials as flexible sheets for use at X-band. 2007; Piscataway, NJ 08855-1331, United States: Institute of Electrical and Electronics Engineers Inc.; 2007. p. 488-91.

[22] Abbas SM, Chandra M, Verma A, Chatterjee R, Goel TC. Complex permittivity and microwave absorption properties of a composite dielectric absorber. Composites Part A: Applied Science and Manufacturing. 2006;37(11):2148-54.
[23] Chen X, Wang G, Duan Y, Liu S. Electromagnetic characteristics of barium titanate/epoxide resin composites in X and Ku bands. Journal of Alloys and Compounds. 2008;453(1-2):433-6.
[24] Li X, Gong R, Feng Z, Yan J, Shen X, He H. Effect of particle size and concentration on microwave-absorbing properties of CuxCo2-xY (x=0, 1) hexaferrite composites. Journal of the American Ceramic Society. 2006;89(4):1450-2.
[25] Dishovski N, Petkov A, Nedkov I, Razkazov I. Hexaferrite contribution to microwave absorbers characteristics. Magnetics, IEEE Transactions on. 1994;30(2):969-71.
[26] Dishovsky N, Grigorova M. On the correlation between electromagnetic waves absorption and electrical conductivity of carbon black filled polyethylenes. Materials Research Bulletin. 2000;35(3):403-9.
[27] Kirkpatrick S. Percolation and Conduction. Reviews of Modern Physics. 1973;45(4):574.
[28] Balberg I. A comprehensive picture of the electrical phenomena in carbon black-polymer composites. Carbon. 2002;40(2):139-43.
[29] Yui H, Wu G, Sano H, Sumita M, Kino K. Morphology and electrical conductivity of injection-molded polypropylene/carbon black composites with addition of high-density polyethylene. Polymer. 2006;47(10):3599-608.
[30] Bar H, Narkis M, Boiteux G. The electrical behavior of thermosetting polymer composites containing metal plated ceramic filler. Polymer Composites. 2005;26(1):12-9.
[31] Chekanov Y, Ohnogi R, Asai S, Sumita M. Electrical properties of epoxy resin filled with carbon fibers. Journal of Materials Science. 1999;34(22):5589-92.
[32] Saib A, Bednarz L, Daussin R, Bailly C, Lou X, Thomassin J-M, et al. Carbon nanotube composites for broadband microwave absorbing materials. IEEE Transactions on Microwave Theory and Techniques. 2006;54(6):2745-53.
[33] Cheah K, Simon GP, Forsyth M. Effects of polymer matrix and processing on the conductivity of polymer blends. Polymer International. 2001;50(1):27-36.
[34] Kato H, Miyashita Y. Qualification of the electrical conducitivity of carbon black filled polymeric materials. 1990; Pocono Manor, PA, USA: Publ by IEEE, Piscataway, NJ, USA; 1990. p. 417-24.
[35] Schueler R, Petermann J, Schulte K, Wentzel H-P. Agglomeration and electrical percolation behavior of carbon black dispersed in epoxy resin. Journal of Applied Polymer Science. 1997;63(13):1741-6.
[36] Yoon HG, Kwon KW, Nagata K, Takahashi K. Changing the percolation threshold of a carbon black/polymer composite by a coupling treatment of the black. Carbon. 2004;42(8-9):1877-9.
[37] Grunlan JC, Bloom FL, Gerberich WW, Francis LF. Effect of dispersing aid on electrical and mechanical behavior of carbon black-filled latex. Journal of Materials Science Letters. 2001;20(16):1523-6.
[38] Weber M, Kamal MR. Estimation of the volume resistivity of electrically conductive composites. Polymer Composites. 1997;18(6):711-25.
[39] Bryning MB, Islam MF, Kikkawa JM, Yodh AG. Very low conductivity threshold in bulk isotropic single-walled carbon nanotube-epoxy composites. Advanced Materials. 2005;17(9):1186-91.
[40] Bigg DM. EFFECT OF COMPOUNDING ON THE CONDUCTIVE PROPERTIES OF EMI SHIELDING COMPOUNDS. Advances in Polymer Technology. 1984;4(3-4):255-66.
[41] Martin CA, Sandler JKW, Shaffer MSP, Schwarz MK, Bauhofer W, Schulte K, et al. Formation of percolating networks in multi-wall carbon-nanotube-epoxy composites. Composites Science and Technology. 2004;64(15):2309-16.

[42] Song YS, Youn JR. Influence of dispersion states of carbon nanotubes on physical properties of epoxy nanocomposites. Carbon. 2005;43(7):1378-85.
[43] Lau K-T, Lu M, Lam C-K, Cheung H-Y, Sheng F-L, Li H-L. Thermal and mechanical properties of single-walled carbon nanotube bundle-reinforced epoxy nanocomposites: The role of solvent for nanotube dispersion. Composites Science and Technology. 2005;65(5 SPEC ISS):719-25.
[44] Chun K-Y, Choi SK, Kang HJ, Park CY, Lee CJ. Highly dispersed multi-walled carbon nanotubes in ethanol using potassium doping. Carbon. 2006;44(8):1491-5.
[45] Huang J-C. Carbon black filled conducting polymers and polymer blends. Advances in Polymer Technology. 2002;21(4):299-313.
[46] Donnet J-B, Bansal RC, Wang M-J. Carbon black : science and technology. 2nd ed. New York: Dekker 1993.
[47] Donnet J-B. Fifty years of research and progress on carbon black. Carbon. 1994;32(7):1305-10.
[48] Brosseau C, Boulic F, Queffelec P, Bourbigot C, Le Mest Y, Loaeca J, et al. Dielectric and microstructure properties of polymer carbon black composites. Journal of Applied Physics. 1997;81(2):882-91.
[49] Kaynak A, Polat A, Yilmazer U. Some microwave and mechanical properties of carbon fiber-polypropylene and carbon black-polypropylene composites. Materials Research Bulletin. 1996;31(10):1195-206.
[50] Das NC, Khastgir D, Chaki TK, Chakraborty A. Electromagnetic interference shielding effectiveness of carbon black and carbon fibre filled EVA and NR based composites. Composites Part A: Applied Science and Manufacturing. 2000;31(10):1069-81.
[51] Kwon SK, Ahn JM, Kim GH, Chun CH, Hwang JS, Lee JH. Microwave absorbing properties of carbon black/silicone rubber blend. Polymer Engineering and Science. 2002;42(11):2165-71.
[52] Barba AA, Lamberti G, D'Amore M, Acierno D. Carbon black/silicone rubber blends as absorbing materials to reduce Electro Magnetic Interferences (EMI). Polymer Bulletin. 2006;57(4):587-93.
[53] Wen B, Jijun Z, Yuping D, Xingguo Z, Yanbo Z, Chuang D, et al. Electromagnetic wave absorption properties of carbon powder from catalysed carbon black in X and ku bands. Journal of Physics D (Applied Physics). 2006;39(9):1960-2.
[54] Chin WS, Lee DG. Development of the composite RAS (radar absorbing structure) for the X-band frequency range. Composite Structures. 2007;77(4):457-65.
[55] Cooper CA, Ravich D, Lips D, Wagner HD, Mayer JJ. Distribution and alignment of carbon nanotubes and nanofibrils in a polymer matrix. Composites Science and Technology. 2002;62(7-8):1105-12.
[56] Van Hattum FWJ, Serp P, Figueiredo JL, Bernardo CA. Effect of morphology on the properties of vapour-grown carbon fibres. Carbon. 1997;35(6):860-3.
[57] Tibbetts GG, Lake ML, Strong KL, Rice BP. A review of the fabrication and properties of vapor-grown carbon nanofiber/polymer composites. Composites Science and Technology. 2007;67(7-8):1709-18.
[58] Miyagawa H, Rich MJ, Drzal LT. Thermo-physical properties of epoxy nanocomposites reinforced by carbon nanotubes and vapor grown carbon fibers. Thermochimica Acta. 2006;442(1-2):67-73.
[59] Uchida T, Anderson DP, Minus ML, Kumar S. Morphology and modulus of vapor grown carbon nano fibers. Journal of Materials Science. 2006;41(18):5851-6.
[60] Thostenson ET, Li C, Chou T-W. Nanocomposites in context. Composites Science and Technology. 2005;65(3-4):491-516.

[61] Yanagisawa T, Hayashi T, Kim YA, Fukai Y, Endo M. Structure and basic properties of cup-stacked type carbon nanofiber. 2002; Philadelphia PA, PA 19106, United States: Taylor and Francis Inc.; 2002. p. 391167-5171.
[62] Yang S, Lozano K, Lomeli A, Foltz HD, Jones R. Electromagnetic interference shielding effectiveness of carbon nanofiber/LCP composites. Composites Part A: Applied Science and Manufacturing. 2005;36(5):691-7.
[63] Zhang C-S, Ni Q-Q, Fu S-Y, Kurashiki K. Electromagnetic interference shielding effect of nanocomposites with carbon nanotube and shape memory polymer. Composites Science and Technology. 2007;67(14):2973-80.
[64] Lee BO, Woo WJ, Kim M-S. EMI Shielding Effectiveness of Carbon Nanofiber Filled Poly(vinyl alcohol) Coating Materials. Macromolecular Materials and Engineering. 2001;286(2):114-8.
[65] Yang Y, Gupta MC, Dudley KL, Lawrence RW. Electromagnetic interference shielding characteristics of carbon nanofiber-polymer composites. Journal of Nanoscience and Nanotechnology. 2007;7(2):549-54.
[66] Thostenson ET, Ren Z, Chou TW. Advances in the science and technology of carbon nanotubes and their. Composites Science and Technology. 2001;61(13):1899-912.
[67] Coleman JN, Khan U, Gun'ko YK. Mechanical reinforcement of polymers using carbon nanotubes. Advanced Materials. 2006;18(6):689-706.
[68] Xie X-L, Mai Y-W, Zhou X-P. Dispersion and alignment of carbon nanotubes in polymer matrix: A review. Materials Science and Engineering R: Reports. 2005;49(4):23.
[69] Thostenson ET, Ziaee S, Chou T-W. Processing and electrical properties of carbon nanotube/vinyl ester nanocomposites. Composites Science and Technology.In Press, Corrected Proof.
[70] Dervishi E, Li Z, Saini V, Sharma R, Xu Y, Mazumder MK, et al. Multifunctional coatings with carbon nanotubes for electrostatic charge mitigation. 2008; Piscataway, NJ 08855-1331, United States: Institute of Electrical and Electronics Engineers Inc.; 2008. p. 4658903.
[71] Potschke P, Gedan-Smolka M, Pegel S, Villmow T, Tuschla M. Polymer - Carbon nanotube composites for electrostatic powder painting applications. VDI Berichte. 2008(2027):221-4.
[72] Huang Y, Li N, Ma Y, Du F, Li F, He X, et al. The influence of single-walled carbon nanotube structure on the electromagnetic interference shielding efficiency of its epoxy composites. Carbon. 2007;45(8):1614-21.
[73] Jung R, Kim H-S, Kim Y, Kwon S-M, Lee HS, Jin H-J. Electrically conductive transparent papers using multiwalled carbon nanotubes. Journal of Polymer Science, Part B: Polymer Physics. 2008;46(12):1235-42.
[74] Gojny FH, Wichmann MHG, Fiedler B, Kinloch IA, Bauhofer W, Windle AH, et al. Evaluation and identification of electrical and thermal conduction mechanisms in carbon nanotube/epoxy composites. Polymer. 2006;47(6):2036-45.
[75] Breuer O, Sundararaj U. Big returns from small fibers: a review of polymer/carbon nanotube composites. Polymer Composites. 2004;25(6):630-45.
[76] Wu J, Kong L. High microwave permittivity of multiwalled carbon nanotube composites. Applied Physics Letters. 2004;84(24):4956-8.
[77] Liu Z, Bai G, Huang Y, Ma Y, Du F, Li F, et al. Reflection and absorption contributions to the electromagnetic interference shielding of single-walled carbon nanotube/polyurethane composites. Carbon. 2007;45(4):821-7.
[78] Umishita K, Okubo T, Takuya N, Hashimoto O. Absorption and shielding effect of electromagnetic wave at GHz frequency by multi-walled carbon nanotube/polymer composites. 2006; Manchester, UK: IEEE; 2006. p. 291-4.
[79] Paton KR, Windle AH. Efficient microwave energy absorption by carbon nanotubes. Carbon. 2008;46(14):1935-41.

[80] Zhao D-L, Chi W-D, Shen Z-M. Preparation of carbon nanotube reinforced epoxy resin coating and its microwave characteristics. Key Engineering Materials. 2007;334-335 II:677-80.
[81] Ying Jie Q, Maosheng C, Liang Z. Investigation on potential microwave absorbability of polyester-composites filled with carbon nanotubes. 2006; Piscataway, NJ, USA: IEEE; 2006. p. 4 pp.
[82] Park K-Y, Lee S-E, Kim C-G, Han J-H. Fabrication and electromagnetic characteristics of electromagnetic wave absorbing sandwich structures. Composites Science and Technology. 2006;66(3-4):576-84.
[83] Lee S-E, Kang J-H, Kim C-G. Fabrication and design of multi-layered radar absorbing structures of MWNT-filled glass/epoxy plain-weave composites. Composite Structures. 2006;76(4):397-405.
[84] Nakamura S, Ito A, Kitagawa K, Sawa G. Resistor and dielectric properties of carbon black-epoxy resin composites. Transactions of the Institute of Electronics, Information and Communication Engineers C-II. 1991;J74C-II(11):749-54.
[85] Nakamura S, Kitagawa K, Sawa G. Dielectric properties of carbon black-epoxy resin composites in high frequency range. 1992; Sestri Levante, Italy: IEEE; 1992. p. 97-101.
[86] Juan-Farfan RS, Hernandez-Lopez S, Martinez-Barrera G, Camacho-Lopez MA, Vigueras-Santiago E. Electrical characterization of polystyrene-carbon black composites. Physica Status Solidi C. 2005(10):3762-5.

# 2 Electromagnetic properties of materials: an overwiev

In this chapter a quick overview of the major dielectric properties of the materials, linked to their microscopic characteristics, is proposed. Moreover some indications on the electromagnetic parameters measuring techniques will be given. Particular attention will be devoted to the description of the mechanisms of polarization, that are the physical basis of the origin of permittivity, and its variation in frequency. Such short dissertation is proposed since some of these concepts will be used in the discussion of the experimental results, where the nature and properties of the used nanofillers together with their dispersion inside the matrix will be ascribed as major feature affecting the permittivity of the composites.

## *2.1 Intrinsic EM parameters*

A material is classified as "dielectric" if it as the ability to store energy when an external electric field is applied. Dielectric properties influence the absorbing and shielding properties of materials. Wave propagation inside materials is influenced by permittivity and permeability, since they influence electric (**E**) and magnetic (**H)** field strengths. The relation between electric and magnetic field and the media in which the wave propagate is through constitutive relations. They relate the electric displacement density **D** and the current density **J** to **E**, and the magnetic flux density **B** to **H**. in the case of free space **D** is collinear with **E** and **B** with **H**.

$$D = \varepsilon_0 E \qquad B = \mu_0 H \qquad J = 0$$

Where $\varepsilon_0$ and $\mu_0$ are known as permittivity and permeability of free space, that present constant values of:

$$\varepsilon_0 = 8{,}854 \cdot 10^{-12} \text{ Farad/meter} \qquad \mu_0 = 4\pi \cdot 10^{-7} \text{ Henry/meter}$$

There is a wide class of materials, within which the above mentioned collinearity relations of the vectors **D** and **J** with **E,** and **B** with **H** are still valid, but they cannot be related by $\varepsilon_0$ and $\mu_0$ alone. They can nevertheless be expressed as scalar relations:

$$D = \varepsilon E \qquad B = \mu H \qquad J = \sigma E$$

Where $\varepsilon$, $\mu$ and $\sigma$ are the permittivity, permeability and conductivity of the medium, those are the *intrinsic EM parameters* of the medium. Quite often the permittivity and permeability of the material are expressed relative to the free space constants $\varepsilon_0$ and $\mu_0$.

$$\varepsilon = \varepsilon_r \varepsilon_0 \qquad\qquad \mu = \mu_r \mu_0$$

Where $\varepsilon_r$ is the relative permittivity or dielectric constant, and $\mu_r$ is called the relative permeability.

To a given **E** the resulting value of **D** and **B** are different if the waves propagates in free space or through a medium. At the macroscopic level this is explained by the fact that $\varepsilon$ and $\mu$ of the medium are different than those of the free space. On at the microscopic level this is explained by the fact that the medium is constituted by charged particles. When an electric or magnetic field is applied on a medium, the molecules and the atomic particles tend to align along the impressed field. This led to the concept of electric and magnetic polarization of materials. The electric polarization **P** is defined as:

$$P = \varepsilon_0 \chi_e E \quad \text{(eq 2.1)}$$

Where $\chi_e$ is the electric susceptibility of dielectric medium. The magnetic polarization, or magnetization, is similarly defined in terms of $\chi_m$ the magnetic susceptibility of medium as:

$$M = \mu_0 \chi_m \quad \text{(eq. 2.2)}$$

The electric (or magnetic) polarization of the materials alters the electric displacement (or magnetic flux) density within a medium due to an impressed field. Thus the electric displacement density within a dielectric medium may be expressed as the superposition of the electric polarization on the free space

$$D = \varepsilon_0 E + P = \varepsilon_0 (1 + \chi_e) E \Rightarrow \chi_e = \varepsilon_r - 1 \quad \text{(eq. 2.3)}$$

The same can be written regarding $\chi_m$.

It is apparent that the electric displacement density and the magnetic flux density vectors **D** and **B,** corresponding to the free space fields, are linear. Hence, if the electric polarization **P** is linear with respect to **E**, and so also the magnetic polarization **M** with respect to **H**, the corresponding expressions for **D** and **B** are also linear. Media obeying these conditions are said to be *linear* media. It is also possible that the polarization resulting from the applied field is not linear. Such media are identified as *nonlinear* in which $\chi_e$ and $\chi_m$ become non linear functions of **E** and **H**, respectively. Examples of such nonlinearity are frequently encountered in the cases of ferroelectric materials, e.g. barium titanate.

The electric polarization **P** resulting from an impressed alternated electric field **E** in a medium tend to lag behind it. This can be mathematically represented by assuming a complex form for the electric susceptibility and hence the dielectric constant of the medium.

$$\varepsilon_r = \varepsilon_r' - i\varepsilon_r'' \quad \text{(eq. 2.4)}$$

The real part of permittivity ($\varepsilon_r'$) is a measure of how much energy from an external electric field is stored in a material. The imaginary part of permittivity ($\varepsilon_r''$) is called the loss factor and is a measure of how dissipative or "lossy" a material is to an external electric field.

It includes the effect of both dielectric loss and electric conductivity. Being the two related by

$$\varepsilon'' = 2\pi f \sigma \quad \text{(eq. 2.5)}$$

Commonly, in everyday practice, the electromagnetic performance of a material is represented by the loss tangent $\tan\delta$ which is the ratio of $\varepsilon''$ to $\varepsilon'$.

$$\tan\delta = \frac{\varepsilon''}{\varepsilon'} \quad \text{(eq. 2.6)}$$

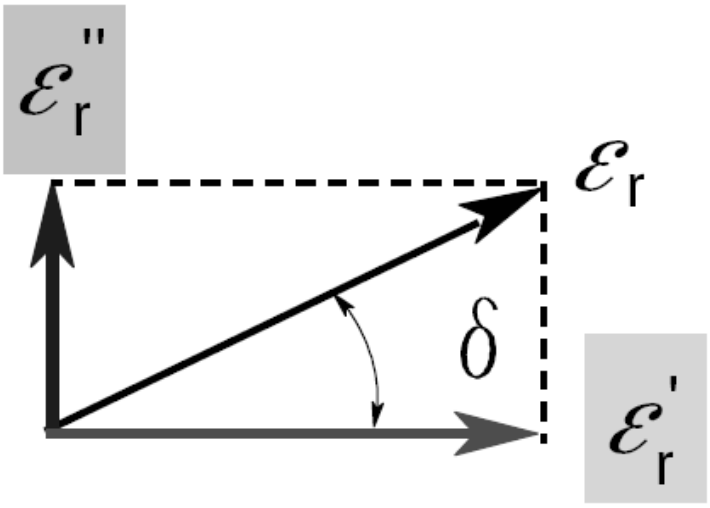


**Fig. 2-1 Graphic representation of relative permittivity ($\varepsilon_r$) and it relationship with real (ε') and imaginary (ε") permittivity through δ [1]**

In the present thesis this term is almost completely omitted since it is not the most appropriate in the discussion of the results to establish a clear correlation between the single ε' and ε" term and the material microstructure.

A similar expression can be obtained from the magnetic polarization **M** as:

$$\mu_r = \mu_r' - i\mu_r'' \quad \text{(eq. 2.7)}$$

The imaginary parts of relative permittivity and permeability are related to the polarization losses within the medium. Yet another loss mechanism is due to the finite but small conductivity of the dielectric medium. All those materials where either of the two mechanisms result in an appreciable loss of energy are said to be *dissipative* or *lossy*. Otherwise the medium is a *nondissipative* one. Other important definitions that derive from $\varepsilon$ and $\mu$ are *homogeneous* when the intrinsic properties remain invariant regardless of spatial coordinates; *dispersive* in which $\varepsilon$ and $\mu$ are frequency dependent; *isotropic* when they are independent of direction.

### *2.1.1 Microscopic approach to permittivity*

As just introduced above, the macroscopic effect of the reduced intensity of the electric field **E** inside the dielectric material has a microscopic explanation in the polarization of the medium.

Metals are typical conductors, their microstructure is characterized by long range order and atoms placed in specific places on the reticular lattice, the energy that binds the electrons to the nuclei (band) is low enough to allow some of the electrons in the outer orbit to escape. These "free"

electrons provide plenty of charge transport, when an electric field is applied they will move in an orderly way (electric current).

Dielectric materials have electrons bind much more tightly and the energy needed to get them unstuck is high, thus they are not free to move when an electric field **E** is applied and there will be no electrical current flowing through then in this condition. What the applied electric field causes on the dielectric material is the creation/orientation of electric dipoles present inside the material, leading to four different polarization mechanisms, orientation, electronic, atomic and interfacial polarization.

#### *2.1.1.1 Orientation polarization*

Some molecules have permanent polar dipole moments, due to the way they combine when forming (e.g. water). The rearrangement of electrons caused by the chemical link may cause an imbalance in charge distribution creating a permanent dipole moment. These moments are oriented in a random manner in the absence of an electric field so that no polarization exists. The electric field **E** will exercise torque **T** on the electric dipole, and the dipole will rotate to align with the electric field causing orientation polarization to occur, if the filed changes direction, the torque will also change [1].

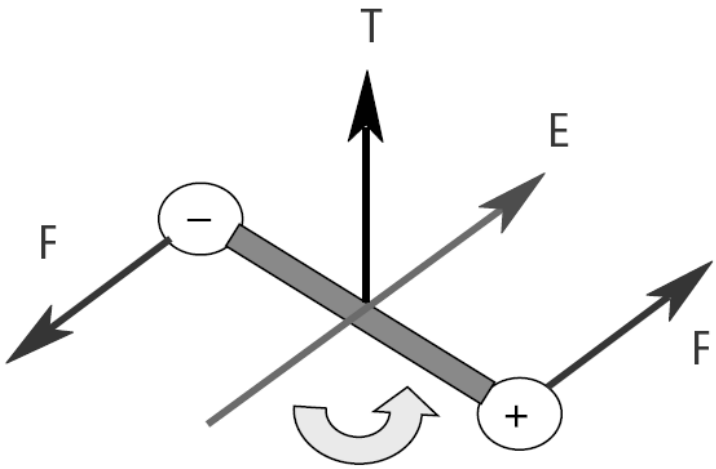


**Fig. 2-2 Forces caused by an electric field perpendicular to a dipole [1]**

#### *2.1.1.2 Electronic and atomic polarization*

Electronic polarization occurs in neutral atoms when an electric field displaces the nucleus with respect to the electrons that surround it. Atomic polarization occurs when adjacent positive and negative ions “stretch” under an applied electric field. For many solids, these are the dominant polarization mechanism at microwave frequencies, although the actual resonance occurs at much higher frequency. An atom can be sketched as a positive charged nucleus surrounded by a

symmetric “cloud” of negative charges, the electrical dipole is then zero. When an electric field is applied the atom lose its symmetry and acquires a dipole moment $\vec{p}$.

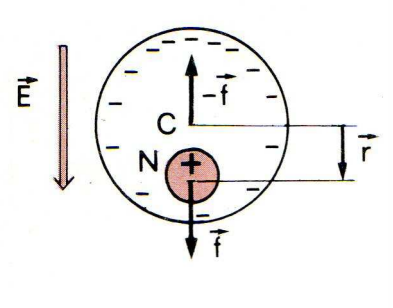


**Fig. 2-3 electronic polarization**

A similar effect to the electronic polarization takes place in an ionic material, i.e. one that has permanent dipoles that can not freely turn. One of such materials is NaCl, when not subjected to an electric field polarization the material is neutral (an equal number of negative $Cl^-$ and positive charged ions $Na^+$) and the ions are repeated regularly in the lattice. When an electric field is applied the ions lose the lattice symmetry by increasing the distance from the opposite ion (and shortening it from another opposite ion) thus producing a net dipole moment.

#### *2.1.1.3 Interfacial or face charge polarization*

Electronic, atomic and orientation polarization occur when charges are locally bound in atoms, molecules, or structures of solids or liquids. Charge carriers also exist in a bulk material that can migrate over a distance through the material when a low frequency electric field is applied. Interfacial or space charge polarization occurs when the motion of these migrating charges is impeded. The charges can become trapped within the interfaces of a material. The filed distortion caused by the accumulation of these charges increases the overall capacitance of a material which appears as an increase in $\varepsilon_r'$.

### *2.1.2 Polarization caused by an alternating electrical field*

When a non-stationary electric field **E** is applied to the medium, the dipoles cycle from the non-oriented (non-polarized) to oriented (polarized) status and back. The dipoles masses are accelerated and decelerated. Since the dipole alignment is not instantaneous, **P** lags **E** and losses occour. There are “cutoff frequency” specific to various polarization mechanisms, as frequency increases the slower mechanism cannot keep pace and drop out in turn, leaving the faster ones to contribute to $\varepsilon'$, the predominant polarization mechanism is then a function of the frequency. As the frequency

shifts to very high values none of the polarization mechanism is able to follow the orientation cycles, and as the frequency moves toward infinite, no polarization occurs and tends to its limit value, i.e. one. The polarization of a medium is the sum of all the different mechanism described, the case of an ideal material that presents all the four mechanisms are depicted in Fig. 2-4.

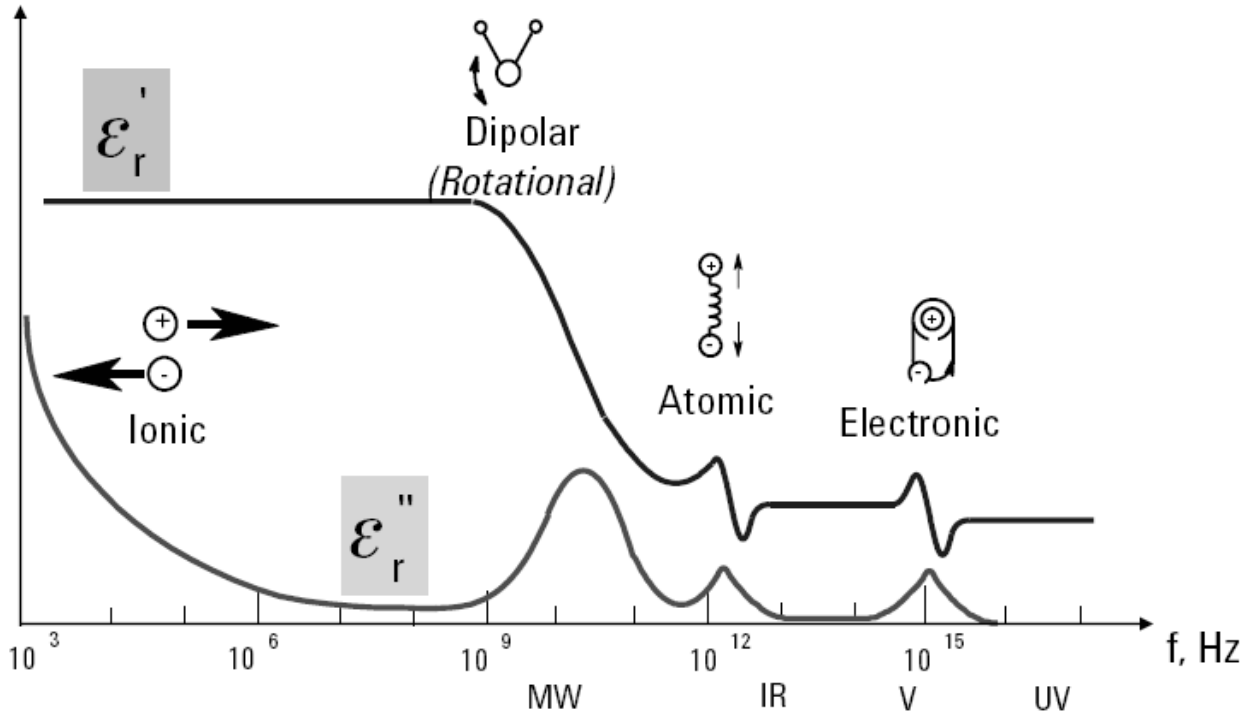


**Fig. 2-4 Principal polarization mechanism from 1kHz to 1THz [1]**

Electronic and ionic polarization mechanism act by moving the charge apart, while the medium resists with an opposite force that is roughly proportional to the distance. It is an oscillator system that will resonate at a certain frequency. Orientation polarization does not have a recognizable force that brings the orientated dipoles back to the non-polarized status, but a series of statistical events that rearrange the dipoles when the external electric field is removed. In this case the quantity representing the phenomenon is the relaxation time $\tau$, defined as the time required for a displaced system aligned in an electric field to return to $1/e$ of its random equilibrium value.

Before ending this paragraph, the author wishes to put into evidence that all the reported polarization mechanisms are always referred to bulk materials, while the materials under test in this thesis are composites. The study of the origin of the EM properties of composite materials is still undergoing, and this is why till now a complete and reliable modelization of the EM behaviour of composite materials in waves is not available yet. Nevertheless, as will be shown in the following

chapters, the major contribution to polarization in the frequency range considered in this study is the interfacial polarization among the nanofillers or nanofiller aggregates and the insulating polymer resin.

### *2.1.3 Absorbing mechanism in dielectric materials*

Broadly speaking EM energy absorption in a dielectric medium is caused by two different mechanisms:

- Dielectric relaxation

  Takes origin in the presence of molecular dipoles (permanent or induced) that follow the polarizing cycles at low frequency. At increasing frequency, though, the dipoles struggle to follow the changes of field due to the viscosity of the medium, and, as a consequence, part of the energy dissipated throughout the media
- Resonance

  The polarization mechanism arising from rotation or vibration of atoms, ions or electrons, as described above, can be described as an oscillator system that, as happens in mechanics, is characterized by the phenomenon of resonance. In EM resonance happens at peculiar frequencies and is clearly visible by the presence of absorption peaks.

Materials that exhibit a single relaxation time constant can be modelled by the Debye relation, which appears as a characteristic response in permittivity as a function of frequency (Fig. 2-5). $\varepsilon_r'$ is constant above and below the relaxation with the transition occurring astride the relaxation frequency. Additionally $\varepsilon_r''$ is small above and below relaxation but peaks in the transition region at the relaxation frequency.

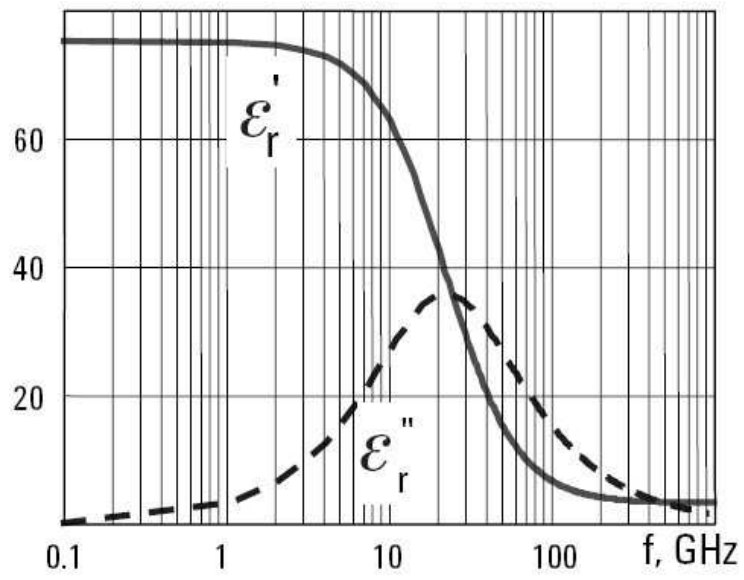


**Fig. 2-5 Debye relaxation [1]**

## 2.2 Measuring equipment

The electromagnetic properties of a material (i.e. Permittivity and permeability) are usually derived from the measurement of the reflection from and/or transmission coefficients of it along with knowledge of its physical dimensions, by means of different techniques. The most suitable instrument, reporting both amplitude and phase of the scattered waves, is the network vector analyzer.

### *2.2.1 Vector network analyzer*

A vector network analyzer (VNA) consists of a signal source, a receiver and a display. The source launches a signal at a single frequency to the material under test (MUT). The receiver is tuned to that frequency to detect the reflected or transmitted signals from the material. The measured response, compared to the reference stored in the VNA, produces the magnitude and phase data at that frequency. The source is then stepped to the next frequency and the measurement is repeated to display the reflection or transmission measurement response as a function of frequency.

These data are the scattering parameters, identified with the notation $S_{xy}$, where x identify the receiving channel and y the emitting one. Thus $S_{11}$ identify a reflection measurement, where the sample is backed by metal, to assure complete reflection of the emitted wave, $S_{21}$ is the transmission scattering parameter. Calibration is used to eliminate the systematic (stable and repeatable) measurement errors caused by the imperfections of the system. Random errors due to noise, drift, or the environment (temperature, humidity, pressure) cannot be removed with a measurement

calibration, this makes a microwave measurement susceptible to errors from small changes in the measurement system.

## 2.3 Measuring techniques

Several method exist to measure the intrinsic properties of materials, all of them have their pro and cons, the most common methods are illustrated briefly

### *2.3.1 Coaxial probe*

The open-ended coaxial probe is a cut off section of transmission line. The material is measured by immersing the probe into a liquid or touching it to the flat face of a solid (or powder) material. The fields at the probe end "fringe" into the material and change as they come into contact with the MUT. The reflected signal ($S_{11}$) can be measured and related to $\varepsilon_r^*$.

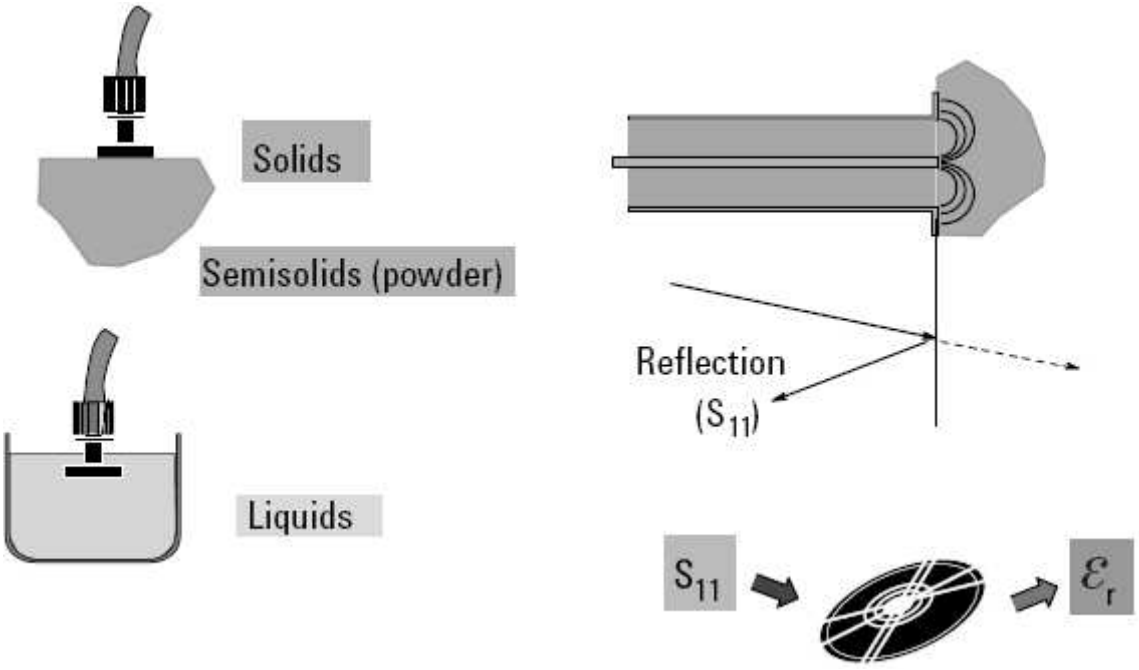


**Fig. 2-6 Examples of coaxial probe uses and what it measures [1]**

This method assumes that the material is of semi-infinite thickness (or at least ⟩⟩ thicker than skin-depth at the frequency used), homogenous and isotropic. Since it is only possible to measure the reflection of the wave ($S_{11}$) it is not possible to analyse magnetic materials (it is not possible to fit a system of two equations with just a set of data). This method has a low resolution but it is broadband and can be used without damaging the material.

### *2.3.2 Transmission line methods*

Transmission line methods involve placing the material inside a portion of an enclosed transmission line. The line is usually a section of rectangular waveguide or coaxial airline (Fig. 2-7). $\varepsilon_r^*$ and $\mu_r^*$ are computed from the measurement of the reflected signal $S_{11}$ and transmitted signal $S_{21}$.

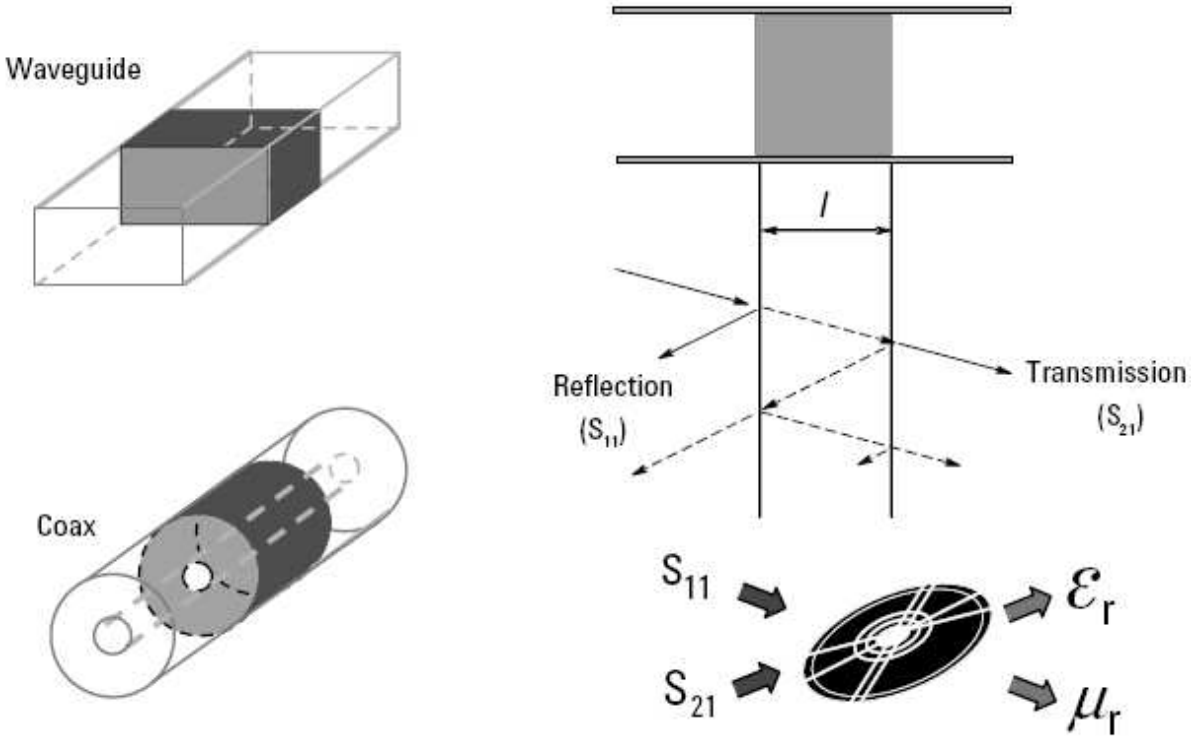


**Fig. 2-7 Examples of transmission line methods, and what they measure [1]**

This method allows to measure both reflection ($S_{11}$) and transmission ($S_{21}$) and as such it allows the measurement of magnetic samples, great care shall be taken in making sure the sample completely fills the cavity and doesn't leave any air gap, at the same time the sample must have perfectly flat surface and be flush to the sample holder. Coaxial transmission lines cover a broad frequency range, but toroid shaped samples are more difficult to manufacture. Waveguide fixtures extend to the mm-wave frequencies and the samples are simpler to machine, but their frequency coverage is banded. This technique was used[2] in the EM measurements carried out during this thesis

[2] EM measurements were carried out at the facilities of CEMIN s.r.l. , VIA DELLA FARNESINA 363, 00194 ROMA, to which special thanks are given

### *2.3.3 Free space*

Free-space methods use antennas to focus microwave energy at or through a slab of material without the need for a test fixture. This method is non-contacting and can be applied to materials to be tested under high temperatures and hostile environments. Frequency range possible is broad and depends only on the antennas, on the other hand the calibration and measurement is tricky, and the method is very expensive since it needs special anechoic rooms to provide useful data not marred by spurious reflections. Major drawback of this method is the dimension of the specimens that are usually wide more or less depending on the frequencies under test. Moreover, particular attention has to be paid to the presence of scattering effects at sample boundaries that can heavily affect the final measurements. A typical freespace measurement setup, specially designed to limit this effect, is depicted in Fig. 2-8 [2, 3].

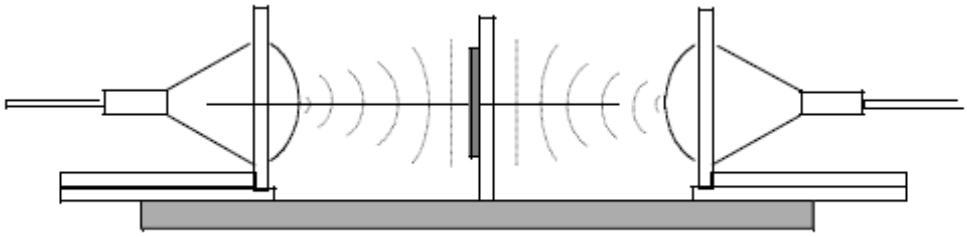

**Fig. 2-8 Focalized aerials free space measurements [1].**

## *2.4 Scattering parameters elaboration*

The scattering parameters obtained with the above methods, describe the interaction of the emitted-reflected/transmitted wave with the MUT. Knowing the thickness of the sample it is possible to derive the value of the intrinsic parameters. Three different kind of scattering parameters were collected during the measurement, reflection $S_{11}$ where samples were backed by metal, indicated as $\rho$, transmission $S_{21}$ designated as $\tau$, and a reflection measurement taken with the transmission set-up ( the material wasn't backed by metal) indicated as $\rho_t$. This further measurement was made to provide a further set of data to allow a closer match of the iterative software routine to the measured data.

When an EM wave ($E_i$) propagating into a medium (medium 1) impinges on a different material surface (medium 2), due to the materials impedance mismatch part of it is reflected ($E_r$), and part is transmitted inside the material ($E_t$). Energy is conserved:

$$\vec{E}_i + \vec{E}_r = \vec{E}_t \text{ (eq. 2.9)}$$

The characteristic impedance can be employed to relate EM field vectors for incident, reflected and transmitted waves.

(eq 2.10) $H_i = \frac{E_i}{Z_1}$ $H_r = -\frac{E_r}{Z_1}$ $H_t = \frac{E_t}{Z_2}$

Where $Z_1$ and $Z_2$ are the characteristic impedances of media 1 and 2, respectively. Substituting

$$\frac{E_i}{Z_1} - \frac{E_r}{Z_1} = \frac{E_t}{Z_2} \Rightarrow E_r = \left(\frac{E_i}{Z_1} - \frac{E_t}{Z_2}\right) Z_1 \text{ (eq. 2.11)}$$

By substituiting for $E_r$ in eq. 2.9 with the expression above, and rearranging, the transmitted electric field can be obtained.

$$E_t = \frac{2Z_2}{Z_1 + Z_2} E_i \text{ (eq. 2.12)}$$

The ratio $E_t / E_i$ is defined as the transmission coefficient $\tau$ at the interface between two media,

$$\tau = \frac{E_t}{E_i} = \frac{2Z_2}{Z_1 + Z_2} \text{ (eq. 2.13)}$$

Eliminating $E_i$ between eqs. 2.13 and 2.9, the reflected electric field $E_r$ becomes

$$E_r = \frac{Z_2 - Z_1}{Z_2 + Z_1} E_i \text{ (eq. 2.14)}$$

The ratio $E_r / E_i$ is called the reflection coefficient and is denoted by $\rho$ which in terms of the characteristic impedance of the two media is:

$$\tau = \frac{E_r}{E_i} = \frac{Z_2 - Z_1}{Z_2 + Z_1} \text{ (eq. 2.15)}$$

Once $\rho$, $\rho_t$ and $\tau$ are measured and knowing d, the material thickness, it is possible to calculate $Z_2$, since $Z_1$ is the impedance of air, known. Then an iterative routine try to find the best fit using the least square method. It should be noted that this process is rather complicated and the solution is just a best match and not the exact solution.

## 2.5 References


[1] Agilent. Basics of measuring the dielectric properties of materials.

[2] Seo IS, Chin WS, Lee DG. Characterization of electromagnetic properties of polymeric composite materials with free space method. Composite Structures. 2004;66(1-4):533-42.

[3] Hollinger RD, Jose KA, Tellakula A, Varadan VV, Varadan VK. Microwave characterization of dielectric materials from 8 to 110 GHz using a free-space setup. Microwave and Optical Technology Letters. 2000;26(2):100-5.

# 3 Material and methods

In this chapter the detailed description of materials and manufacturing processes is presented. Particular attention will be devoted to the main processes that were common to all samples, while little variations, possibly brought in specific preparation will be respectively discussed in the chapter about each type of nanofiller. Main differences in manufacturing procedures have to be found in the dispersion processes (for example use of additives, type of solvent, process parameters) that were always aimed to increase a better nanofiller dispersion .

### *3.1.1 Acronym*

The quite large variety of samples produced is responsible for the difficulty in finding a general naming procedure. In this paragraph the acronym used are reported in order to facilitate the reading of the following parts. Samples naming follows a this form

AAxxx-SB

Where

- The first two letters AA identify the filler used or if a surfactant is used the surfactant added.
- The digits that follows the first two letters report the nanofiller weight percent of filler
- S identify the resin used, and it is constant throughout the thesis
- If more identifying features are needed (usually related to different methods of production) a suffix is added after S

### *3.1.2 Resin*

The resin used is a 2 component epoxy resin based on Bisfenol A-epichloridrine that offers low viscosity and good wetting of fillers. It was decided to employ an epoxy resin from the start due to its superior mechanical and thermal qualities than thermoplastic polymers, on the other hand the dispersion of filler inside a thermoset is not as easy as in thermoplastics where several melting can be successively carried out [1] in order to improve the dispersion or keep it in a molten state for as long as it is useful. Polycondensation is a one way reaction and it is only possible to choose how quick it will be, using different hardening agents. Isoforon Diammine was used in all the samples produced, it gives about 45 minutes before gel time, enough time to be able to mix it thoroughly without the need of very quick and thus turbulent stirring of the resin-filler dispersion.

### *3.1.3 Determination of filler content*

To calculate the weight of the filler it is necessary to know how much resin and hardener is employed. First the resin is weighted then the hardener is calculated and weighted following the stechiometric ratio of 4 grams of hardener to 10 grams of resin. Filler weight is calculated using equation 2.1

$$X\text{: mass \% wanted} = (R + H + X):100 \quad \text{(eq. 3.1)}$$

Where R is resin weight, H is Hardened weight and X is the weight needed to reach the desired mass % of filler, all in grams. Eq. 3.1 can be written in a more practical way as

$$X = \frac{(R + H) \cdot \text{mass \% wanted}}{100\text{- mass \% wanted}} \quad \text{(eq. 3.2)}$$

If solvent is used, as in CNF and CNT samples, then the volume is calculated using the ratio to the filler as outlined in the respective chapters. Surfactants were used in some of the CNT samples, and their amount is not computed into the total weight of the samples, as in the case of the filler, but it is calculated as a percent of the filler weight (cfr §6.1.1).

### *3.1.4 VNA measurement sample requirements and preparation*

Electromagnetic Measurements were carried out in the X-band (8,2-12,4 GHz) , that was chosen since it is one of the most used and congested band. Just to report some examples of what is already in use or in development that occupies such band, there is the polarimetric radar [2], medical applications [3, 4], space radars [5] etc.

as previously reported, waveguide measurements require the sample to touch perfectly against the sample holder, because even a small air gap between the flange and the material under test can cause significant errors. To overcome this problem, the samples were directly casted in the flanges, that were 4 mm thick conventional k-band flanges ( 22,86x10,16 mm). The thickness of 4 mm was chosen as a good compromise between minimum material required and a good interaction of the waves with the material.

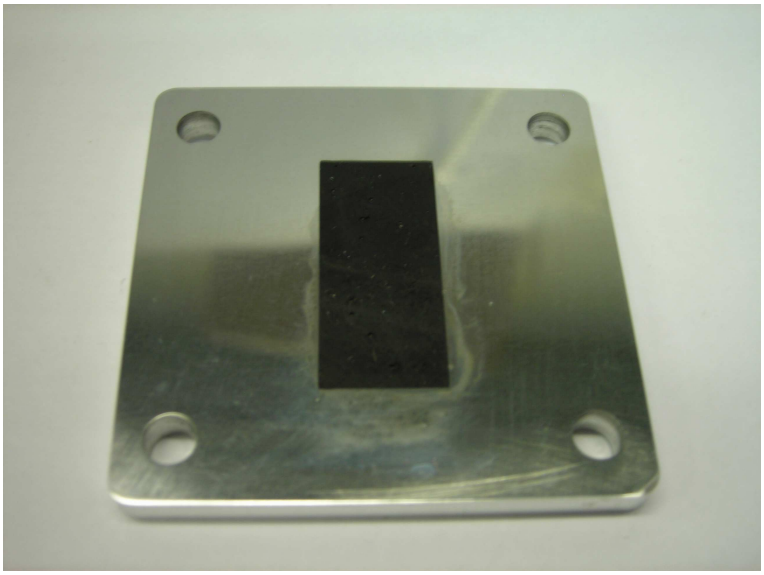

**Fig. 3-1 X-band sample holder and sample ready to be measured**

Another requirement for waveguide measurement is specimen surface flatness, which was achieved by grinding and polishing the samples.

Scattering parameters were measured in both reflection and transmission ($S_{11}$ and $S_{21}$). The collected data were successively elaborated inferring the ε and μ coefficients by minimizing an error function between the measured and the numerically calculated S complex parameters with respect to ε', ε" [6]. Due to the complexity of the mathematical relations involved in this procedure, together with the extreme sensitivity of the measurements, the results of these elaborations can be considered reliable with a confidence of about 5-8%. Moreover, as largely known, the waveguide technique is not particularly suitable for ε" evaluation, that is usually more precisely measured by resonance methods. Nevertheless this technique offer the possibility to measure ε" as a function of frequency whereas the resonance method give usually the values of ε" only at two or three frequencies.

Always from the same waveguide measurements it was possible to determine the absorption loss of all samples. The reported results are those achieved by $S_{11}$ measurements using a metal baking. Simulations were then carried out to evaluate the absorption performance at different thicknesses always less that 4mm, being larger thickness un-useful for practical applications.

### *3.1.5 Dielectric percent variations calculations*

Percent variations of the real and imaginary permittivity will be encountered during the discussion of the dielectric properties of samples and their relationship with microstructure. The percent values presented are calculated using eq. 3.3:

$$\frac{\varepsilon(X_{i+1}) - \varepsilon(X_i)}{\varepsilon(X_i)} \cdot 100 \quad \text{(eq. 3.3)}$$

When samples with the same weight percent of filler but different filler or production methods are compared, the same formula is used and “A/B variance” is found as the header of the column, in this case A replaces $X_{i+1}$ and B replaces $X_i$.

## 3.2 References


[1] Yang Y, Gupta MC, Dudley KL, Lawrence RW. The fabrication and electrical properties of carbon nanofibre-polystyrene composites. Nanotechnology. 2004;15(11):1545-8.

[2] Anagnostou MN, Anagnostou EN, Vulpiani G, Montopoli M, Vivekanandan J. Evaluation of X-band polarimetric radar estimates of drop size distributions from coincident S-band polarimetric estimates and measured raindrop spectra. 2008; Piscataway, NJ, USA: IEEE; 2008. p. 3575-8.

[3] Gambaccini M, Taibi A, Del Guerra A, Frontera F. Small-field imaging properties of narrow energy band x-ray beams for mammography. 1995; Piscataway, NJ, USA: IEEE; 1995. p. 1388-91.

[4] Hanna SM. Applications of X-band technology in medical accelerators. 1999; Piscataway, NJ, USA: IEEE; 1999. p. 2516-8.

[5] Mizuhara A. Bandwidth and group delay extension for an X-band 250 kW CW klystron for JPL/NASA deep space radar. 2004; Piscataway, NJ, USA: IEEE; 2004. p. 77-8.

[6] Knott EF. Radar cross section measurements. Raleigh, NC: SciTech Pub. 2006

# 4 Carbon Black samples

This chapter deals with the production and testing of carbon black (CB) filled epoxy samples.

## *4.1 Experimental*

### *4.1.1 Degussa Printex XE2-B and Timcal Super-P*

As reported in paragraph §1.2.1, some of the most important characteristics that influence the shape of CB network inside the matrix are [1] and surface area [2] of nanofillers and the resulting structure. Increasing the surface area of CB would result in decreasing the gaps between the polymer and conductive aggregates, in particular, it is well known [1] that carbon nanoparticles with high surface area and oil absorption number (OAN) present the so-called “high structure”, i.e. highly branched aggregates, which leads to the formation of the conductive network at lower carbon content (low percolation threshold) [3]. In this experimentation two different types of carbon black powders. Named Xe-2b and Sp, were employed to produce the samples. Table 4-1 reports their main characteristics. Highly conductive Xe2-b is used in electrical conductive coatings and in antistatic or electrical conductive modification of polymer systems, Super-p is used as conductive additive primary in zinc-carbon battery.

**Table 4-1 CB filler properties as found in the respective datasheet**

| | Particle size nm | DPB Absorption (structure) ml/100 g | Specific surface area $m^2/g$ |
|---|---|---|---|
| Printex XE2-B | 30 | 411 | 1000 |
| Super-P | 40 | 380 | 62 |

### *4.1.2 Fabrication procedure*

CB powders are the less difficult to disentangle among the filler used in this thesis, disagglomeration was achieved directly into the resin, skipping the solvent step used in CNF and CNT samples. High speed mechanical stirring is enough to disperse them into the resin, since it generates high shear forces [4]. Five minutes stirring at 700 revolutions per minutes (RPM) was used on all the CB samples, followed by other 5 minutes stirring after the hardener was added, before casting.

Table 4-2sums the samples produced.

**Table 4-2 CB samples produced**

| Name | Weight % of filler produced | Name example |
|---|---|---|
| Xe | 2; 3; 4; 5; 6 | Xe4-s |
| Sp | 2; 3; 4; 5; 6 | Sp3-s |

### *4.1.3 Specimens characterization*

EM characterization of the samples has been carried out following the procedure reported in §3.1.4 . Microstructural characterization, aimed to analyze the CB dispersions of the two types of specimens in the cured resin, was carried out by scanning electron microscopy (SEM mod. Leo-supra 35). The observations were carried out on highly polished samples using charging phenomena [5].

## *4.2 Results and discussion*

### *4.2.1 Conducting paths morphologies*

The morphologies of the two different fillers in cured composites are outwardly similar but differ on the scale of the aggregate dimension. As can be seen in Fig. 4-1a and as noted in §1.2.1 the smaller specific surface area of Xe produces smaller, shorter and close spaced aggregates, that form a continuous network throughout sample cross section, leading to percolation.

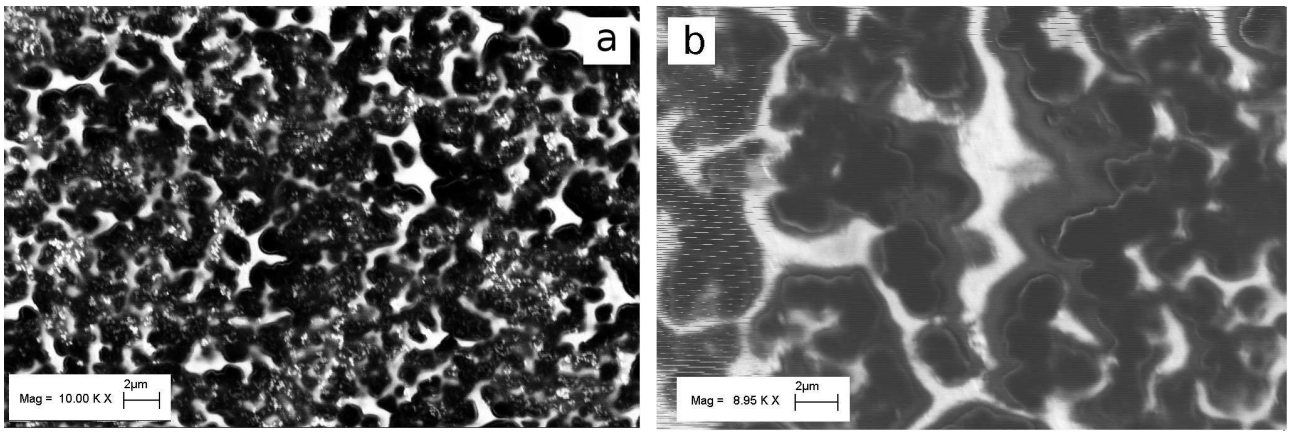


**Fig. 4-1 SEM micrographyes a) XE 5%w; b) Super-P 5%w**

On the other hand, Sp samples present long, broad meandering aggregates that develops in 3d forming a semi-continuous reticule of conducting paths, but in this case, on equal conditions, the layers of resin separating the conductive aggregates is larger than in case of Xe. This difference has

wide ranging influence on the resulting properties of the samples when electrical and dielectric properties are concerned.

### *4.2.2 XE loaded samples*

The dielectric properties of XE loaded samples show a regular increase in the value of permittivity, both real and imaginary, at increasing filler loading. As described in §1.3 the increase in filler content increases the equivalent capacity and decreases the resistivity. Real permittivity is a measure of the ability of the material to store energy and so it increases when filler is increased until direct contact among the conductive particles is achieved. The 2%w loading is too low to present any change in dielectric constant with respect to the neat resin (3-j0.05) (Fig. 4-2), while an increase of this quantity is recorded started from 3%w. The big increase in dielectric constant from xe5-s to xe6-s (59%, Table 4-3) is due to the inset of percolation, whose occurring at this loading is documented in [6].

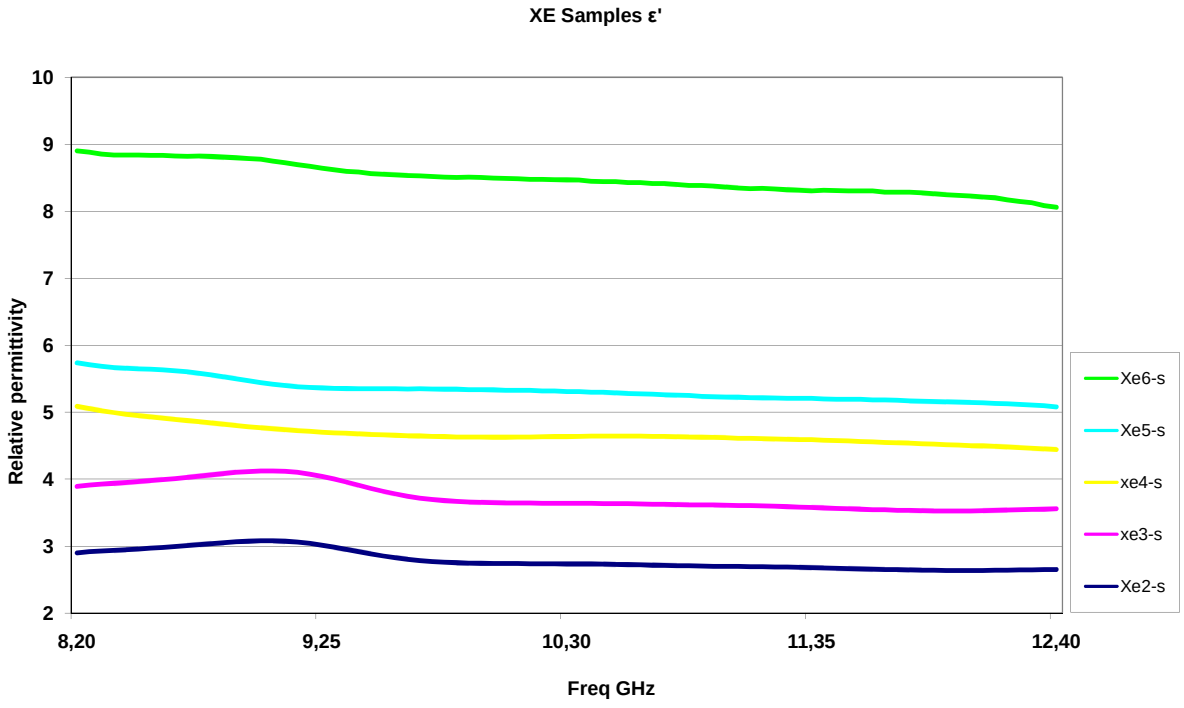


**Fig. 4-2 XE samples real permittivity in X-band**

Even imaginary permittivity increases at filler increase, (Table 4-3). In this case, though, the imaginary permittivity is immediately incremented, even at a 2%w CB, form that of neat resin (ε”=0.05), due to the conductive nature of the filler (see eq. 2.5 ). The important progressive increase of ε” is due to the reduced spacing between clusters, enabling some tunnelling and/or

hopping conduction. The formation of new clusters and the decreased distance among them, occurring when more filler is added, lead to a more close spaced structure with more opportunities of tunnelling/hopping.

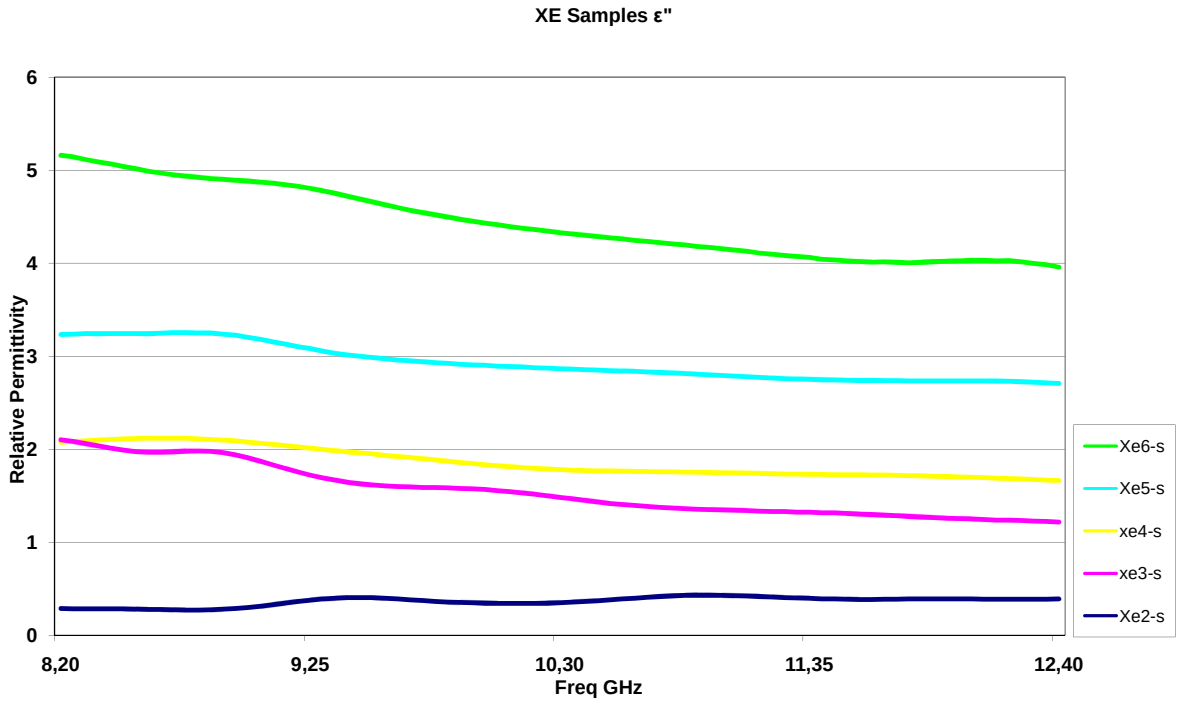


**Fig. 4-3 XE samples imaginary permittivity in X-band**

**Table 4-3 Percent increases in filler weight load, average real and imaginary XE samples**

| Filler weight % | Weight increment | Average ε’ | ε’ increment | Average ε" | ε" increment |
|---|---|---|---|---|---|
| 2% | | 2,99 | | 0,36 | |
| 3% | 50% | 3,73 | 34% | 1,55 | 325% |
| 4% | 33% | 4,67 | 25% | 1,86 | 20% |
| 5% | 25% | 5,33 | 14% | 2,93 | 58% |
| 6% | 20% | 8,49 | 59% | 4,43 | 51% |

Fig. 4-4 report the microwave absorbing performances of XE samples, referred to 4mm thickness. Very interesting results were achieved in the case of 3 and 4%w loaded samples, the latter reaching a peak of -38 db. 5 and 6%w loading loose absorbing properties, due to the too high conductivity of the specimens, which become mostly reflective. 2%w specimens were not included in the graph, due to their very low permittivity.

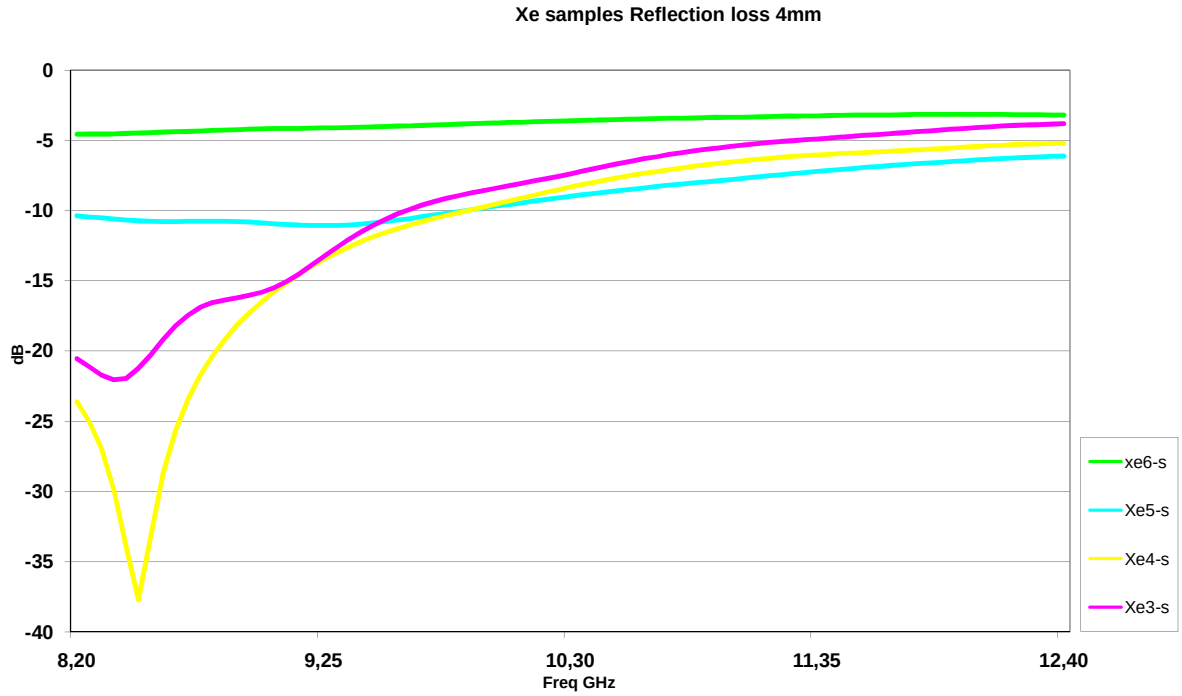


**Fig. 4-4 XE samples reflection loss in X-band 4 mm thickness**

### *4.2.3 Super-P*

Super-P samples raise of real permittivity ε' (Fig. 4-5) dovetails nicely with the percent increase in filler (Table 4-4), with the exception of the 6%w specimen whose increment is double the increase of filler. Many SEM observations suggested that with this type of filler, the increase of its amount is primary used to augment the dimension of clusters instead of forming new clusters. As a result a wide spread conductive network is achieved later. In these conditions, using the circuit analogy, the overall capacity is then increased by the bigger surfaces of the micro-condenser formed by CB aggregates.

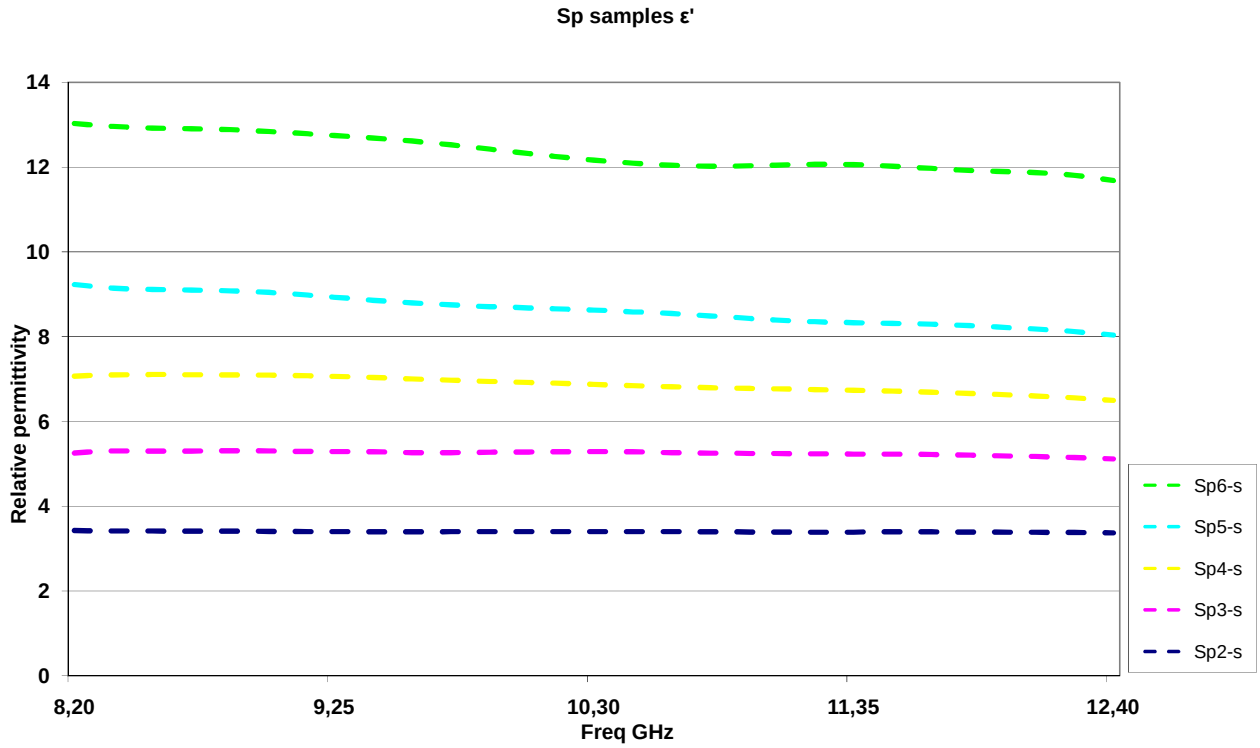


**Fig. 4-5 S-P samples real permittivity in X-band**

Again, imaginary permittivity ε" (Fig. 4-6, Table 4-4) increases with filler content, nevertheless their absolute values are lower than in the case of XE samples, representing the lower conductivity achieved in this case as a consequence of the peculiar microstructure. In this case, in fact, the presence of broader and less branched aggregates leads to a more difficult formation of the conductive pattern an electrical conductivity, again represented in ε".

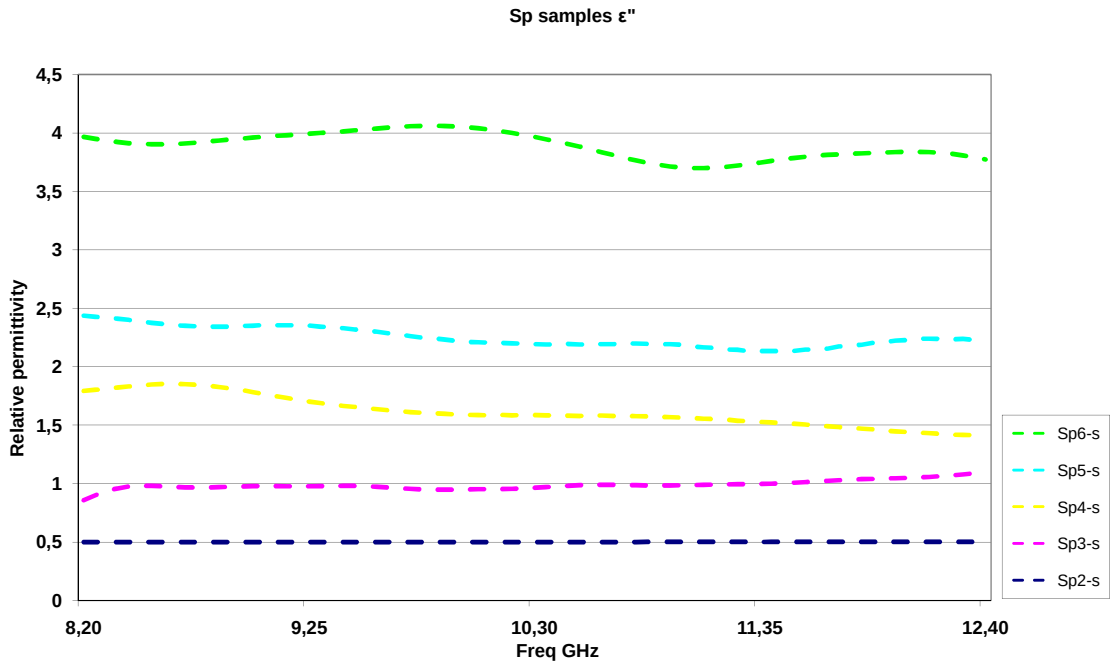


**Fig. 4-6 SP samples imaginary permittivity in X-band**

**Table 4-4 Percent increases in filler weight load, average real and imaginary Super-P samples**

| Filler weight % | Weight increment | Average ε’ | ε’ increment | Average ε" | ε" increment |
|---|---|---|---|---|---|
| 2% | | 3,40 | | 0,50 | |
| 3% | 50% | 5,25 | 55% | 0,99 | 97% |
| 4% | 33% | 6,87 | 31% | 1,61 | 63% |
| 5% | 25% | 8,63 | 26% | 2,25 | 40% |
| 6% | 20% | 12,33 | 43% | 3,89 | 73% |

Absorption performances of Sp samples is globally lower that that of the corresponding XE samples. In 2%w specimen the filler content is too low to provide any useful absorption, while Sp-3-s sample is the only one providing at least some interesting results (-16db). Possibly, even Sp4-s has an absorbing peak comparable to that of the previous samples, nevertheless it is shifted at lower frequencies, outside the x-band. Eventually, Sp5-s and Sp6-s have too much filler, and therefore too much conductivity, to be able to absorb EM waves (Fig. 4-7).

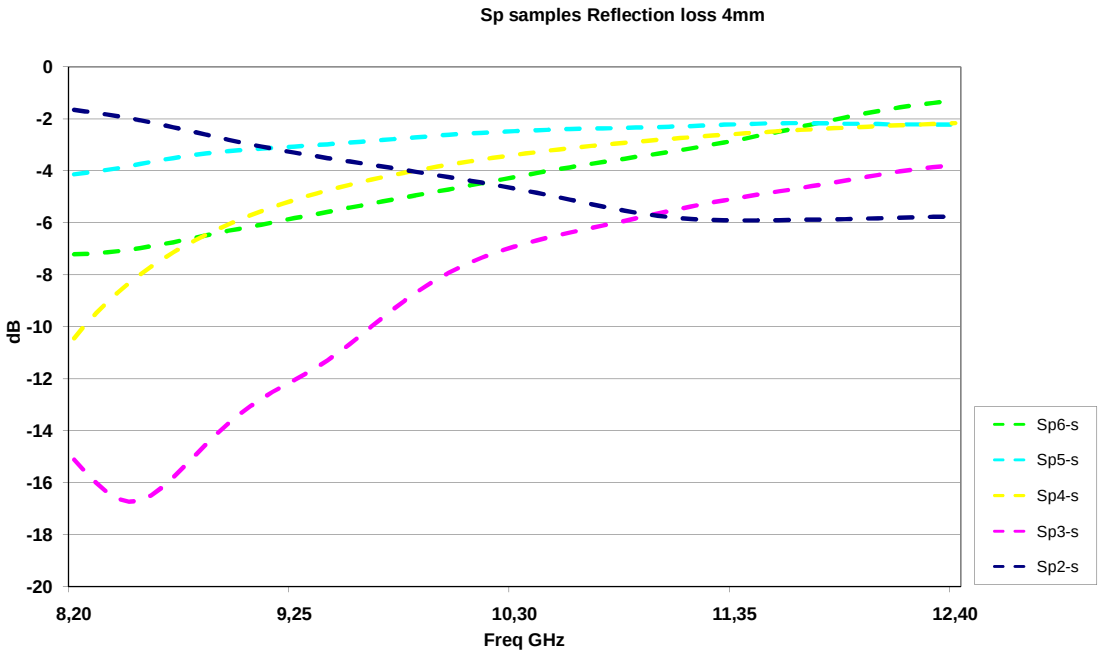


**Fig. 4-7 SP samples reflection loss in X-band 4 mm thickness**

### *4.2.4 Electric interpretation of the conducting path morphologies and comparison on same filler basis*

The author believes that the dielectric behaviour found in the produced materials can be interpreted using the equivalent circuit analogy. As noted above, both CB fillers produce meandering clusters inside the matrix, that can be seen as parallel cylinders capacitor (Fig. 4-8). This capacitance in this case follows the law

$$C = \varepsilon_0 \varepsilon_r \frac{l}{\arccos h\left(\frac{d}{2R}\right)} \quad \text{(eq. 4.1)}$$

Where $l$ is the length and $R$ is the radius of the cylinders, $d$ is the distance between them. Sketching Fig. 4-9 the different systems of cylinder capacitors formed inside the polymer matrix by the two different fillers, can help to understand the different dielectric behaviour, i.e. Permittivity against frequency, found in the two cases.

XE samples present short, thin clusters closely spaced, while SP specimens produce long, thick, meandering, quite far apart spaced, clusters (Fig. 4-9). The distance *d* and the radius *R* vary in the same way, but, form eq. 4.1, it is possible to assume that the parameter most affecting the capacity is the length of clusters *l*.

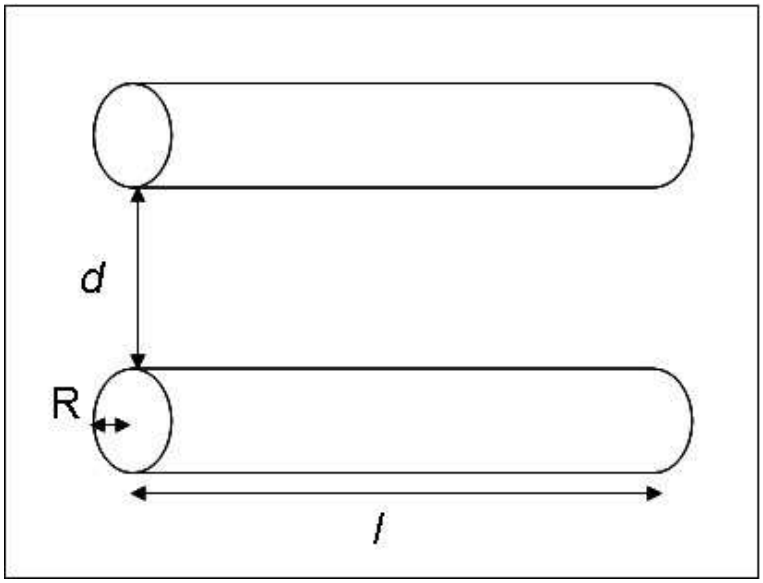


**Fig. 4-8 Sketch of a parallel cylinder capacitor and its characteristic dimensions**

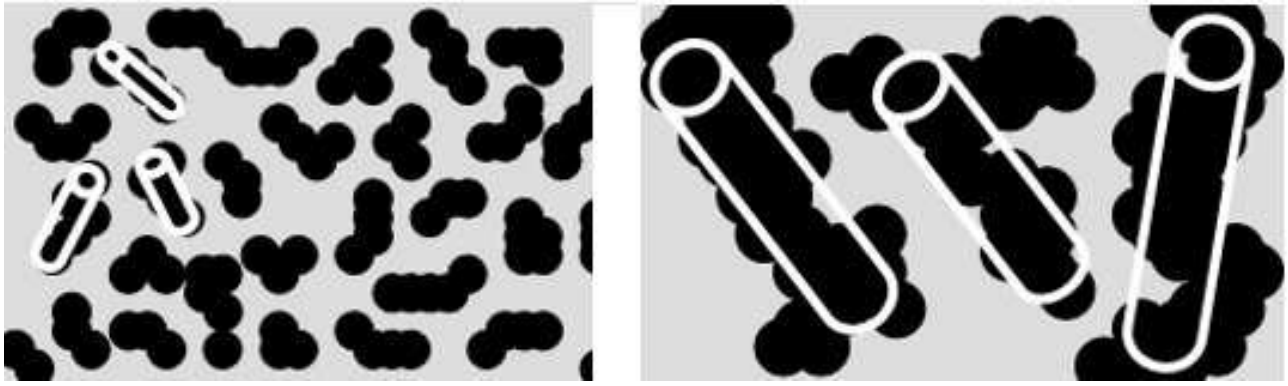

**Fig. 4-9 Sketch of the different conducting patterns created by the filler, overlaid the possible interpretation as parallel cylinders capacitors.**

At same filler amount, XE clusters are smaller and in larger number than SP ones, moreover, when filler quantity is incremented the clusters do not increase in length, but in number, with a less evident effect on the overall capacitance of the composite. SP clusters, instead, have *R* and *l* that work toward increasing the real permittivity, as filler increases clusters get thicker and longer while d remains roughly constant, giving a net contribution to composite capacitance, Table 4-5 allows a rapid comparison between average real permittivity on a same filler percent loading basis.

A comparison among the dielectric properties of the two type of samples is proposed in (Fig. 4-10 and Fig. 4-11). Again, it is here evident that Sp specimen present a more capacitive behaviour, characterized by higher values of ε', while, as far as imaginary permittivity is concerned, XE clusters are more numerous and closer to allow tunnelling and hopping conduction. Thereby, on a same filler basis, its values of ε" are in this case higher than Super-p samples (Table 4-6).

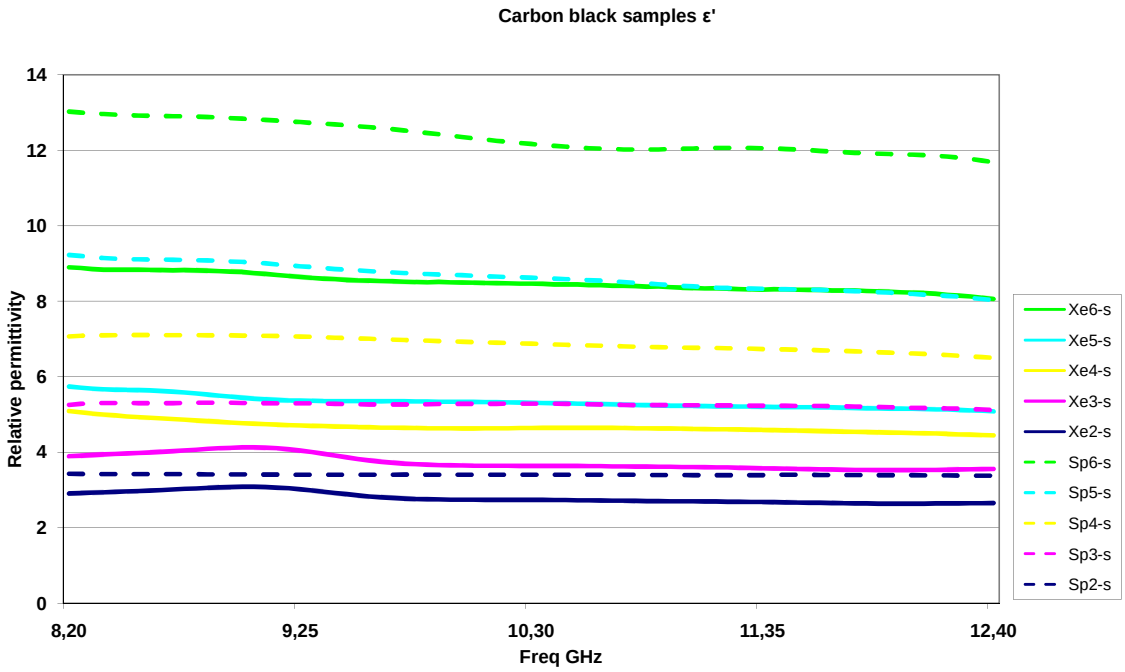


**Fig. 4-10 Comparison between XE and Super-P real permittivity in X-band**

**Table 4-5 Same filler percent load comparison, real permittivity**

| Filler weight % | Xe samples average ε' | SP samples average ε' | SP/Xe variance |
|---|---|---|---|
| 2% | 2,99 | 3,40 | 14 |
| 3% | 3,73 | 5,25 | 41 |
| 4% | 4,67 | 6,87 | 47 |
| 5% | 5,33 | 8,63 | 62 |
| 6% | 8,49 | 12,33 | 45 |

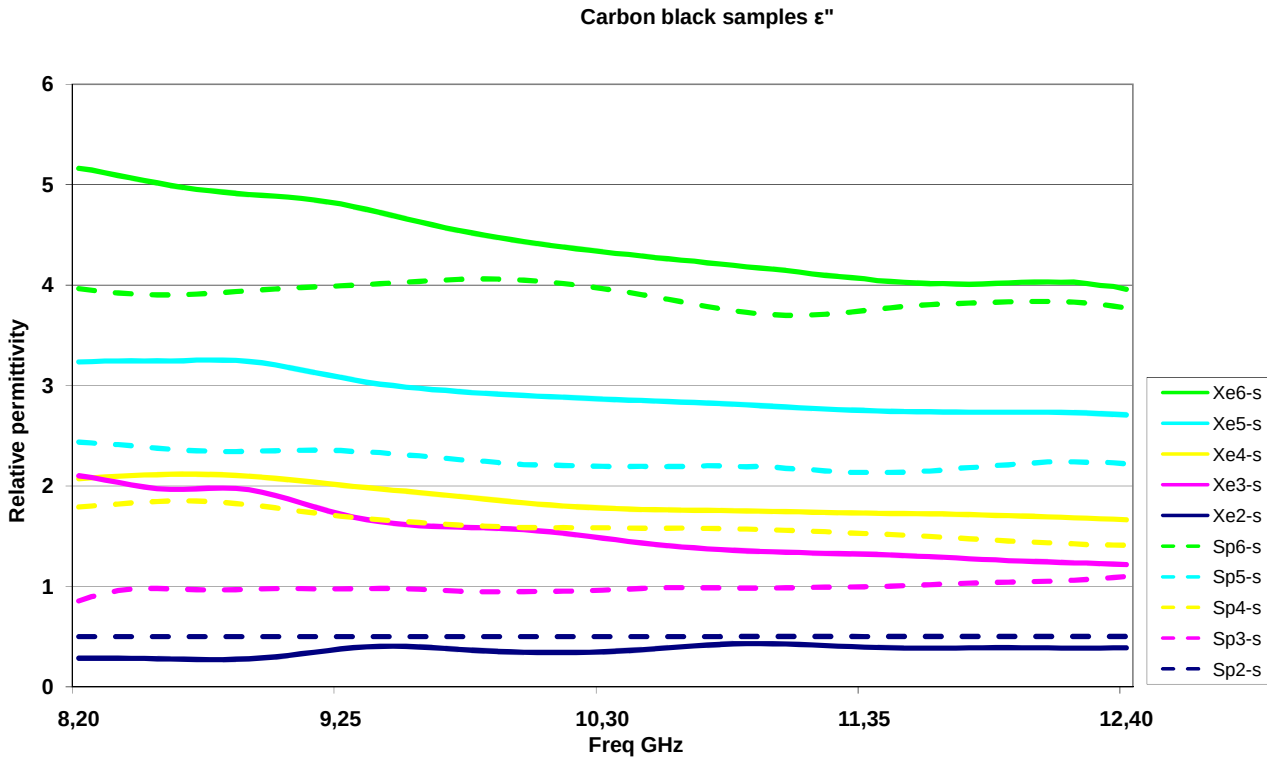


**Fig. 4-11 Comparison between XE and Super-P imaginary permittivity in X-band**

**Table 4-6 Same filler percent load comparison, imaginary permittivity**

| Filler weight % | Xe samples average ε” | SP samples average ε” | SP/Xe variance |
|---|---|---|---|
| 2% | 0,36 | 0,50 | 38 |
| 3% | 1,55 | 0,99 | -36 |
| 4% | 1,86 | 1,61 | -13 |
| 5% | 2,93 | 2,25 | -23 |
| 6% | 4,43 | 3,89 | -12 |

## *4.3 Conclusions*

Samples loaded with CB were produced and tested in X-band using the waveguide method. It was found by SEM analysis that paths of CB clusters are formed in both XE and SP samples, whereas, in the former case, a more fine distribution of smaller and shorter aggregates is achieved. EM measurements show that the microstructures influence the dielectric and EM behaviour of samples, and an explanation was suggested, using the circuit analogy. It was assumed that it is possible to relate the shape of clusters to a parallel cylinders capacitor, that are smaller in the case of XE samples, leading to lower ε’ compared to that shown by sp specimens. At the same time, in the case

of XE nanofiller, the more close spaced clusters create more possibility of hopping and tunnelling conduction, causing higher ε". Absorbing performances of these composites are very good at 4 mm of thickness, achieving a remarkable -38 db peak at 8,5 GHz in the case of XE4-s.

## *4.4 References*


[1] Balberg I. A comprehensive picture of the electrical phenomena in carbon black-polymer composites. Carbon. 2002;40(2):139-43.

[2] Brosseau C, Boulic F, Queffelec P, Bourbigot C, Le Mest Y, Loaeca J, et al. Dielectric and microstructure properties of polymer carbon black composites. Journal of Applied Physics. 1997;81(2):882-91.

[3] Huang J-C. Carbon black filled conducting polymers and polymer blends. Advances in Polymer Technology. 2002;21(4):299-313.

[4] Schueler R, Petermann J, Schulte K, Wentzel H-P. Agglomeration and electrical percolation behavior of carbon black dispersed in epoxy resin. Journal of Applied Polymer Science. 1997;63(13):1741-6.

[5] Chung KT, Reisner JH, Campbell ER. Charging phenomena in the scanning electron microscopy of conductor-insulator composites: a tool for composite structural analysis. Journal of Applied Physics. 1983;54(11):6099-112.

[6] Nanni F, Ruscito G, Travaglia P, Madau F, Gusmano G. Self-diagnosis composite material properties for civil application. In: Society PP, editor. PPS 24; 2008; Salerno; 2008

# 5 Carbon nanofibers samples

This chapter deals with the production and testing of carbon nanofibres as filler of epoxy resin. EM and microstructural characterization were carried out in order to link the dielectric properties to the found microstructures.

## *5.1 Experimental*

### *5.1.1 Pyrograf PR-19-XT-HHT*

CNF used in the experimentation are produced by Pyrograf products inc. using the chemical vapour deposition method (CVD). They present a herringbone arrangement of the graphene planes and, due to their morphology, are thicker than CNT. They are subjected to a post-production thermal treatment to 3000 °C, to produce a complete graphitic structure, that imparts better conducting properties [1]. Catalyst residues (iron) are present in very small quantity. Table 5-1 sums the relevant properties as reported in the relevant datasheet (http://www.apsci.com/ppi-pyro3.html).

**Table 5-1 Pyrograf PR-19-XT-HHT**

| | |
|---|---|
| Fibre diameter | 100-200 nm |
| Fibre length | 30-100 µm |
| Specific surface area | 15-25 $m^2/g$ |
| Dispersive surface energy | 265-285 $MJ/m^2$ |
| Iron | <100 ppm |

### *5.1.2 Sample production methods*

CNF as delivered appear as tightly packed bundles of various sizes, as can be observed by SEM (Fig. 5-1). To exploit the properties of CNF, especially their aspect ratio, the first step is to "disassemble" these bundles into the component fibres. There are several ways suggested to achieve this goal, nevertheless after reviewing the literature [2], it was decided to employ sonication in a liquid, since this method was reported to accomplishes very good dispersion of filler inside the matrix, so to reach percolation at the lowest filler content [3, 4]. During the experimentation, it was found that direct sonication in the resin or in the hardener is ineffective, because the volume of resin or harderner was too low to allow the fibres to separate from the bundles. Several solvents were then tried, among them acetone and ether, but acetone hinders polymerization and ether has such a low boiling point that is difficult to block its evaporation while the dispersion is sonicated. Finally it

was decided to use two different solvent in manufacturing the samples Butil-Glycidyl-Ether (BGE) and chloroform. The ratio of CNF to solvent used in all the following method was kept constant to

$$\frac{CNF}{Solvent} = 0{,}007\ \frac{g}{ml} \quad \text{(eq. 5.1)}$$

#### *5.1.2.1 BGE solvent method*

After reviewing literature it was decided to try BGE as a solvent, due to its very good compatibility with epoxy resin [5], and its boiling point temperature is high enough to allow sonication at room temperature without the need to control solution temperature. After 1 hour sonication in Elna C 30 sonicator bath, the dispersion is placed on a magnetic stirrer at 100 RPM until BGE completed evaporation at room temperature. Determination of complete evaporation of solvent was done by weighting the dispersion. Samples produced with this method range from 1%w to 4%w loading of CNF.

#### *5.1.2.2 Coprecipitation method*

A different way to achieve a good dispersion of CNF inside the resin after disagglomeration is to take advantage of the insolubility between chloroform and methanol [6, 7]. In this case the procedure used in the same, till sonication, as that reported in §5.1.2.1, with the difference that the solvent used is chloroform. After one hour of room temperature stirring at 100 RPM, the temperature of the dispersion is increased to 50°C and methanol is added. Chloroform and methanol are insoluble, therefore adding the latter to the solution causes the precipitation of resin and CNF. Chloroform and methanol are much more volatile than BGE and the complete evaporation of both is achieved in a matter of hours instead of days.

Samples with a weight percent of 1; 2; 3; 4%w CNF were produced using this method. The 4%w sample, however, did not polymerize completely and it is then not included in the results and discussion paragraph.

#### *5.1.2.3 Filtration method*

An even quicker way to separate the solvent from the disaggregated fibre (suggested by Ing. Valentini in his master thesis) is filtration of the colloidal dispersion of BGE and CNF using laboratory filter paper. It was expected a lower efficiency in the final filler dispersion in the cured composite, nevertheless, this way was tried thinking to possible future industrial exploitations. As done with the other two methods, CNF and BGE were sonicated for one hour, then the dispersion

was filtered, the CNF were left on the filter for about 30 minutes. CNF were then scraped from filter paper and added to the resin to stir for 30, to improve filler distribution uniformity in the resin. Samples with the same weight percents of the Chloroform method were produced. Table 5-2 summarises all the samples produced and the suffixes used to distinguish the various methods used.

**Table 5-2 Summary of samples produced**

| Suffix | Method of production used | Sample produced (%w of filler) | Name example |
|---|---|---|---|
| P | BGE | 1; 2; 3; 4 | NF1-SP |
| CL | Chloroform | 1; 2; 3; 4 | NF1-SCL |
| F | Filtration | 1; 2; 3; 4 | NF1-SF |

### *5.1.3 Characterization*

The different disagglomeration methods were evaluated by FEG-SEM. Droplets of the dispersions after the sonication were deposited on SEM stubs, then after complete evaporation of the solvent and gold sputtering, SEM micrographs were taken and compared to the CNF micrographs shot before the sonication. Dispersion of the filler inside the cured resin was evaluated by charging phenomena on highly polished samples following what reported in [8]. EM measurements were carried out as reported in §2.3.2

## *5.2 Results and discussion*

### *5.2.1 CNF Disagglomeration*

As delivered CNF fibres are assembled in tightly wound ball-like fibres agglomerates (Fig. 5-1), negating one of their most important feature, aspect ratio.

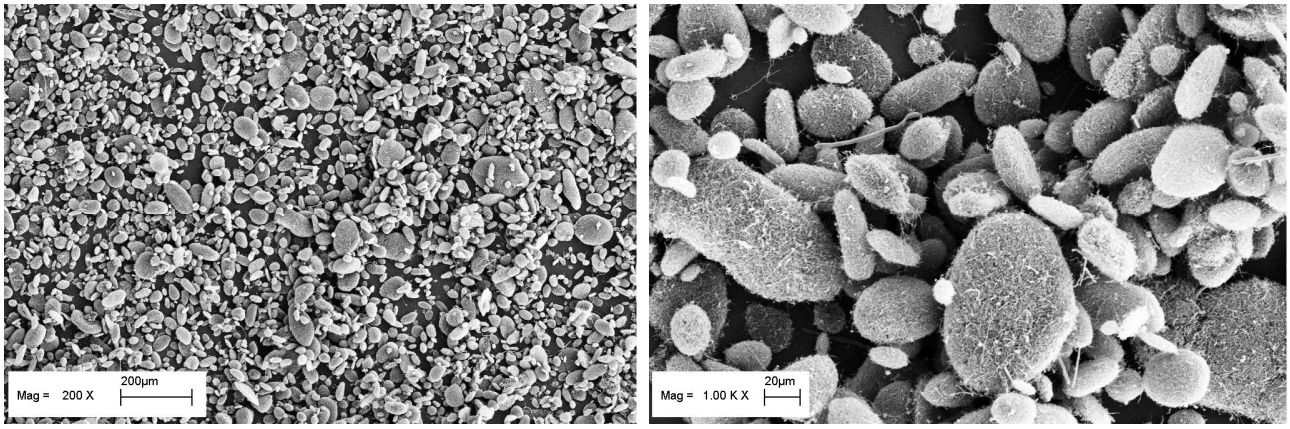


**Fig. 5-1 Pyrograf III as delivered**

It is then central to disentangle these agglomerates into the component fibres since their value is the possibility of creating a conductive path inside the matrix using less filler.

#### *5.2.1.1 Dispersion in BGE*

The result of one 1 hour of sonication in BGE as described in §5.1.2.1 and §5.1.2.3 is shown in Fig. 5-2. Average size of the agglomerated bundles is now 30 µm compared to the 70 µm of untreated CNF. A tight web of fibres now connects the remaining agglomerates and no single fibres are present.

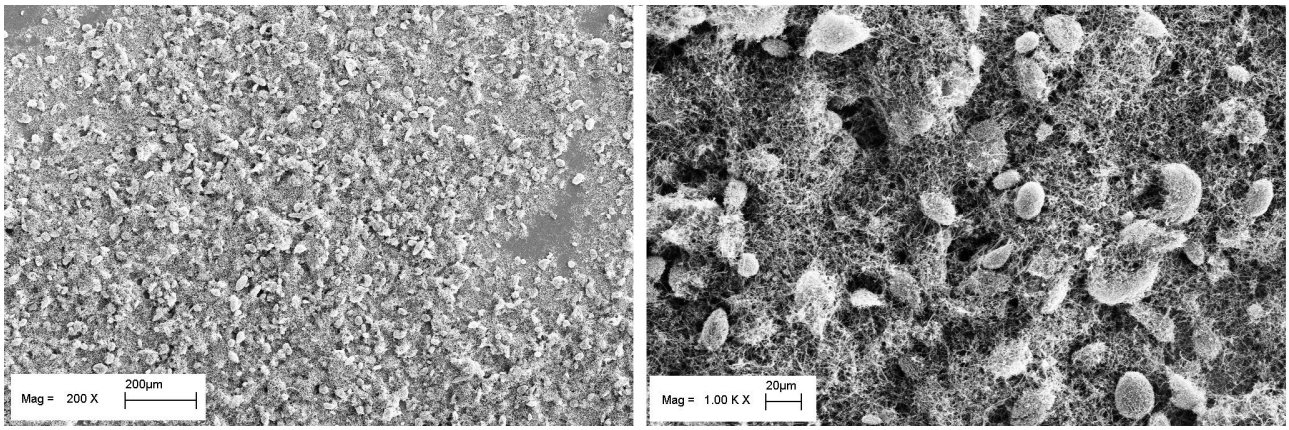


**Fig. 5-2 Pyrograf III after 1 hour sonication**

Tests were made to check if a longer sonication time would produce better results, therefore using the same ratio of solvent to CNF, samples were sonicated for 2 and 3 hours (Fig. 5-3). After 2 or 3 hours the samples did present only little improvements, being present the same morphology of a tight mesh of fibres with few bundles. It is then clear that the sonicator bath used in the dispersion process is not powerful enough to disrupt and disagglomerate properly all bundles. The resulting fibres, even if they more disentangled than the “as delivered”, do not present complete

disagglomeration and CNF aspect ratio won't be, therefore, fully exploited. As a way to balance processing time and performance, sonication of CNF was standardized at 1 hour.

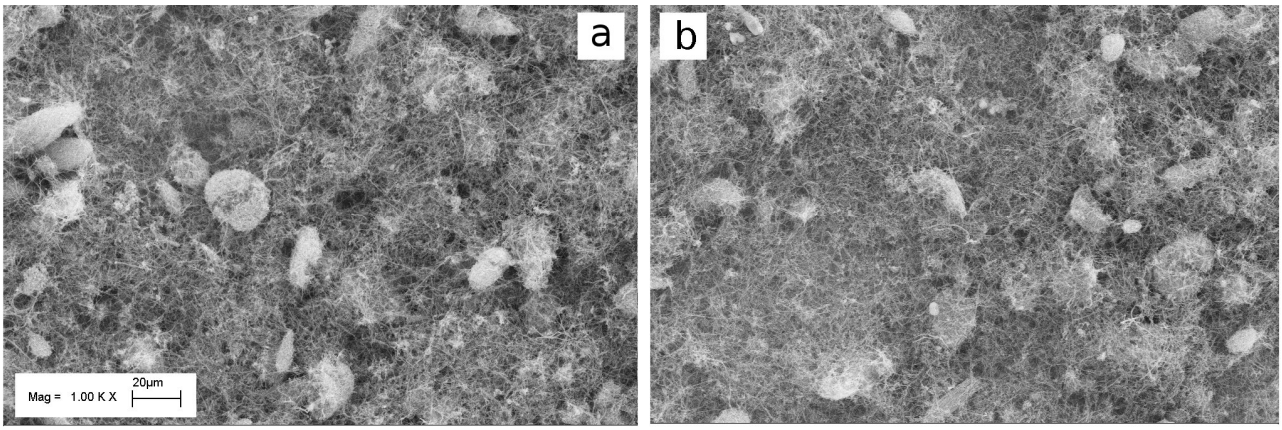


**Fig. 5-3 Pyrograf III after 2 hours sonication (a) and 3hours (b).**

#### *5.2.1.2 Dispersion in chloroform*

Samples produced using the method outlined in §5.1.2.2 had CNF sonicated using chloroform instead of BGE as a solvent. It is possible to see in Fig. 5-4 that samples have the same general morphology but the aggregates are bigger than in the previous case.

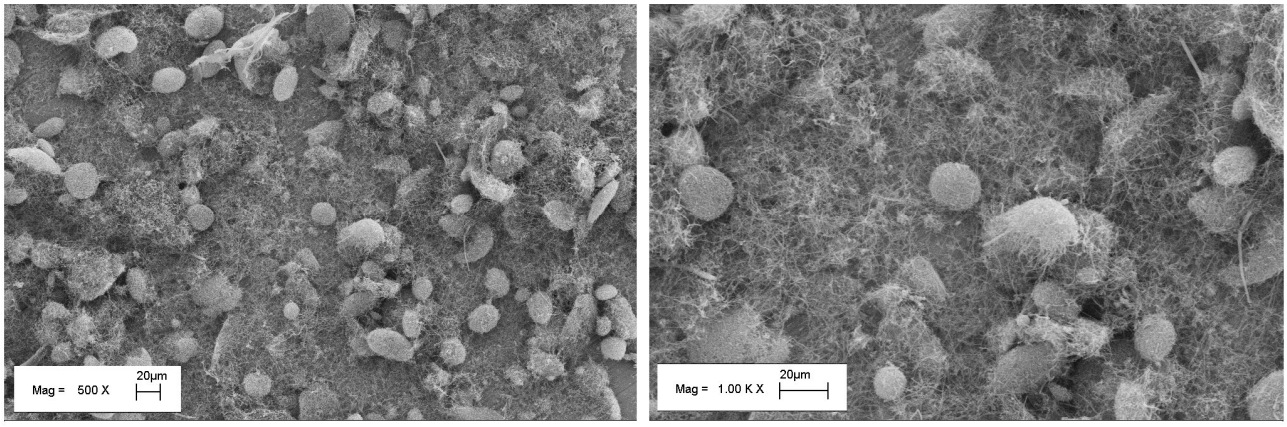


**Fig. 5-4 Pyroraf III after 1 hour sonication in chloroform.**

### *5.2.2 Dispersion in resin and dielectric properties*

Despite the differences in solvent dispersion, CNF processed with all three methods were successively added to the resin to obtain cured epoxy nanocomposites. In this paragraphs the EM performance as well as the microstructure of all CNF manufactured samples are reported and discussed.

#### *5.2.2.1 Nanocomposites produced via BGE method*

Samples produced with this method present a sufficient dispersion of fibres in the matrix, but some bigger agglomerates are still present (Fig. 5-5).

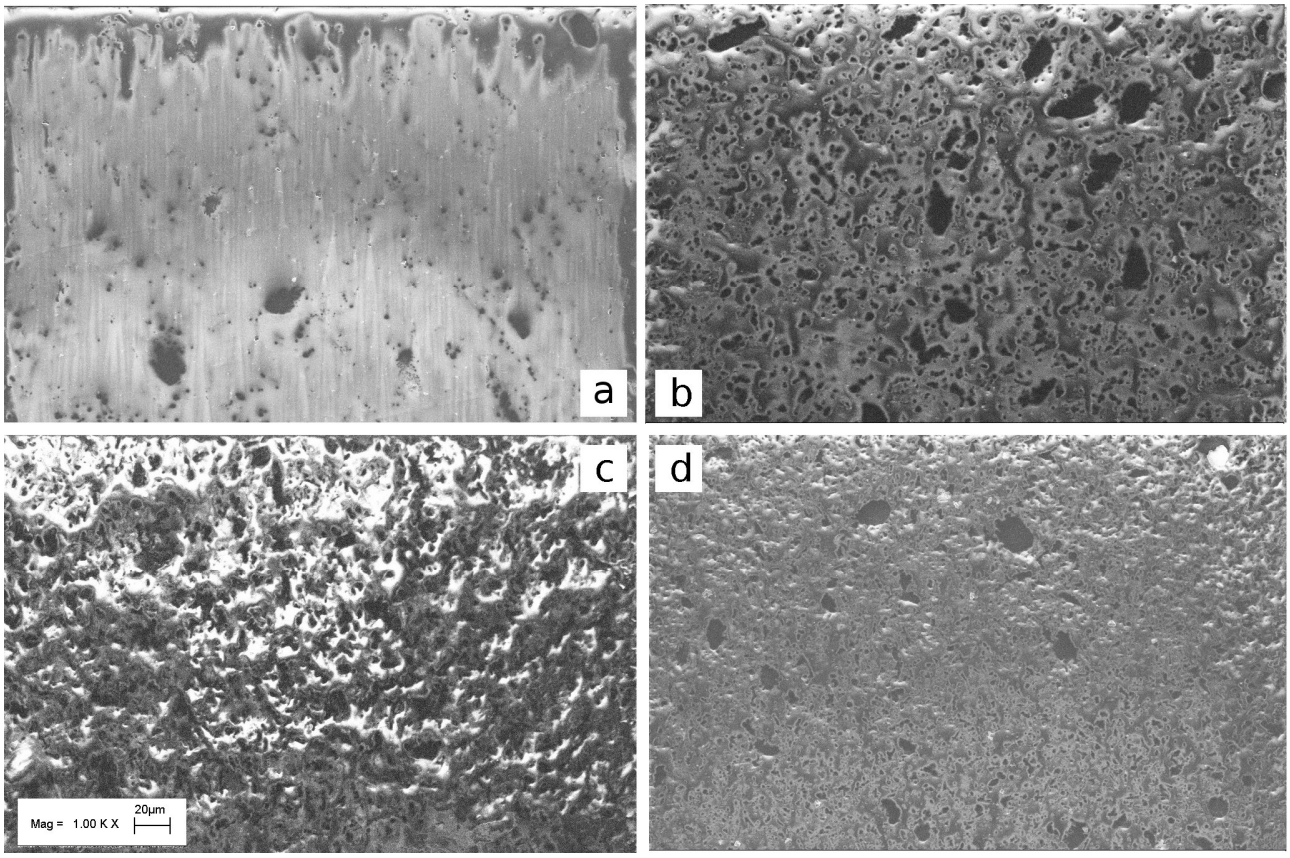


**Fig. 5-5 SEM micrographs of BGE produced samples, 1%w (a); 2%w (b); 3%w (c); 4%w (d)**

The high boiling point of BGE and the constant ratio of solvent to filler means samples produced with this method have different times of stirring: 1 day for 1%w sample to 6 days for the highest loaded sample of 4%w. This leads to a range of different morphologies AND the highest loaded samples present better dispersed filler inside the matrix (Fig. 5-5), in contrast to what is usually achieved when comparing samples produced with same time of processing.

In detail the sample filled with 1 %w of filler has few big agglomerates and so a bad dispersion of filler. NF2-SP and NF3-SP show similar filler patterns made of few and small agglomerates, evenly distributed inside the matrix. Both samples took nearly the same time of stirring before the solvent was completely evaporated. Lastly 4%w filled sample was stirred the longest and therefore, in the SEM micrograph, fibres appear well dispersed with the presence of agglomerates of very small dimensions. From this experience it is possible to conclude that, when using a low power sonicator bath, stirring time becomes an important factor in dispersing the fibres inside the matrix.

The analysis made on the SEM micrographs is reflected in the dielectric behaviour shown in Fig. 5-6 and Fig. 5-7, that report the results of real and imaginary permittivity.

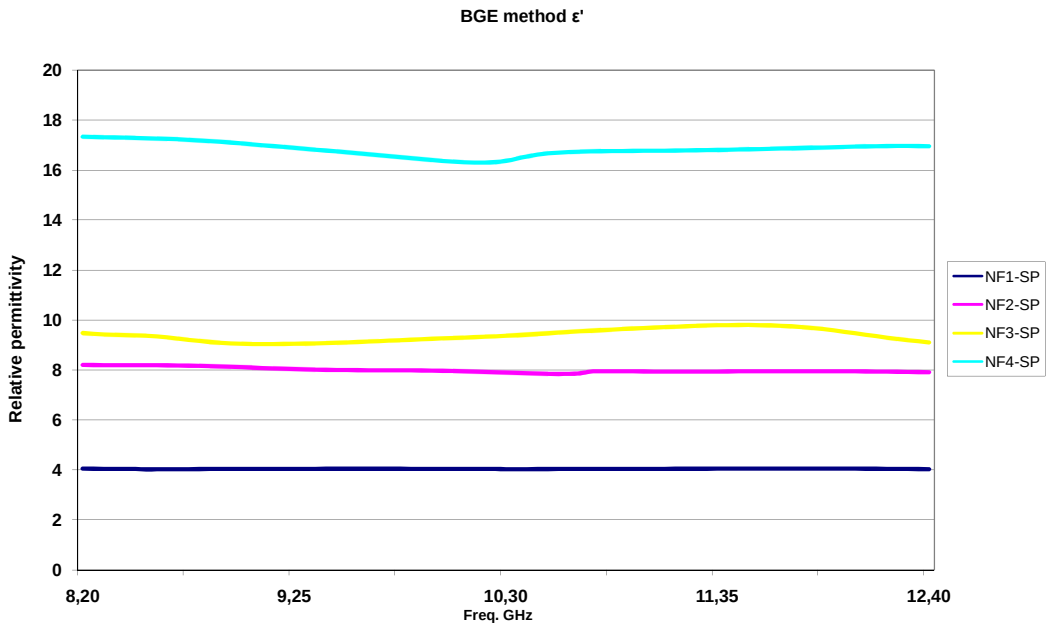


**Fig. 5-6 Real permittivity of samples produced using the BGE method**

The samples show a pattern of small and big agglomerates, being the former prevalent in those cases where a good dispersion was achieved. The aggregate can be seen as conductive regions dispersed in an insulating matrix and the prevalent effect is the resulting interfacial polarization. In this case what matters is the total surface area of the agglomerates, that polarize and, therefore, smaller more numerous agglomerates offer more polarisable surface area, resulting in a higher value of the real part of permittivity, on equal filler content. Imaginary part of permittivity is affected by both filler quantity and dispersion. The former aspect is due to the merely increase of the quantity of conductive particles (cfr. eq. 2.5), while the effect of dispersion is related to the fact that a larger number of smaller and well dispersed aggregates lead more easily to conductivity, by means of tunneling/hopping effects.

Table 5-3 sums the percent increases in real and imaginary permittivity compared to the increase in filler content as described in §1.3, NF1-SP's filler content is low and coupled to the fact that it is niot well dispersed gives low values of ε' and ε". Disappointingly ε' and ε" don't follow mixture laws but it is still possible to get some information, comparing the increase of filler against the increase of permittivity. Compared to NF1-SP, NF2-SP shows a better dispersion and higher values of ε' and ε". On the other hand NF3-SP show a very limited increase in permittivity from NF2-SP, even if the filler increases from 2 to 3%w (50% in relative terms) ε' increases just 17%, it is then possible to say that the dispersion achieved doesn't exploit the increased filler content, and

highlights the influence of stirring time on the resulting dispersion and, as a consequence, on the sample dielectric performance. 4% loaded sample filler is much better dispersed and the value of ε' and ε" have increments of 79 and 252% compared to NF3-SP in contrast filler weight increases just 33% (Table 5-3).

**Table 5-3 Percent increases in filler weight load, average real and imaginary samples BGE method**

| Filler weight % | Weight increment | Average ε' | ε' increment | Average ε" | E" increment |
|---|---|---|---|---|---|
| 1% | | 4,05 | | 0,30 | |
| 2% | 100% | 8,00 | 97% | 1,01 | 236% |
| 3% | 50% | 9,40 | 18% | 1,14 | 13% |
| 4% | 33% | 16,84 | 79% | 4,02 | 252% |

The vast increase in permittivity from NF3-SP to NF4-SP is not just caused by a better dispersion and filler increase, but also by a transition from non conductive to semi conducting status of the composite, the conductive network inside the matrix does not yet encompass the whole sample but it is enough to add a significant contribute to the dielectric performances.

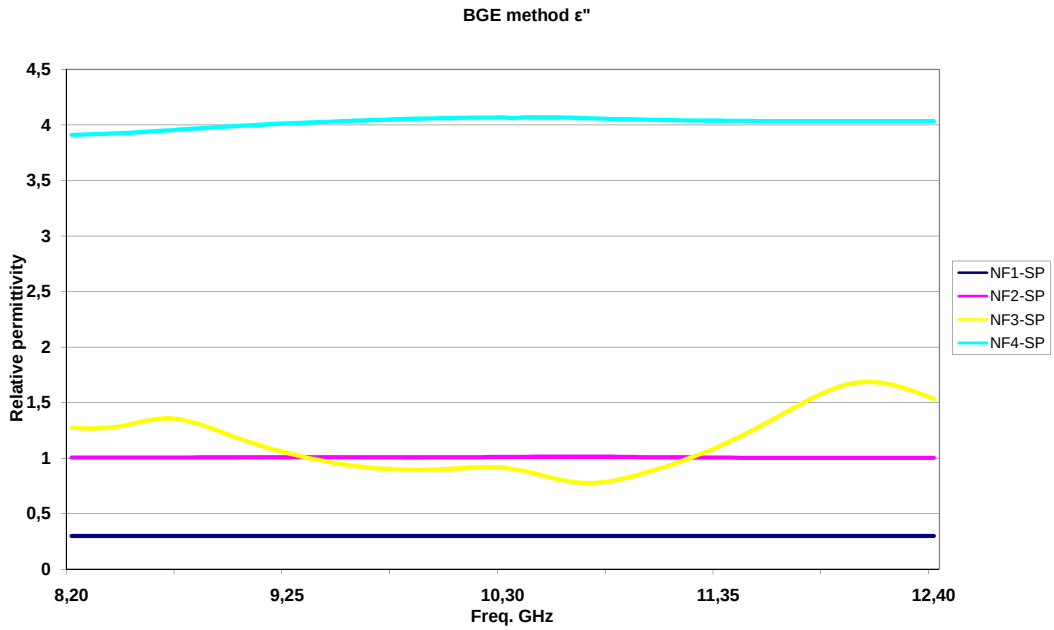


**Fig. 5-7 Imaginary permittivity of samples produced using the BGE method**

#### *5.2.2.2 Nanocomposites produced via the chloroform method*

Samples produced with this method have a quicker and more uniform production time, nevertheless, the large amount of chloroform used in high loaded specimens, to maintain the ratio specified in eq. 5.1, does not permit good polymerization of the matrix. This responsible for the nfact that explains 4%w samples did not cured at all, while 3%w ones only partially cured and the it not possible to trust the resulting ε".

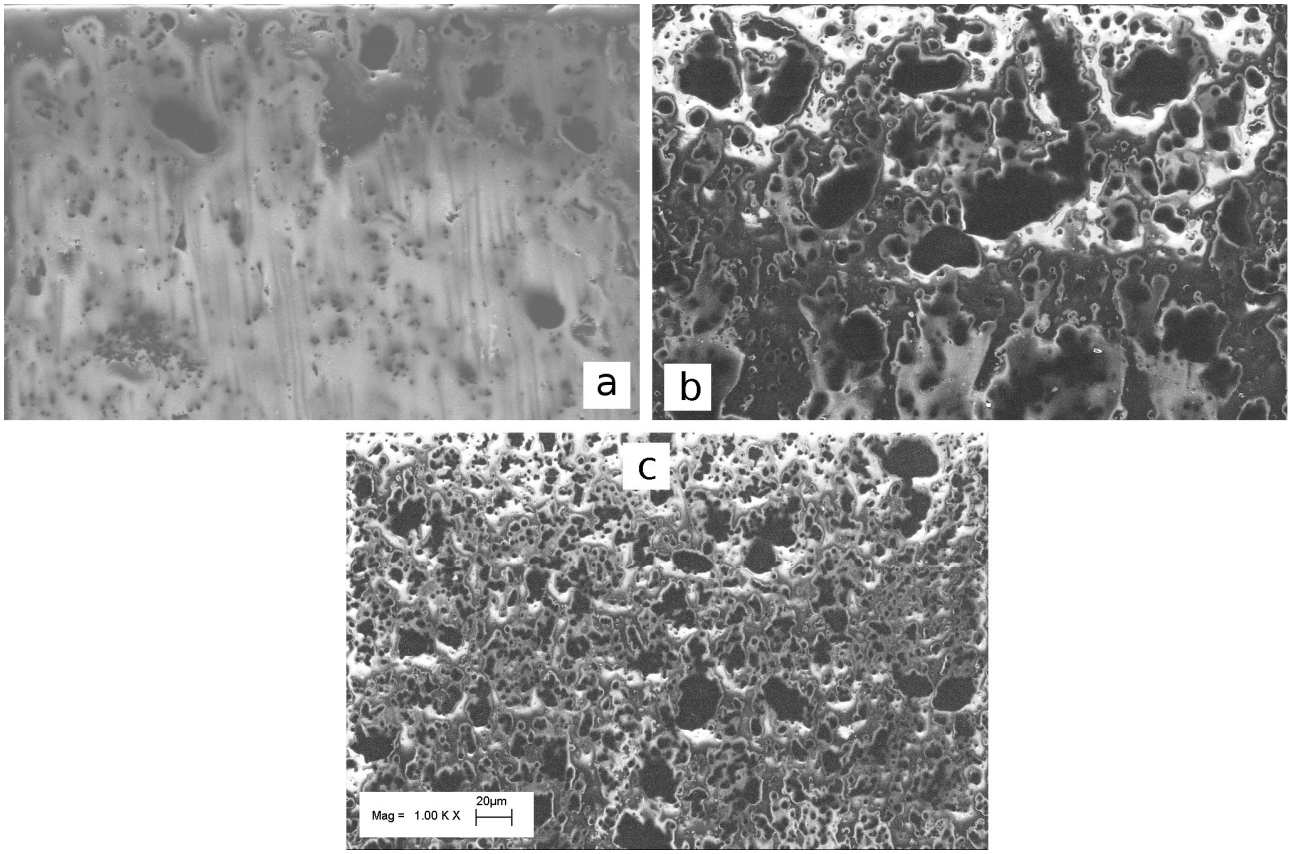


**Fig. 5-8 SEM micrographs of chloroform produced samples; 1%w (a); 2%w (b); 3%w (c)**

In this case the production time, even if not perfectly equal across the range, does not present differences as significant as in the BGE method produced samples.

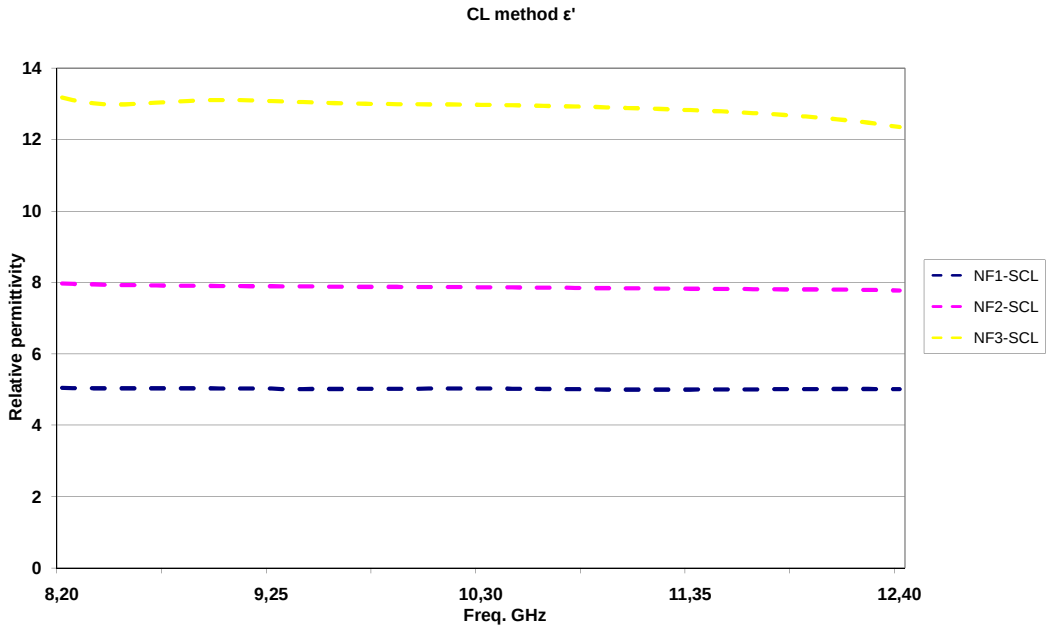


**Fig. 5-9 Real permittivity of samples produced using the chloroform method**

Chloroform samples show a more regular increase in ε' and ε" than BGE samples due to the more uniform manufacturing. The increase of real permittivity from 1%w filled sample to 2%w (100% more filler content) is 57% compared to 97% variation between 1% and 2% BGE samples (Table 5-4).

**Table 5-4 Percent increases in filler weight load, average real and imaginary samples chloroform method**

| Filler weight % | Weight increment | Average ε' | ε' increment | Average ε" | ε" increment |
|---|---|---|---|---|---|
| 1% | | 5,02 | | 0,60 | |
| 2% | 100% | 7,86 | 57% | 1,00 | 67% |

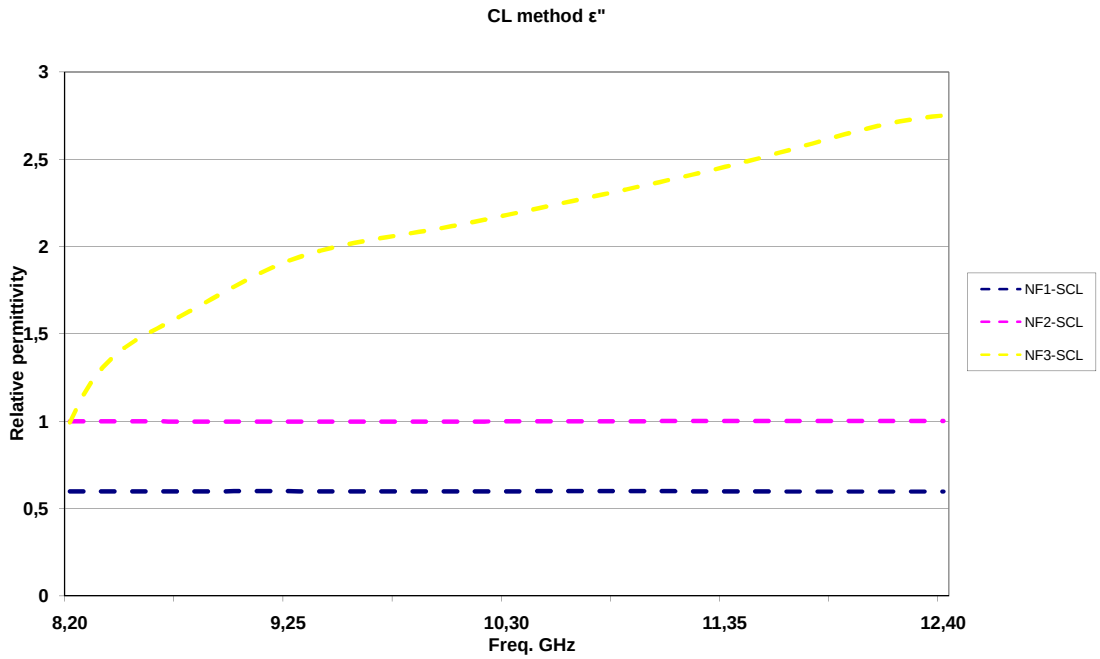


**Fig. 5-10 Imaginary permittivity of samples produced using the chloroform method**

### *5.2.2.3 Filtration method*

Samples produced using this method present some of the worst disagglomerations among all produced samples. As it is possible to notice from the analysis of Fig. 5-11, dispersion patterns in the samples are different The sample loaded with 1%w of filler presents agglomerates of medium dimension uniformly dispersed in the resin, probably the low ratio of filler to resin helps the dispersion and on a lesser level disagglomeration inside the resin. Samples filled with 2 and 3%w show very big agglomerates, in 3%w case of huge size, caused most probably by the compounded effect of scraping the filler from the filter paper and the increasing ratio of filler to resin while stirring. Last, 4%w sample show a very good distribution pattern of small/medium agglomerates evenly dispersed, this marked difference from 2 and 3%w it is probably caused by the operator scraping the filler from the filter paper.

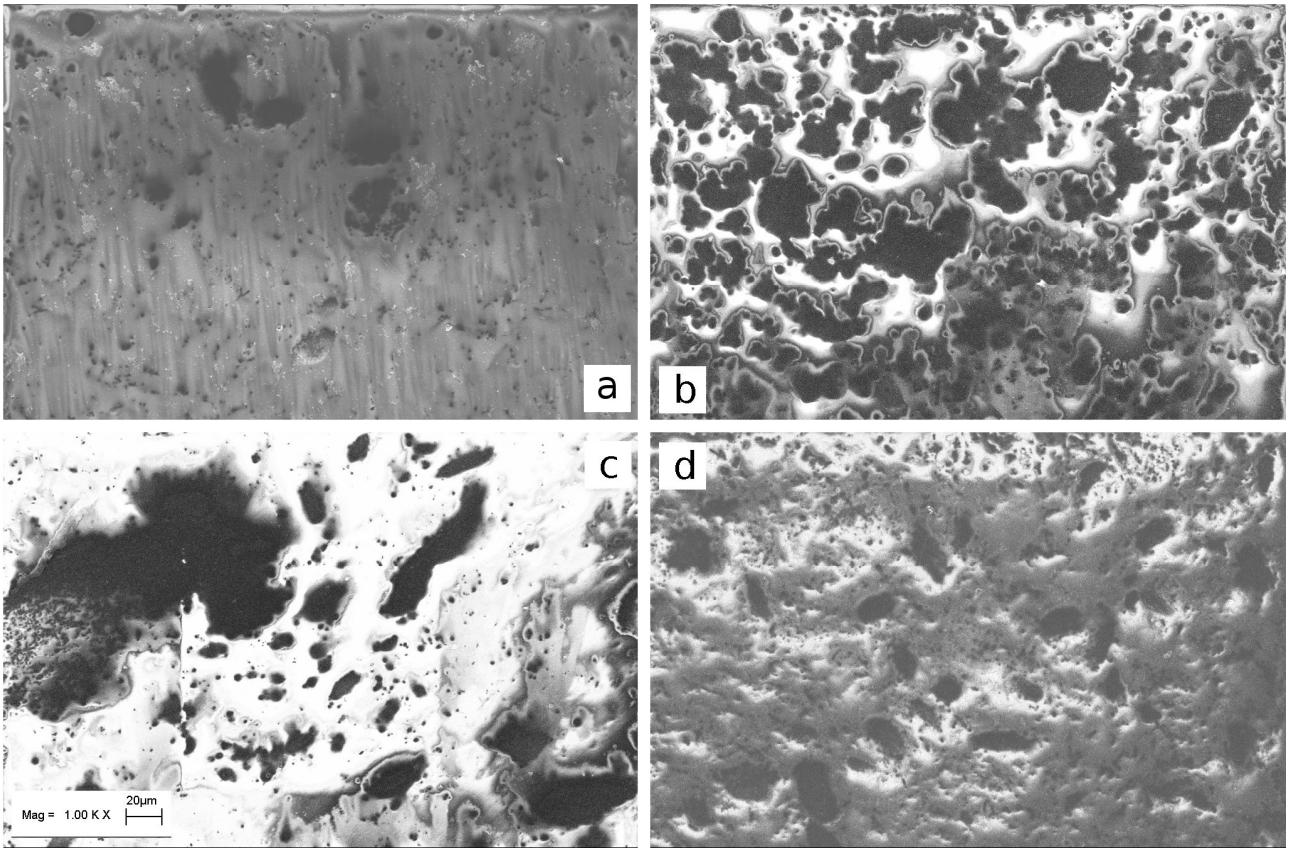


**Fig. 5-11 SEM micrographs of filtration method produced samples; 1%w (a); 2%w (b); 3%w (c); 4%w (d)**

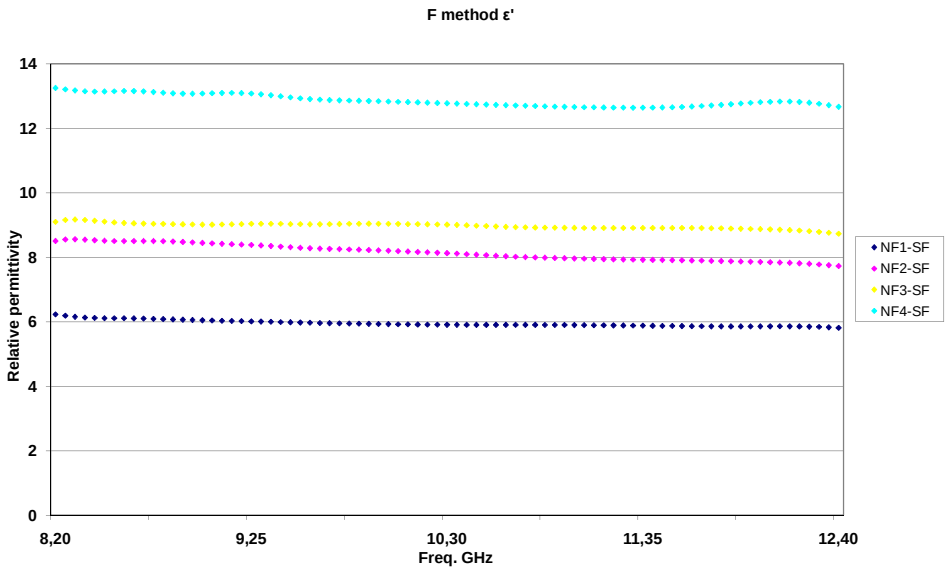


**Fig. 5-12 Real permittivity of samples produced using the filtration method**

As done with the previous two batches of samples, in this section a match between the sample morphology and the dielectric results is attempted (Table 5-5). The different morphology of these samples is reflected in the dielectric measurement. the big agglomerates present across the range of samples produced using the filtration method give the lower increases in ε' and ε" when compared to the samples produced with the other methods. the effect of bad dispersion inside NF3-SF is reflected in the very small increase of 10 and 9% from NF2-SF when ε' and ε" are considered.

**Table 5-5 Filtration method samples percent increase in filler weight load, real and imaginary average permittivity**

| Filler weight % | Weight increment | Average ε' | ε' increment | Average ε" | ε" increment |
|---|---|---|---|---|---|
| 1% | | 5,95 | | 0,65 | |
| 2% | 100% | 8,14 | 37% | 0,96 | 49% |
| 3% | 50% | 8,97 | 10% | 1,05 | 9% |
| 4% | 33% | 12,86 | 43% | 1,82 | 73% |

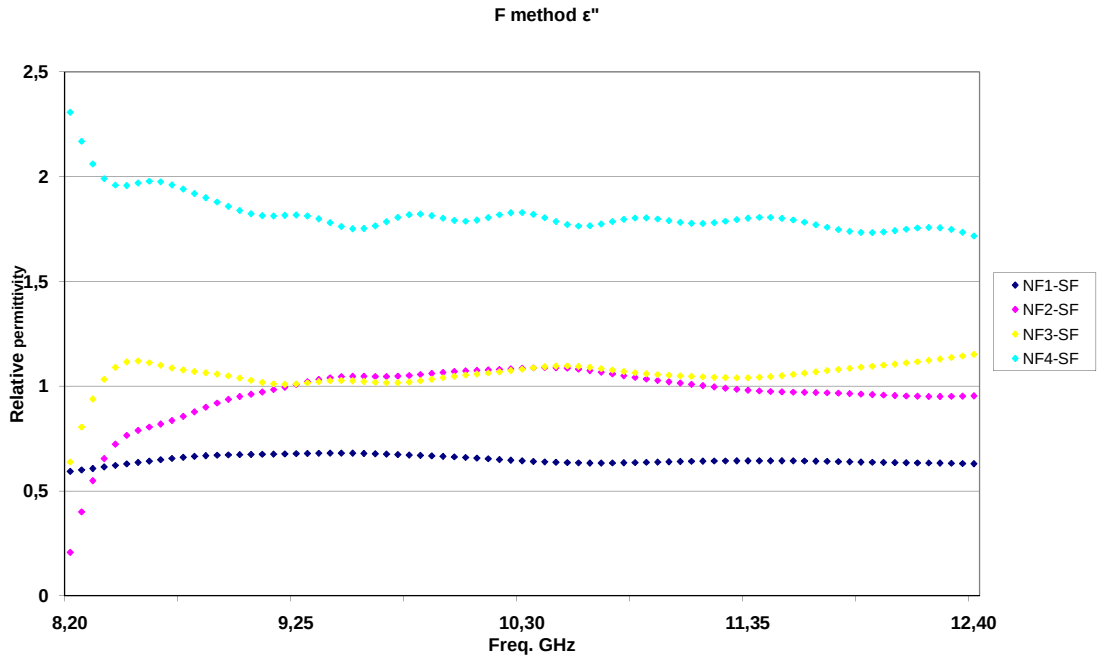


**Fig. 5-13 Imaginary permittivity of samples produced using the Filtration method**

### 5.2.3 *Review of the relationship between microstructure morphology and dielectric properties on the same filler % basis*

Another way to asses the effect of different production methods and relative morphology on the dielectric properties of the resulting composites is to compare ε' and ε" on samples loaded with the same filler percent. Tables  Table 5-6 and Table 5-7 sum up these comparisons in a synthetic way.

**Table 5-6 same filler percent load comparison, real permittivity**

| Filler weight | BGE samples average ε' | CL Samples average ε' | CL/BGE variance | F Samples average ε' | F/BGE variance | F/CL variance |
|---|---|---|---|---|---|---|
| 1% | 4,05 | 5,02 | 24% | 5,95 | 47% | 19% |
| 2% | 8,00 | 7,86 | -2% | 8,14 | 2% | 4% |
| 3% | 9,40 | | | 8,97 | -5% | |
| 4% | 16,84 | | | 12,86 | -24% | |

NF1-SP has the lowest value of all 1%w samples, as described in §5.2.2.1 and shown in Fig. 5-5 its dispersion is not good, NF1-SCL presents a value of ε' 24% and NF1-SF 47% higher, even bigger increments are present when ε" is considered 100% and 116% respectively.

It is possible to explain these big differences analyzing Fig. 5-5, Fig. 5-8 and Fig. 5-11, and noting that in this case there is very few filler involved. The effects of differences in dispersion are then amplified especially when ε" is concerned since conductivity contributes to it.

Samples loaded with 2%w of filler have the same values of ε' and ε" when measurements uncertainties are considered, as is possible to notice from the SEM micrographs cited above they present similar type and quality of dispersion.

**Table 5-7 Same filler load comparison, imaginary permittivity**

| Filler weight | BGE samples average ε" | CL Samples average ε" | CL/BGE variance | F Samples average ε" | F/BGE variance | F/CL variance |
|---|---|---|---|---|---|---|
| 1% | 0,30 | 0,60 | 100% | 0,65 | 116% | 8% |
| 2% | 1,01 | 1,00 | -1% | 0,96 | -4% | -4% |
| 3% | 1,14 | | | 1,05 | -8% | |
| 4% | 4,02 | | | 1,82 | -55% | |

When the filler content is increased the differences between the various methods start to show better. Filtration method samples at 3%w present a coarser dispersion than the NF3-SP, NF3-SF has

a value of ε’ 5% lower than NF3-SP and ε” 8% and lower. The difference is increased in the case of 4%w loaded samples where NF4-SF has a ε’ value 24% lower and ε” 55% lower than the sample with the same filler weight content produced using the BGE method.

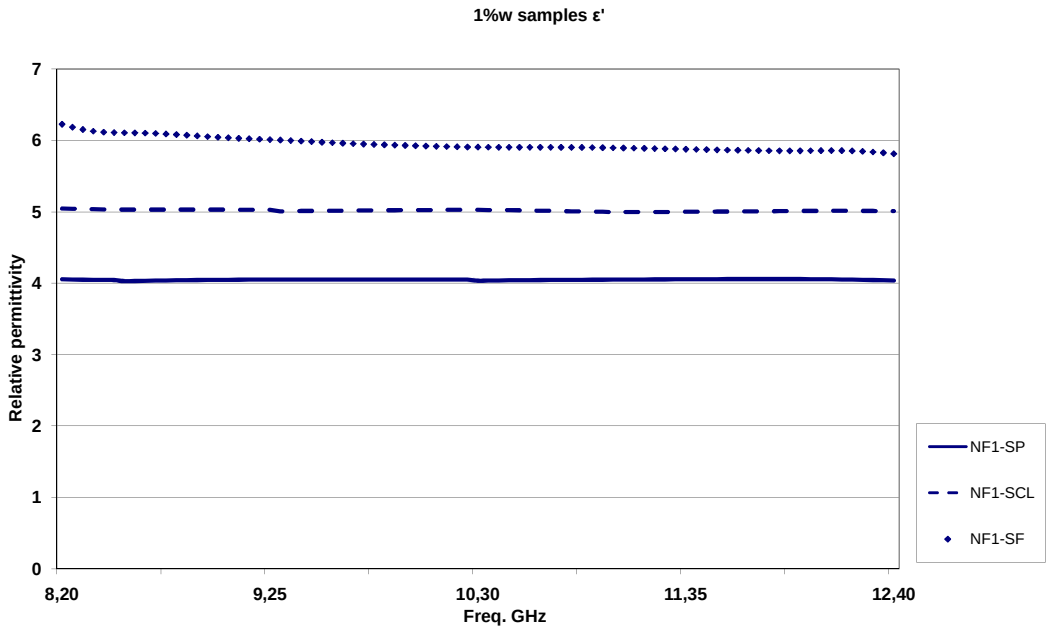


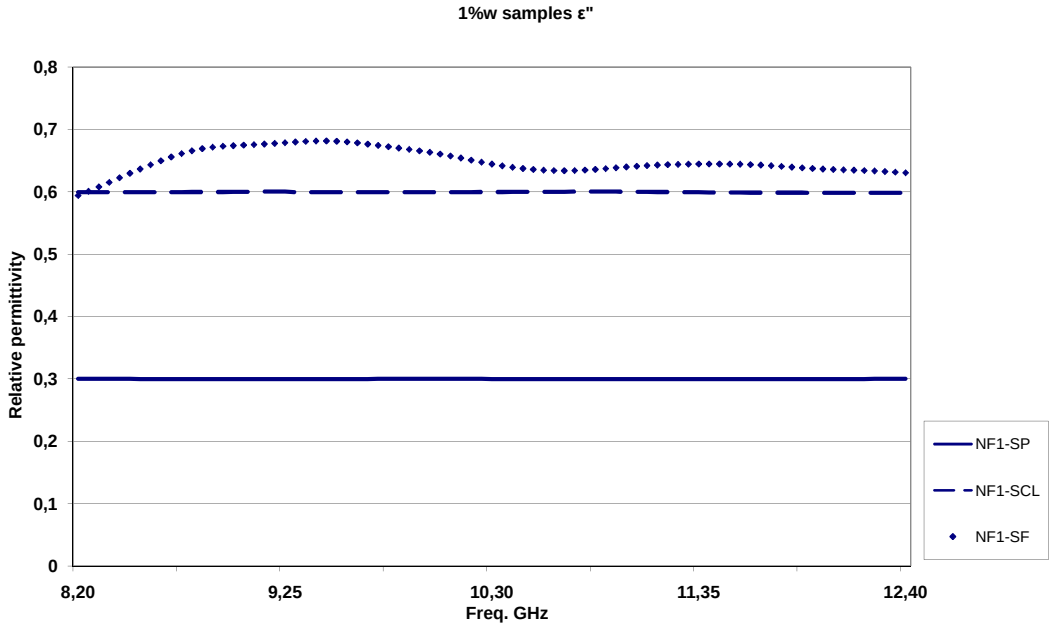

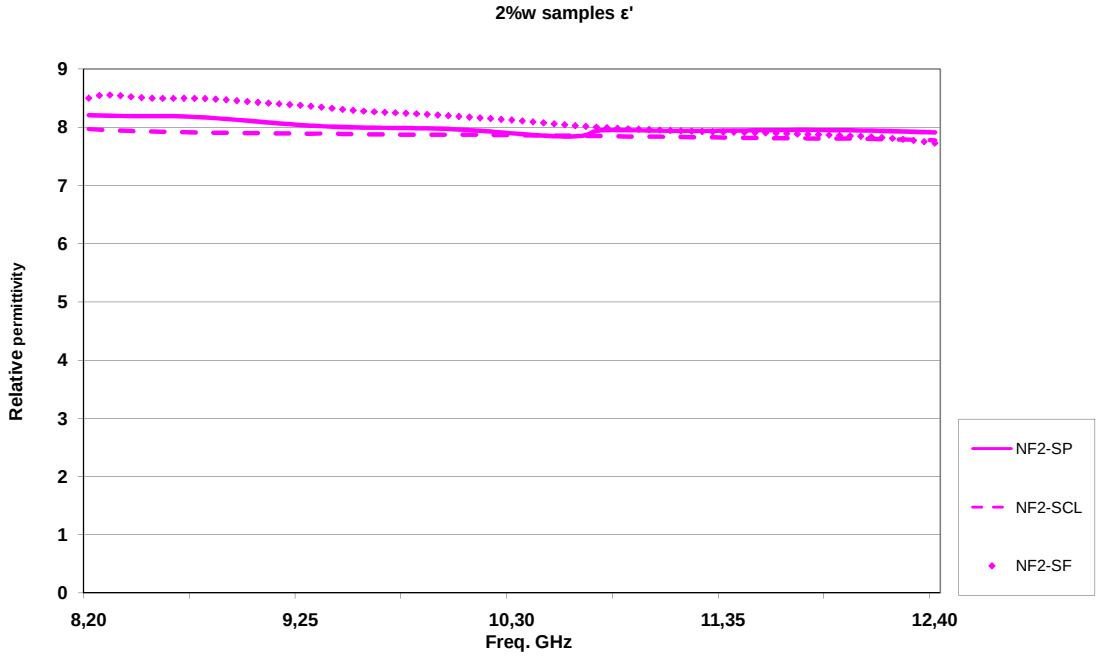
2%w samples ε'
Relative permittivity
9
8
7
6
5
4
3
2
1
0
8,20
9,25
10,30
11,35
12,40
Freq. GHz
NF2-SP
NF2-SCL
NF2-SF

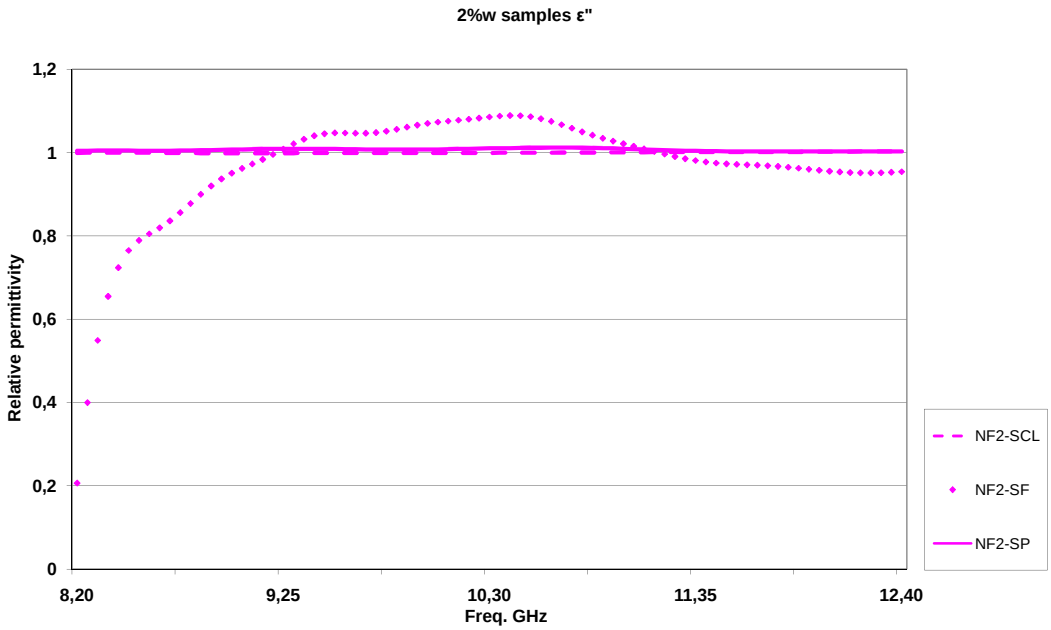
2%w samples ε"
Relative permittivity
1,2
1
0,8
0,6
0,4
0,2
0
8,20
9,25
10,30
11,35
12,40
Freq. GHz
NF2-SCL
NF2-SF
NF2-SP

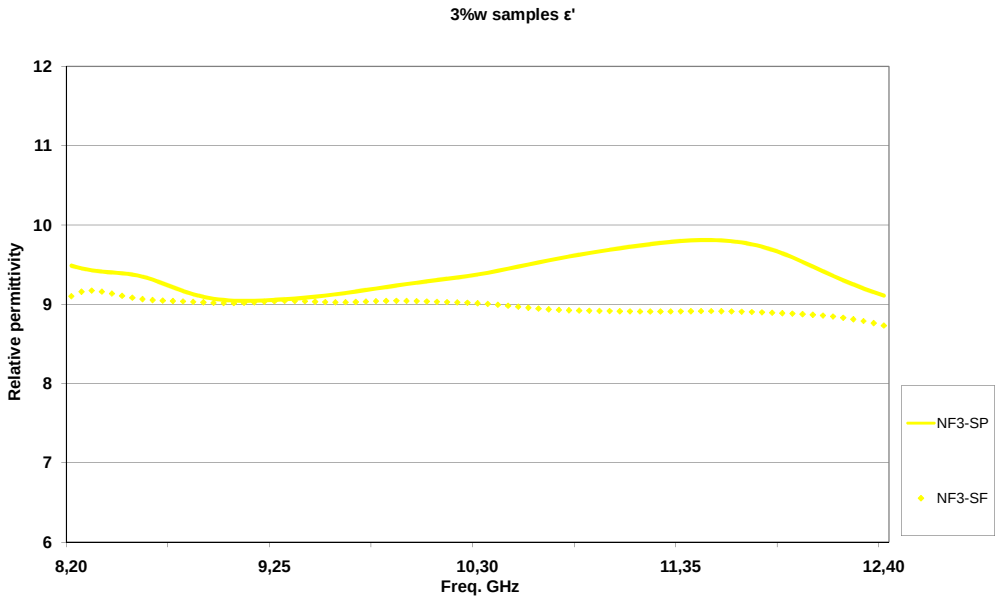
3%w samples ε'
12
11
10
9
8
7
6
Relative permittivity
8,20
9,25
10,30
11,35
12,40
Freq. GHz
NF3-SP
NF3-SF

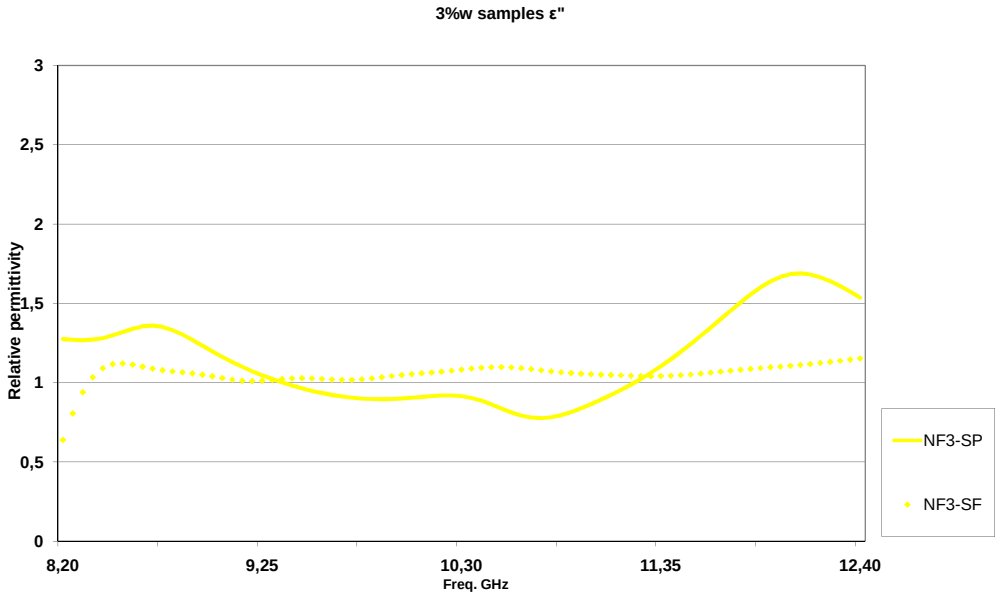
3%w samples ε"
3
2,5
2
1,5
1
0,5
0
Relative permittivity
8,20
9,25
10,30
11,35
12,40
Freq. GHz
NF3-SP
NF3-SF

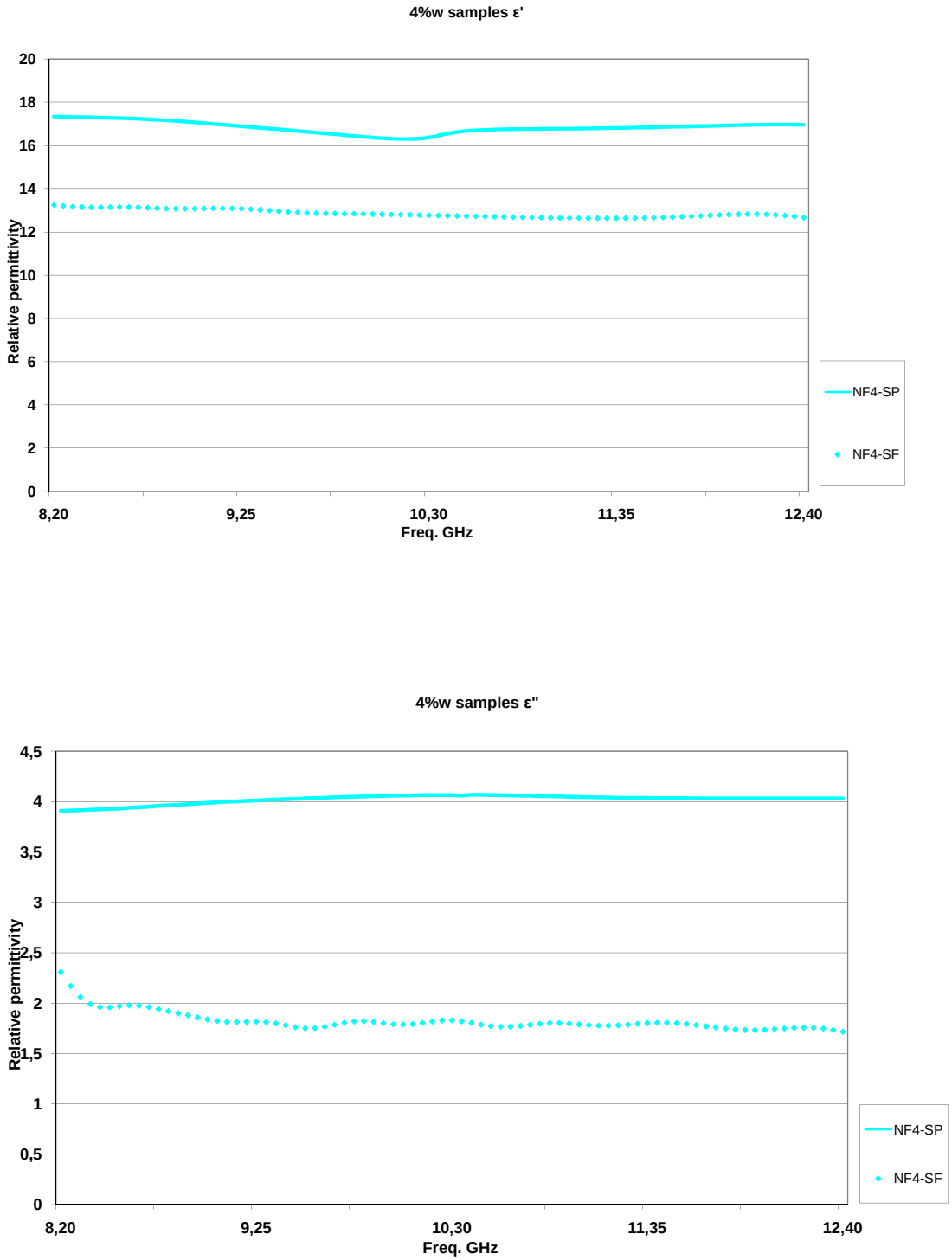


**Fig. 5-14 Same filler loading graphics real and imaginary permittivity.**

Electromagnetic absorbing/shielding performances

Fig. 5-15, Fig. 5-16 and Fig. 5-17 illustrate the absorbing performances Of 4 mm thick specimens, none of which produced present any kind of interesting absorbing performance. As detailed in the introduction, contrary to permittivity, absorbing performance depend on geometrical factors such as thickness. Therefore in order to verify the absorbing performance of the produced materials at differen thicknesses, a simulation, based on the measured dielectric properties, was carried out. The results are summarized in tables Table 5-8 BGE,

Table 5-9 Chlorofom and

Table 5-10 Filtrated, where the possible maximum absorption performance are reported with the respective thickness.

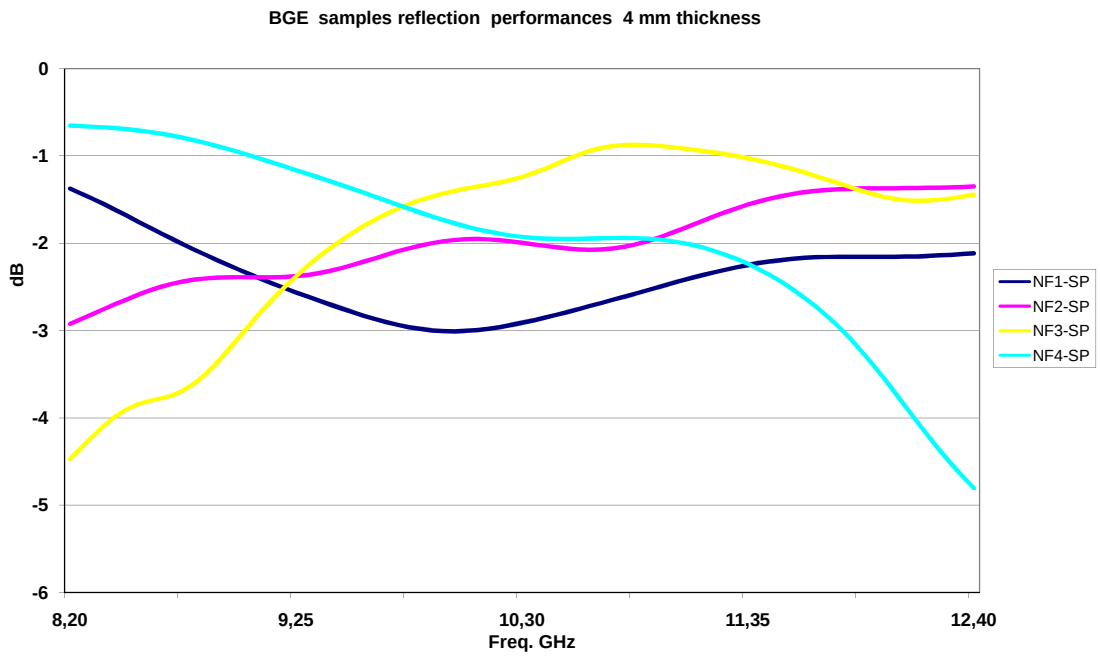


**Fig. 5-15 Reflection loss BGE method produced samples, 4 mm thickness**

**Table 5-8 Peak absorption BGE method produced samples, and thickness it is achieved**

| Sample | Thickness (mm) | Frequency at peak (GHz) | Peak absorption (dB) |
|---|---|---|---|
| NF1-SP | 10 | 11,4 | -6,5 |
| NF2-SP | 10 | 8,2 | -14 |
| NF3-SP | 8 | 10 | -35,5 |

| | | | |
|---|---|---|---|
| NF4-SP | 2 | 9,2 | -18 |

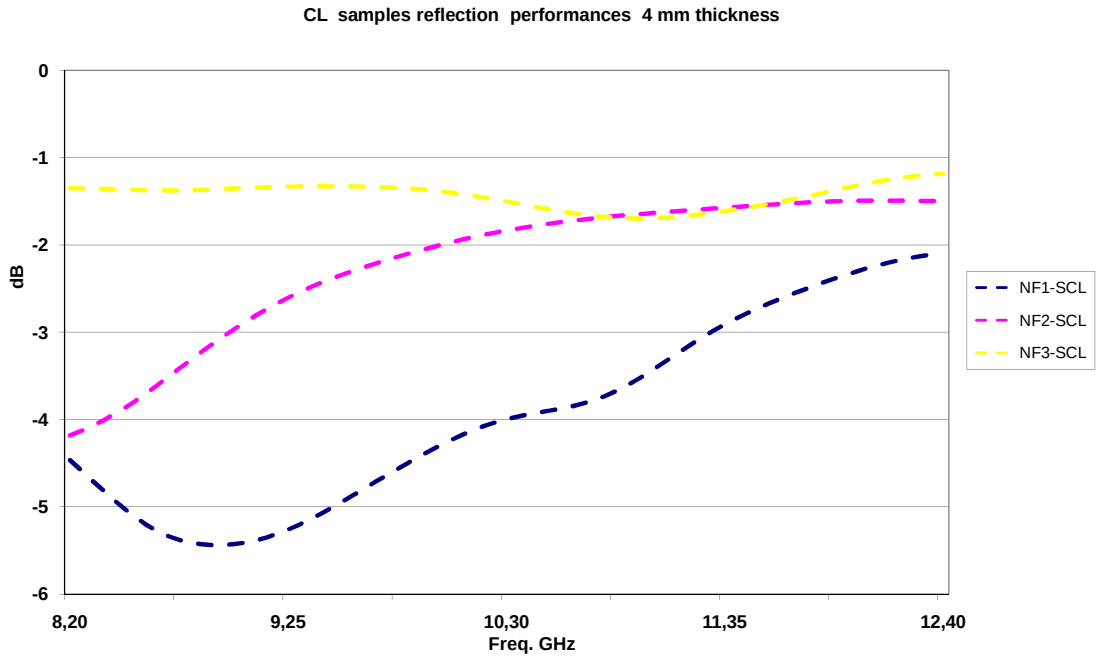


**Fig. 5-16 Reflection loss chloroform method produced samples, 4 mm thickness**

**Table 5-9 Peak absorption chloroform method produced samples, and thickness it is achieved**

| Sample | Thickness (mm) | Frequency at peak (GHz) | Peak absorption (dB) |
|---|---|---|---|
| NF1-SCL | 9 | 11,3 | -12,7 |
| NF2-SCL | 6 | 11,4 | -19,9 |

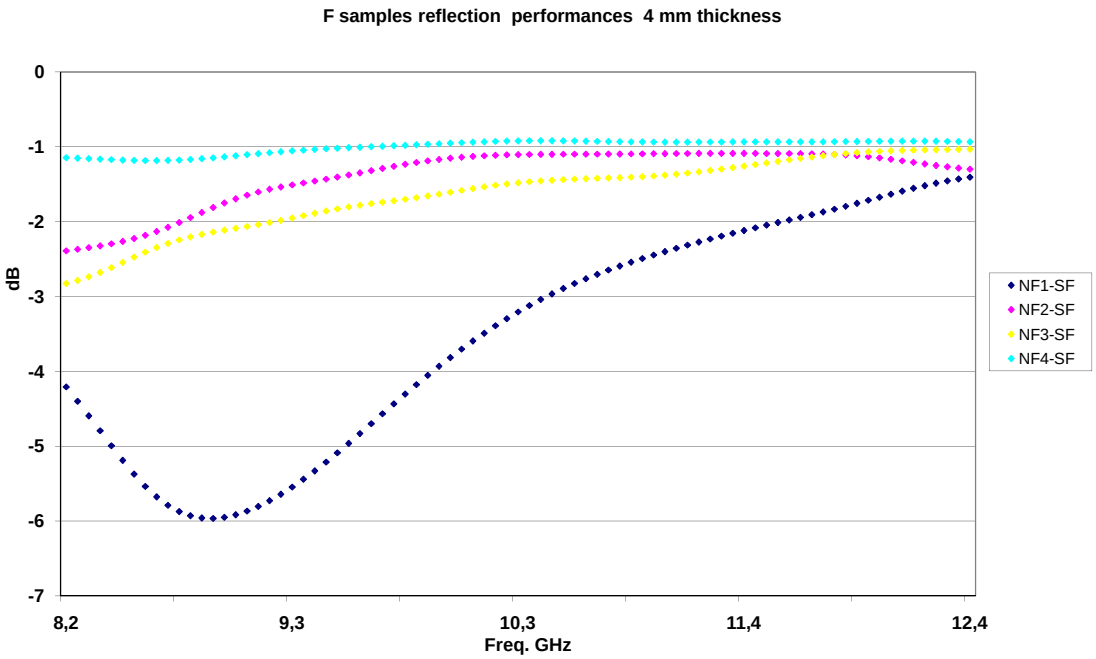


**Fig. 5-17 Reflection loss filtratin method produced samples, 4 mm thickness**

**Table 5-10 Peak absorption filtration method produced samples, and thickness it is achieved**

| Sample | Thickness (mm) | Frequency at peak (GHz) | Peak absorption (dB) |
|---|---|---|---|
| NF1-SF | 9 | 10,3 | 13,8 |
| NF2-SF | 7 | 11,4 | 19,9 |
| NF3-SF | 8 | 10 | 21,1 |
| NF4-SF | 6 | 10,4 | 20,7 |

The results clearly show that almost all CNF samples produced present good absorption performance only with substantial thicknesses, practically limiting the application of such materials as MAM. Only NF4-SP shows good absorbing properties with a reasonable small thickness of 2 mm, with an absorption peak of -18 dB at 9,2 GHz

## *5.3 Conclusions*

In this chapter three different production methods were investigated to produce CNF nanocomposites.

CNF were dispersed using either BGE or chloroform, and solvent was removed by evaporation or filtration. The resulting samples showed different meso and micro-structures whose effect to the

dielectric properties was attempted. SEM observations of better dispersed samples are matched by higher dielectric values on a same filler basis, due to the larger polarisable surface area (increase of e') and to the higher conductivity (increase of e''). Unsatisfying absorption performance at 4 mm sample thickness of all almost all samples was found, and a simulation of the effect of material thickness on this quantity was carried out. The results show that, with the exception of the case of 4%wt BGE material that offers interesting performance with a thickness of 2mm, none of the other samples produced has any significant EM absorption performance at thickness thin enough to be useful in engineering applications.

## 5.4 References


[1] Endo M, Koyama T, Hishiyama Y. Structural improvement of carbon fibers prepared from benzene. Japanese Journal of Applied Physics. 1976;15(11):2073-6.

[2] Al-Saleh MH, Sundararaj U. A review of vapor grown carbon nanofiber/polymer conductive composites. Carbon. 2009;47(1):2-22.

[3] Choi Y-K, Gotoh Y, Sugimoto K-I, Song S-M, Yanagisawa T, Endo M. Processing and characterization of epoxy nanocomposites reinforced by cup-stacked carbon nanotubes. Polymer. 2005;46(25):11489-98.

[4] Choi Y-K, Sugimoto K-I, Song S-M, Gotoh Y, Ohkoshi Y, Endo M. Mechanical and physical properties of epoxy composites reinforced by vapor grown carbon nanofibers. Carbon. 2005;43(10):2199-208.

[5] Jana S, Zhong W-H, Gan YX. Characterization of the flexural behavior of a reactive graphitic nanofibers reinforced epoxy using a non-linear damage model. Materials Science and Engineering A. 2007;445-446:106-12.

[6] Musumeci AW, Silva GG, Liu J-W, Martens WN, Waclawik ER. Structure and conductivity of multi-walled carbon nanotube/poly(3-hexylthiophene) composite films. Polymer. 2007;48(6):1667-78.

[7] Du F, Fischer JE, Winey KI. Coagulation method for preparing single-walled carbon nanotube/poly(methyl methacrylate) composites and their modulus, electrical conductivity, and thermal stability. Journal of Polymer Science, Part B: Polymer Physics. 2003;41(24):3333-8.

[8] Kovacs JZ, Andresen K, Pauls JR, Garcia CP, Schossig M, Schulte K, et al. Analyzing the quality of carbon nanotube dispersions in polymers using scanning electron microscopy. Carbon. 2007;45(6):1279-88.

# 6 Carbon nanotubes samples

The carbon filler commonly used in CPC is carbon black, but due to its close to spherical shape the weight percent needed to achieve good electrical properties is quite high, causing manufacturing problems, and reduced mechanical properties. The focus is now to find a better performing filler to decrease filler content and at the same time increase electrical and mechanical properties. Em properties of carbon filled polymers shall increase in a significant way by using rod-like fillers such as nanofibers or nanotubes (CNT), due to their higher aspect ratio compared to carbon black [1, 2]. The increase in electrical properties shall be even more marked when using CNT due to their excellent electrical properties .

The most important obstacle to overcome before it is possible to take full advantage of CNT filled polymers is CNT agglomeration and dispersion into the polymer matrix. The easier and economic method to produce CNT is by carbon vapour deposition, the CNT produced by this method are highly tangled and assembled in “ropes” due to strong van der Waal’s interaction among them [3]. It is then critical to achieve a good percolation pattern at the lowest weight percent possible that those ropes are separated into their constituent CNT, Several techniques are published to disperse CNT from ball milling [4] mechanical stirring [5], sonication [6] chemical doping [7], coagulation or precipitation [8, 9], these methods vary greatly in complexity and results achieved, as may be gathered by the widely different percolation threshold published. As the best compromise between time, cost, complexity and results achieved, it was decided, to use industrial grade surfactants. Surfactant use is a single step process that can be easily integrated into the overall composite processing without much alteration. Surfactants work by coating the CNT with molecules, which can induce repulsion that counterbalance the strong van der Waals attraction. A diblock copolymer has been used as a surfactant in CNT application with good results by Zhao [10], DisperBYK 2150 structure is composed by “lyophobic (solvent-repelling) and lyophilic (solvent-attracting) blocks. The lyophobic part adsorbs onto the surfaces of CNT while the lyophilic is swollen by the solution. “The repulsion among the lyophilic blocks overcomes the van der waals attractive force between CNT, so the CNT are kept separated” [11, 12]. The adsorption of the lyophobic blocks on the CNTs doesn’t seem to influence the percolation properties greatly as shown by surface resistivity measurements in Sluzarenko [12]. Two other surfactant, typically used to disperse carbon black, were employed, samples made without surfactant were also produced to gauge the effectiveness of the surfactant.

## 6.1 Experimental

### *6.1.1 materials and fabrication procedure*

Multiwall CNT used in this study were Nanocyl 3150, their properties are summarized in Table 6-1.

**Table 6-1 Nanocyl 3150 data as reported by datasheet**

| | |
|---|---|
| Average diameter | 9 nm |
| Average length | <1μm |
| Purity | >95% |

Short and thin CNT were chosen as they are more mobile compared to longer CNT and promote network formation [13]. As reported above, a diblock copolymer was employed as surfactant with a ratio 0,6 to the weight of the filler. Solvent was ethanol absolute, both because it is reported to be fully compatible with the surfactant [10, 11] and has a low boiling point, speeding the evaporation process. Samples with CNT content from 0,25%, to 1,5%w were produced. Sets of samples with the same range of filler content were also produced using BYK 9076 and BYK 9077 surfactants. As reference, samples with the same filler weight content were produced without the aid of surfactant. Table 6-2 summarises all samples produced with the relative nomenclature.

**Table 6-2 Summary of CNT samples produced**

| Name | Surfactant used | Weight % of filler produced | Name example |
|---|---|---|---|
| NT | None | 0,25; 0,5; 0,75; 1; 1,5 | NT1-S |
| SU | DisperBYK2150 | 0,25; 0,5; 0,75; 1; 1,5 | SU0,5-S |
| B6 | BYK9076 | 0,25; 0,5; 0,75; 1; 1,5 | B60,75-S |
| B7 | BYK9077 | 0,25; 0,5; 0,75; 1; 1,5 | B70,25-S |

The process can be summarized in a few points: nanocyl 3150 multi wall CNT and surfactant were weighted and placed in a beaker, solvent was added to a ratio of 1 ml of ethanol to 1 mg of MWCNT, and sonicated 1 hour using a Sonics VC 750 sonicator wand set at 70% of the tip oscillation, ice was used to prevent heating of the suspension. Afterwards the weighted resin was added and the dispersion stirred using a magnetic stirrer. Solvent completely evaporation was determined by weight, and then hardener was added. Cure was carried out at 80°C for 24 h.

### *6.1.2 Characterization*

Surfactant effectiveness and the effect of the sonicator process were first evaluated by TEM (Hitachi H7500), assessing by visual inspection the different degree of dispersion after sonication. Efficiency of CNTs dispersion in the cured polymer matrix was estimated by FEG-SEM analysis of gold-coated fracture surfaces of samples previously fractured under liquid nitrogen.
Dielectric properties were measured as described in §3.1.4.

## *6.2 Results and discussion*

### *6.2.1 Dispersion in solvent and in resin*

The effect of surfactant as well as the dispersion process employed in samples manufacturing has been evaluated by TEM. Fig. 6-1 shows a 100k magnification of CNT, as delivered by the manufacturer before any treatment. It is possible to notice CNT are tightly bundled in “ropes”.

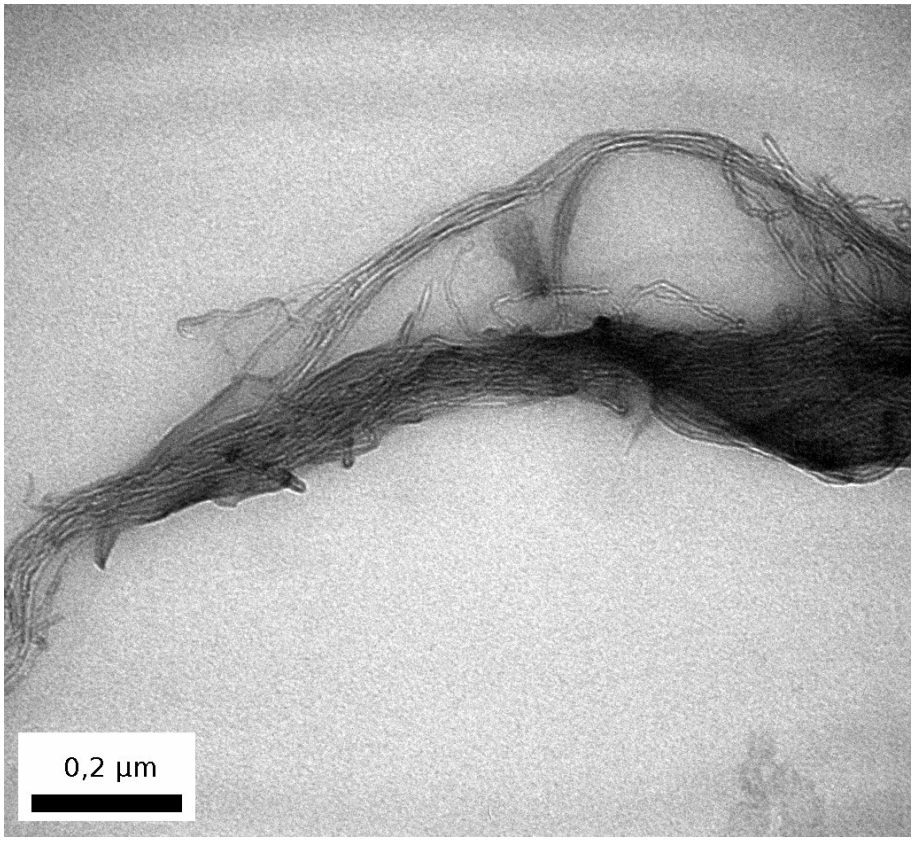


**Fig. 6-1 100K magnification TEM of unsonicated Nanocyl 3150 CNT**

Fig. 6-2a reports a 70k magnification of the CNT in ethanol dispersion as obtained after 1h sonication without any aid of surfactant (NT samples): CNT ropes are not present anymore, although CNT are still bundled together in aggregates. Fig. 6-2b (SU samples) evidences the

dispersion achieved when adding the surfactant, following the above reported procedure. In this latter case, a satisfying dispersion was attained: single nanotubes are visible together with fragments of CNT, indicating the beginning of their cutting. On the bottom, Fig. 6-2c the CNT dispersion is not helped at all by BYK 9076 (B6), on the bottom right (Fig. 6-2d) CNT dispersed using BYK 9077 (B7) show a very good dispersion and CNT fragments of almost equal length uniformly distributed, very few aggregates of very small dimensions are present.

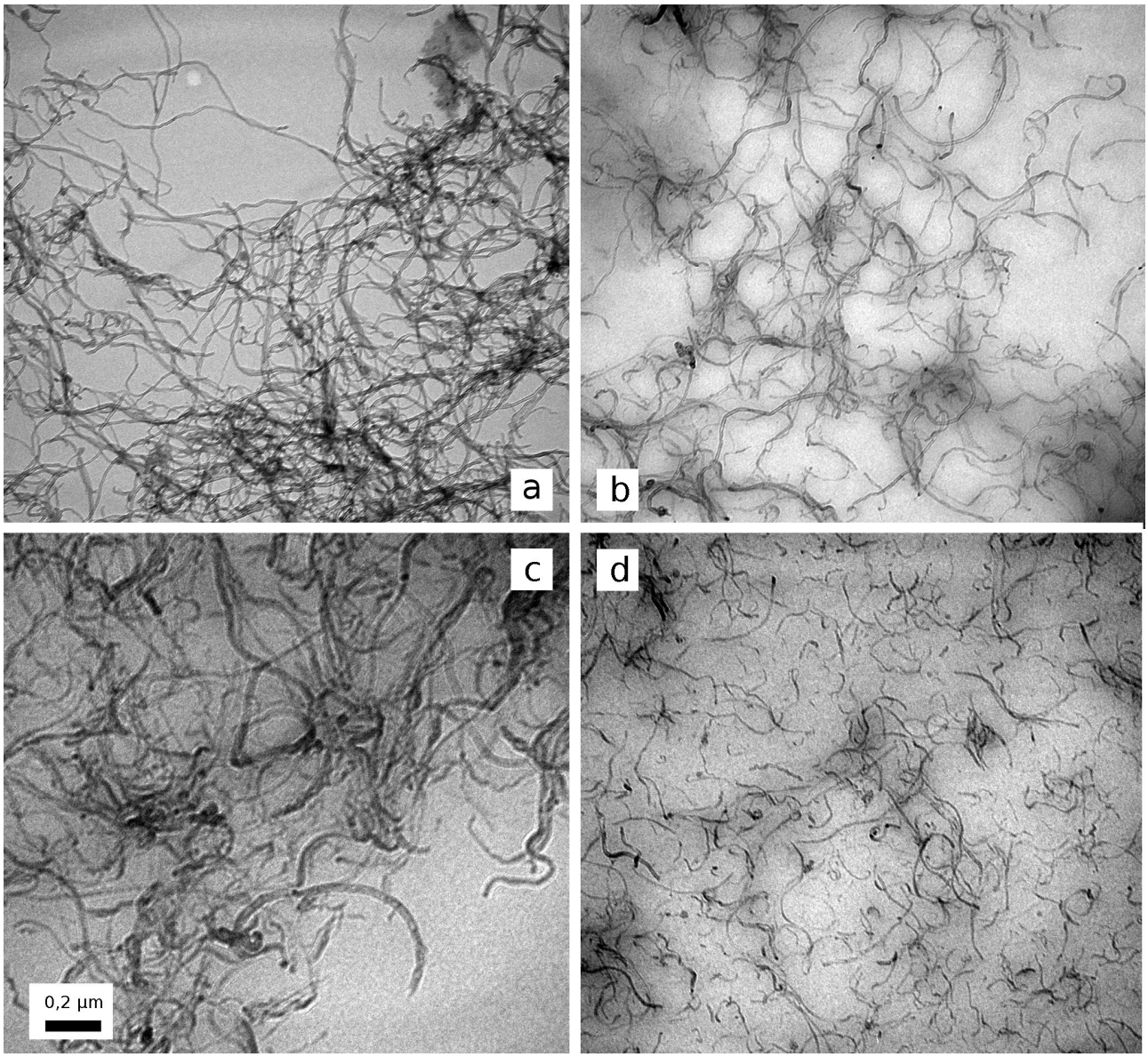


**Fig. 6-2 TEM 60K magnification of ethanol and CNT dispersions. From left to right from top to bottom NT (a), SU (b), B6 (c) and B7 (d) samples**

The stability of CNT dispersion in ethanol was checked in time by visual inspection. As shown in Fig. 6-3, the stability of the dispersions without surfactant or with BYK 9076 surfactant ( NT and B6 samples, respectively a and c in Fig. 6-3) after 5 days is very poor, due to the presence of CNT

bundles that precipitate in a short time. On the contrary, the DisperBYK2150 and BYK9077 surfactant assisted dispersions ( SU and B7 samples, b and d in Fig. 6-3) present single nanotubes or small agglomerates of them able to float for a much longer time.

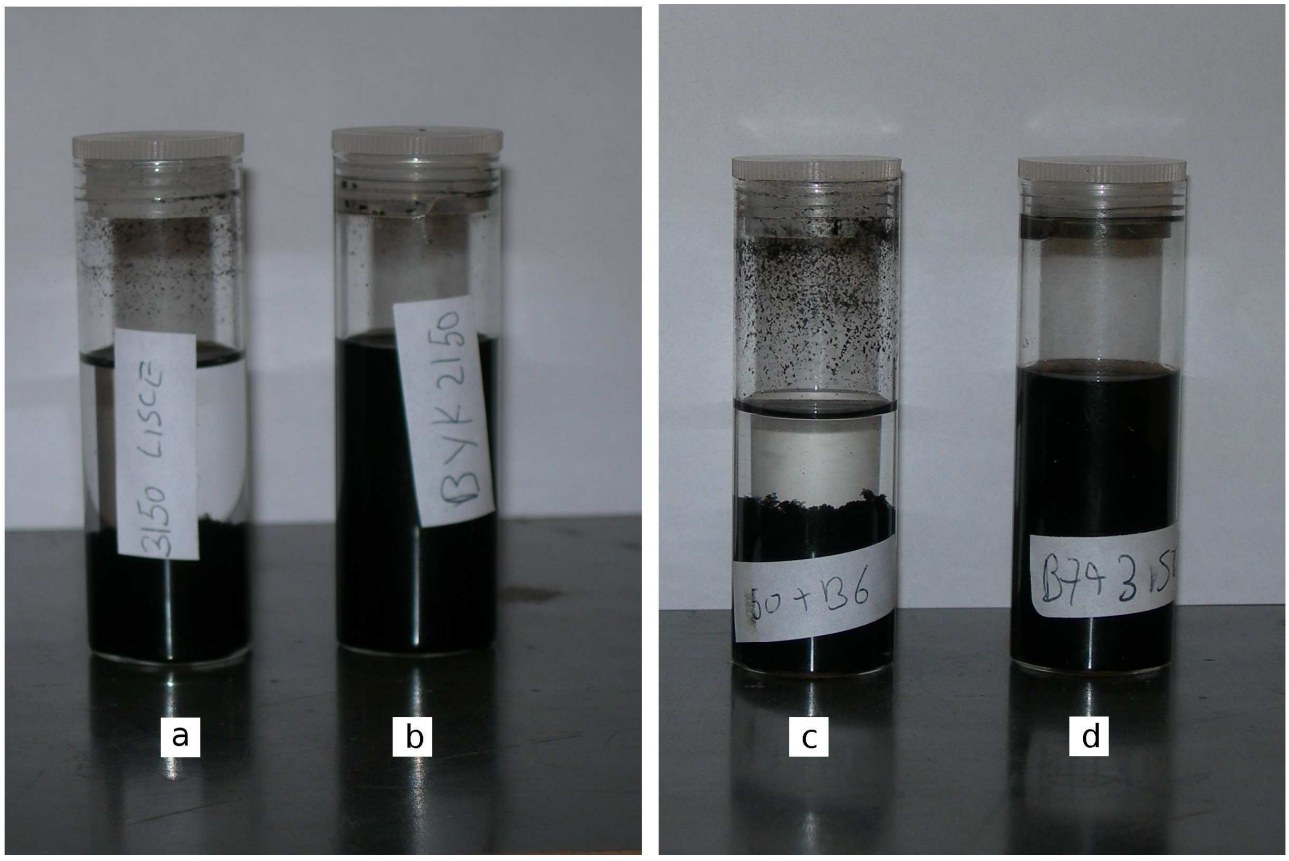


**Fig. 6-3 MWCNT precipitation after 5 days from left to right type NT (a), SU (b), B6 (c) and B7 (d)**

Fig. 6-4 reports the micrographs of 1%wt CNT samples, NT, SU and B6 samples micrograph are in agreement with the assessment of dispersion quality made by TEM (Fig. 6-4 a,b,c respectively), while type B7 dispersion inside the resin is much worse than what it is in ethanol, Fig. 6-4d

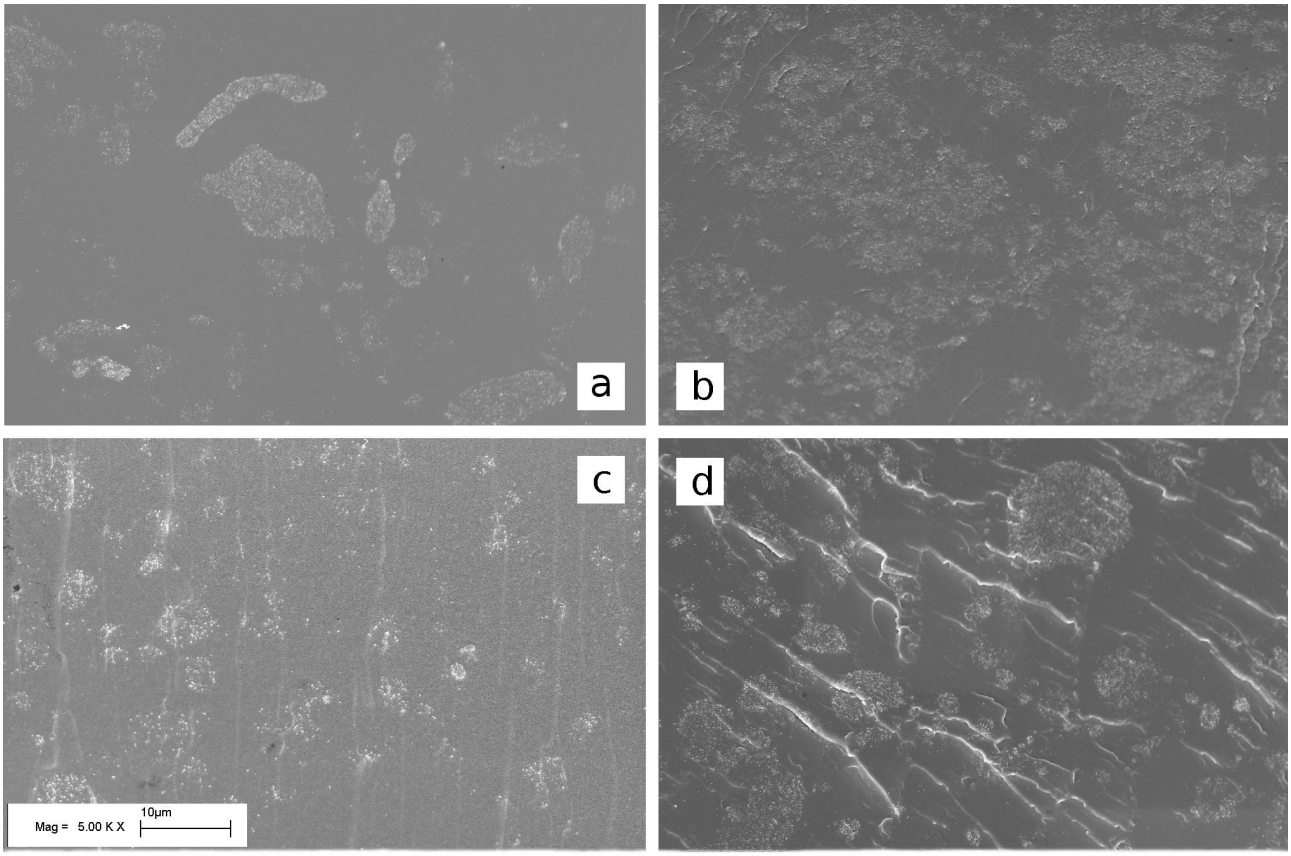


**Fig. 6-4 Cryo-factured surfaces of 1% CNT loaded samples SEM micrograph 5K magnification, from left to right and top to bottom type NT (a), SU (b), B6 (c) and B7 (d).**

In detail NT sample (Fig. 6-4a) shows agglomerates of CNT in the resin, on the other hand SU sample (Fig. 6-4b) demonstrate the effect of surfactant: CNT are almost evenly distributed on the surface. B6 samples (Fig. 6-4c) micrograph IS in agreement with TEM analysis, IT shows that the poor dispersion of the CNT in ethanol is transferred into the finished samples. B7 samples (Fig. 6-4d) instead show bundles of not dispersed CNT even if the dispersion as analysed by TEM is the best of the group. Since the samples produced only differed by the ratio of CNT to solvent used (as required to obtain clearer pictures by TEM) it is possible that BYK9077 works better in more diluted colloidal dispersions.

Fig. 6-5 reports a magnification of a light grey area of Fig. 6-4. It is possible to verify that these areas are agglomerates of CNT that appear as a web of CNT with multiple contacts points.

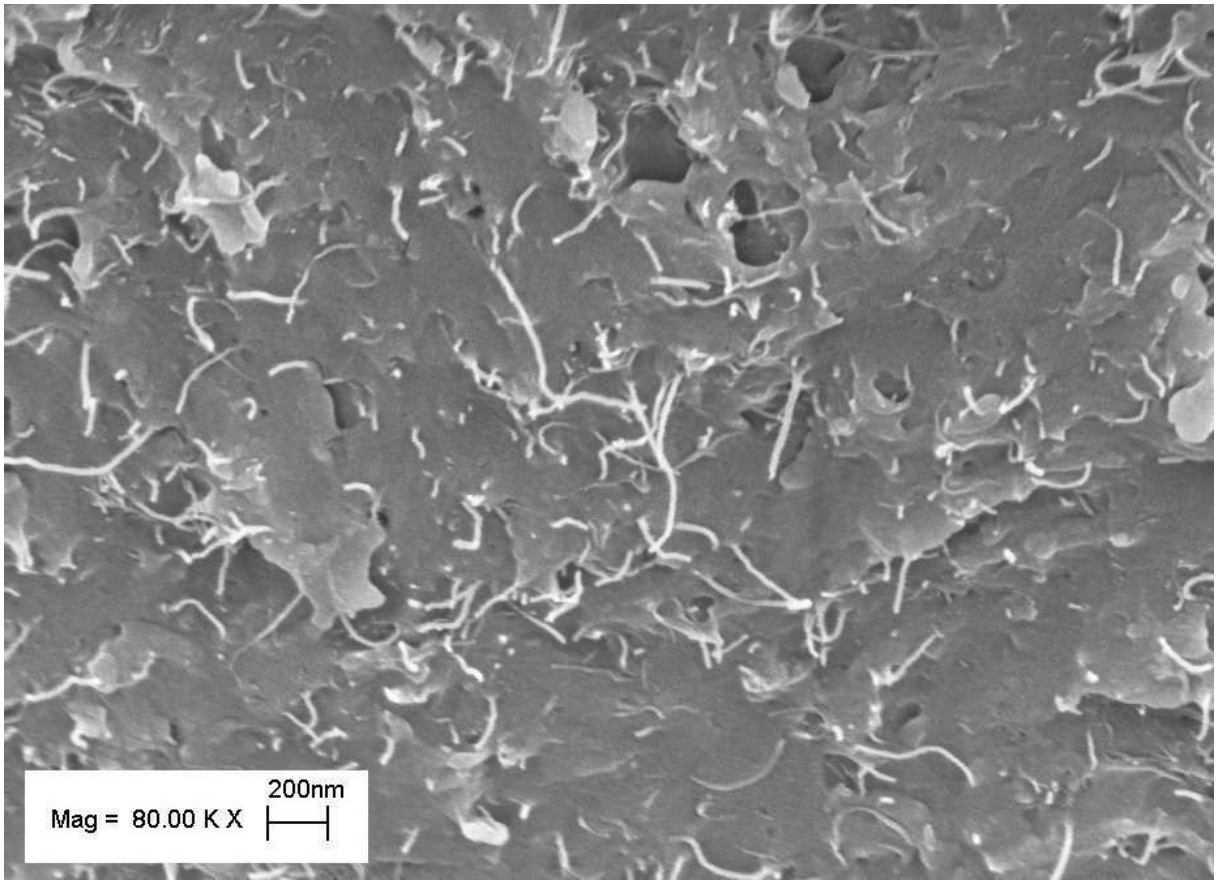


**Fig. 6-5 80kx magnification of a bundle of an agglomeration of nanotubes from NT0,75-S sample**

### *6.2.2 Em measurements and Relationship between microstructure and dielectric properties: Type NT and SU samples*

Fig. 6-6and Fig. 6-7 report respectively the real and imaginary part of permittivity as a function of frequency. On the same %w filler basis, samples produced with DisperBYK 2150 surfactant present higher ε' and lower ε" than those found in NT specimens. As a consequence loss tangent is higher in samples without surfactant.

These initially astonishing results have to be most probably referred to the different microstructure obtained in the two cases. The author in A previous work [14], as well as other authors [15, 16], suggest that it is possible to analyze the matrix-filler samples with an equivalent circuit analogy. If the system is modelled as an equivalent electrical circuit the resistance should decrease while the capacitance increases with filler loading. This kind of behaviour is reflected in ε', the real part of the complex permittivity (ε*), that is related to the capacity of the material to store energy. This term should increase when increasing the number of capacitors and, hence, filler content or filler dispersion. Better dispersed samples produce more equivalent capacitors and more dead end branches, as evidenced in [17] FOR CB SAMPLES (cfr §1.5XXX).

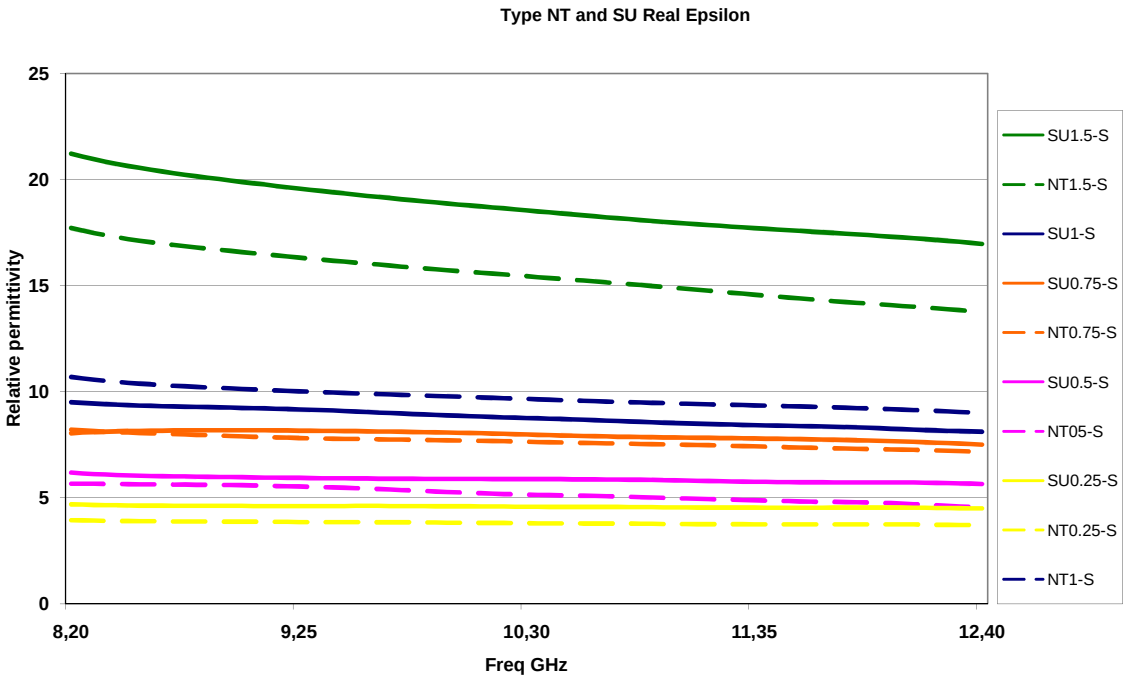


**Fig. 6-6 Real permittivity of SU  compared to NT samples.**

The complex part (ε”), instead, takes into account dissipation and conductivity of the medium.

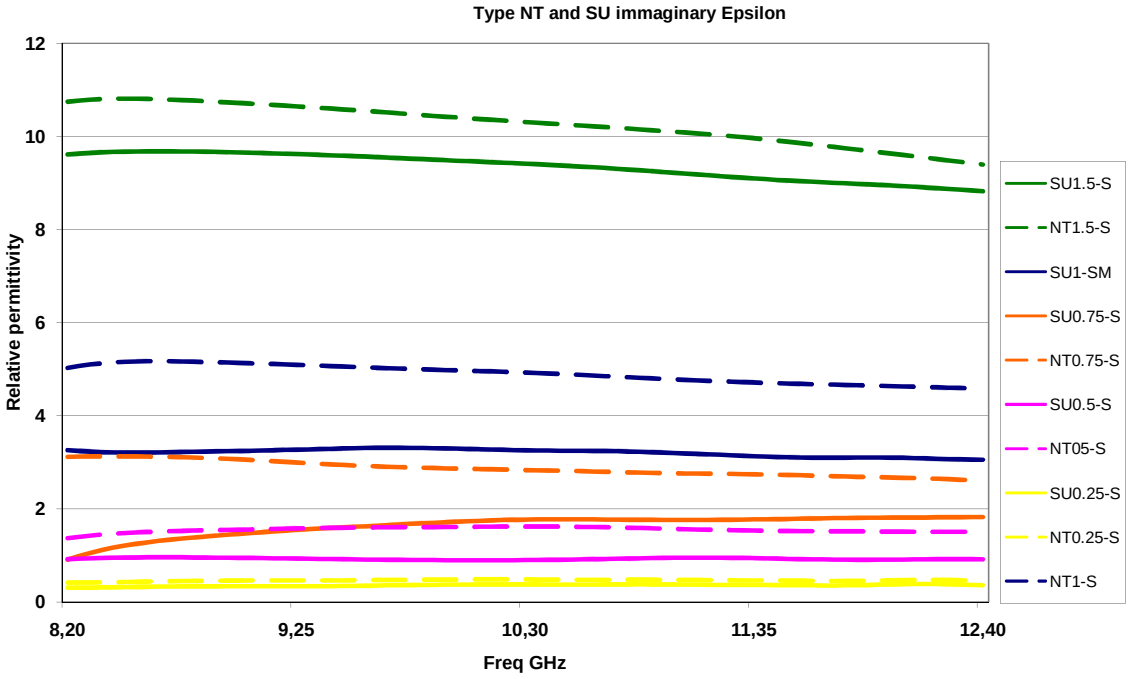


**Fig. 6-7 Imaginary permittivity of SU compared to NT samples**

Regarding energy dissipation it was proven that the major effect is the capacity of quickly dissipate the energy. Gojny et al. At low frequency in [18] showed that not always an optimum dispersion is wanted (especially in the case of very thin fillers). Dissipation, in fact, happens mainly through joule effect and if a good, but not perfect, disagglomeration of CNT is achieved, a large amount of electrical shortcuts occur(Fig. 6-8a), dissipating the energy quickly. On the other hand, the better dispersed CNT offer only few electrical shortcuts, since the single nanotubes are separates one to the other by a thin layer of resin and the energy is stored inside the CNT and dissipates slowly (Fig. 6-8b)

The belief that there is an optimum dispersion threshold, that produces the highest effect on dissipation and conduction for any given weight percent, made its way. Above that threshold, dispersion starts to become counterproductive.

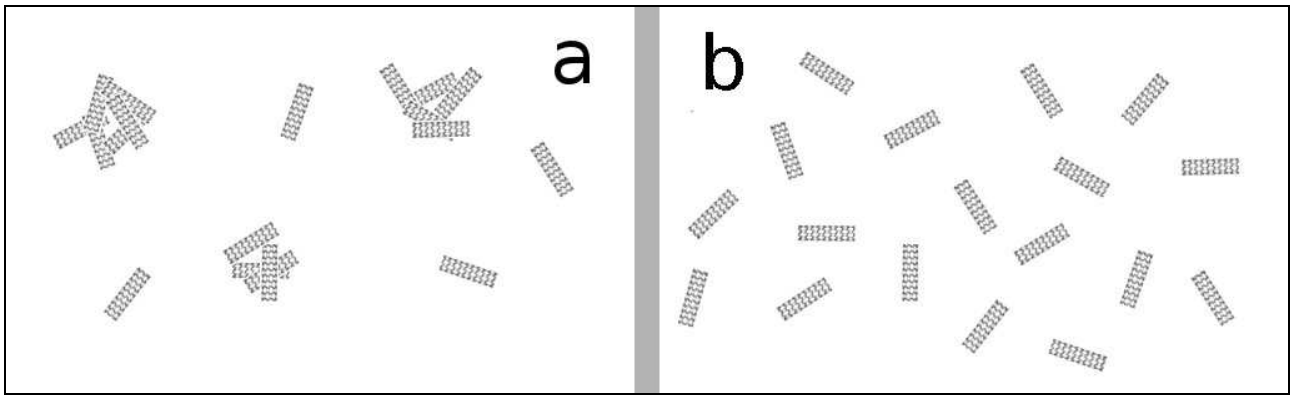


**Fig. 6-8 schematics of different dispersion inside the produced samples a) NT, b) SU**

Table 6-3 and Table 6-4 reassumes the numerical results of the electromagnetic experimentation.

**Table 6-3 Percent increases in filler weight load, average real and imaginary samples produced without surfactant**

| Filler weight % | Weight increment | Average ε' | ε' increment | Average ε" | ε" increment |
|---|---|---|---|---|---|
| 0,25% | | 3,82 | | 0,47 | |
| 0,50% | 100% | 5,19 | 36% | 1,55 | 234% |
| 0,75% | 50% | 7,64 | 47% | 2,87 | 84% |
| 1,00% | 33% | 9,71 | 27% | 4,90 | 71% |
| 1,50% | 50% | 15,49 | 59% | 10,27 | 109% |

**Table 6-4 Percent increases in filler weight load, average real and imaginary samples produced using BYK2150**

| Filler weight % | Weight increment | Average ε' | ε' increment | Average ε" | ε" increment |
|---|---|---|---|---|---|
| 0,25% | | 4,25 | | 0,31 | |

| | | | | | |
|---|---|---|---|---|---|
| 0,50% | 100% | 5,87 | 38% | 0,93 | 199% |
| 0,75% | 50% | 7,95 | 35% | 1,64 | 77% |
| 1,00% | 33% | 8,79 | 11% | 3,21 | 95% |
| 1,50% | 50% | 18,70 | 113% | 9,35 | 191% |

#### *6.2.2.1 SU and NT samples Reflection loss performance*

The absorbing performance of SU and NT samples were evaluated, as usual, by measuring $s_{11}$ of metal backed samples. Since 4mm samples did not report significant absorbing, it was decided to report the results of the numerical simulation carried out considering a thickness of 2.5mm (Fig. 6-9). This because it is an interesting small thickness that produced good absorbing.

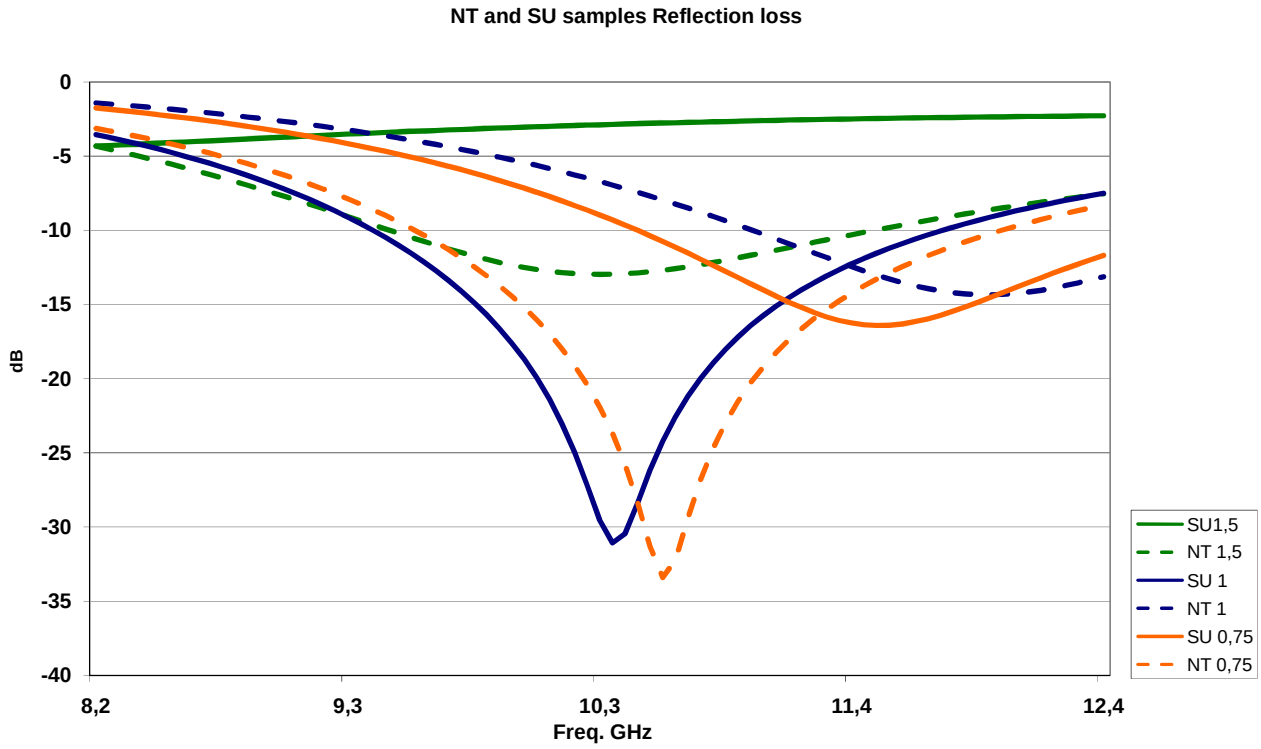


**Fig. 6-9 Absorbing performance of selected samples with a 2,5 mm thickness**

Good absorption peaks were achieved by NT0,75-S and SU1-S at 2,5 mm thickness. As usual, it was found that too conductive samples become mostly reflective, while if the filler is present in a small amount does not produce a sufficiently lossy medium. It is interesting to remark that the absorbing performance of NT0,75-S and SU1-S at are similar, even if the two samples have different CNT amount. This is due to the fact that SU1-S presents a better dispersion of CNT in the resin that, as previously discussed, leads to a decrease of EM performance. Finally, it is worth noting that NT0,75-S shows a wide 10 dB absorption bandwidth from 9,5 to 12 GHz.

### *6.2.3 B6 Dielectric and EM properties*

B6 samples were compared to the reference NT samples, as done with SU samples in the previous paragraph.

An assessment of the dispersion produced using BYK 9076 compared to samples produced without (Fig. 6-2a and c) shows that B6 samples are marginally better dispersed than NT samples. In fact, both specimens present aggregates of CNT that are smaller and more numerous in the case of b6 samples.

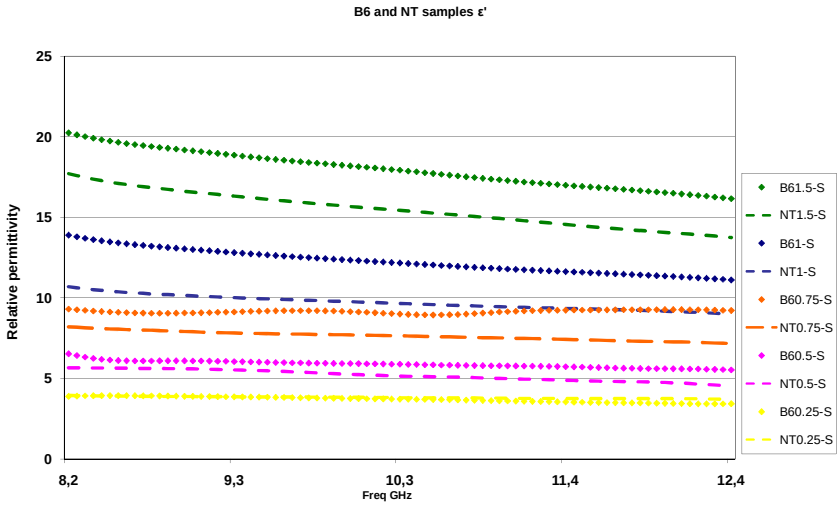


**Fig. 6-10 Real permittivity of B6 compared to NT samples.**

This improvement is reflected in ε' or ε", that are always higher than the respective NT samples.

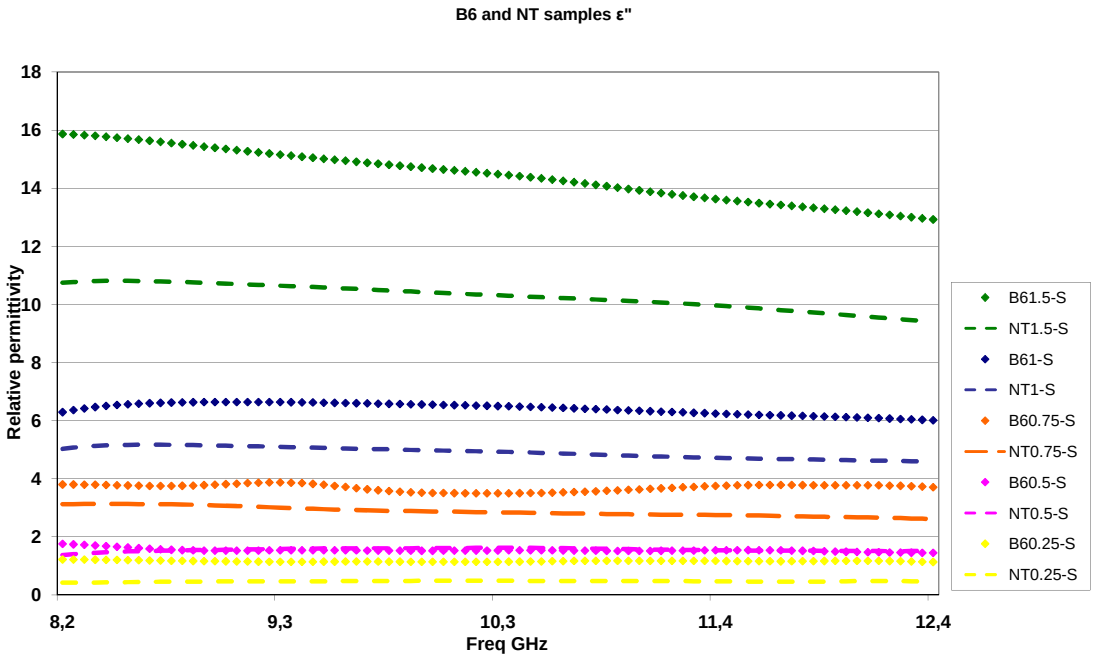


**Fig. 6-11 Imaginary permittivity of B6 compared to NT samples.**

Table 6-5 summarizes the percent increments of weight, real and imaginary permittivity as filler increases.

**Table 6-5 Percent increases in filler weight load, average real and imaginary samples produced using BYK9076**

| Filler weight % | Weight increment | Average ε' | ε' increment | Average ε" | ε" increment |
|---|---|---|---|---|---|
| 0,25% | | 3,70 | | 1,16 | |
| 0,50% | 100% | 5,88 | 59% | 1,53 | 32% |
| 0,75% | 50% | 9,15 | 56% | 3,70 | 141% |
| 1,00% | 33% | 12,26 | 34% | 6,41 | 73% |
| 1,50% | 50% | 17,98 | 47% | 14,43 | 125% |

### *6.2.4 Type B7 Dielectric and EM properties*

Samples produced using BYK9077 have good values of real permittivity (Fig. 6-12) and this ties well with the dispersion of CNT as can be seen from Fig. 6-3d, the quality of BYK9077 aided dispersion of CNT into the resin is lower than B6 samples but better than NT. The EM results reflect the microstructure except for B71-S that show a value of ε' and ε" lower than B70,75-S that can be easily understood by checking the samples microstructure as reported in Fig. 6-14, B70,75-S is very well dispersed and doesn't follow the pattern of dispersion of the other B7 samples.

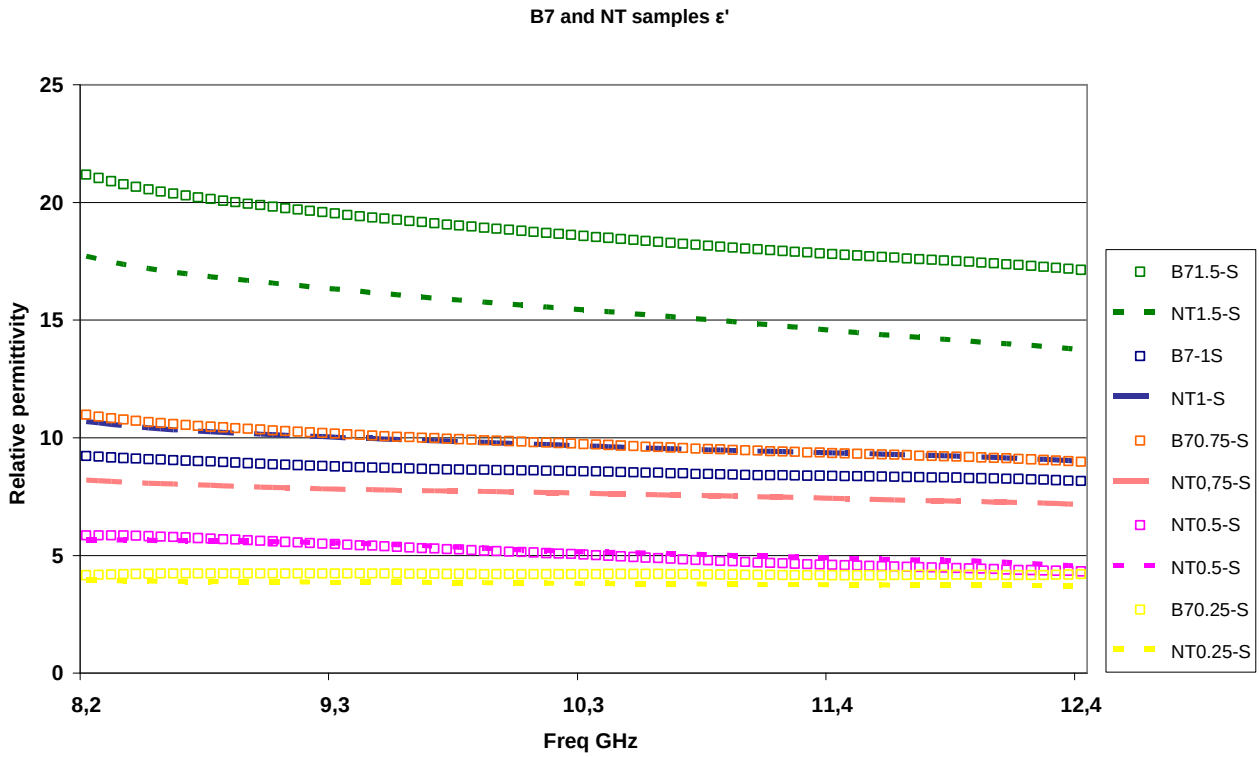


**Fig. 6-12 Real permittivity of B7 compared to NT samples.**

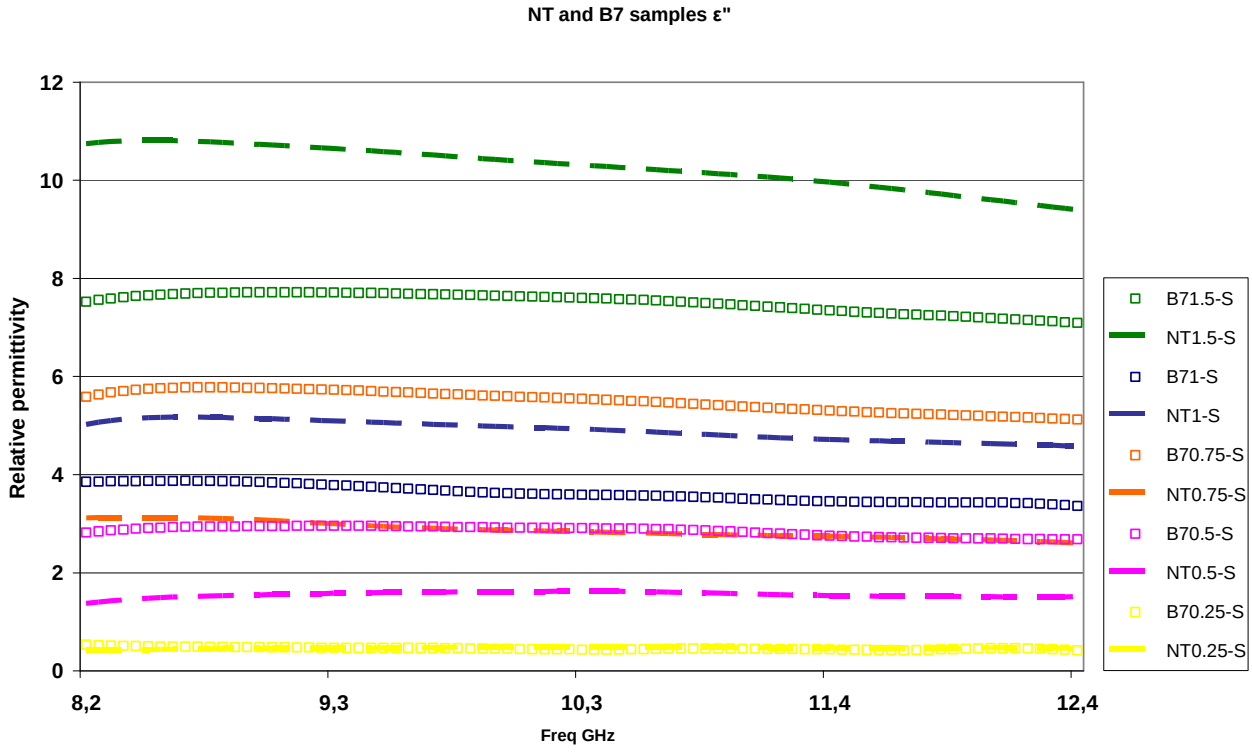


**Fig. 6-13 Imaginary permittivity of B7 compared to NT samples.**

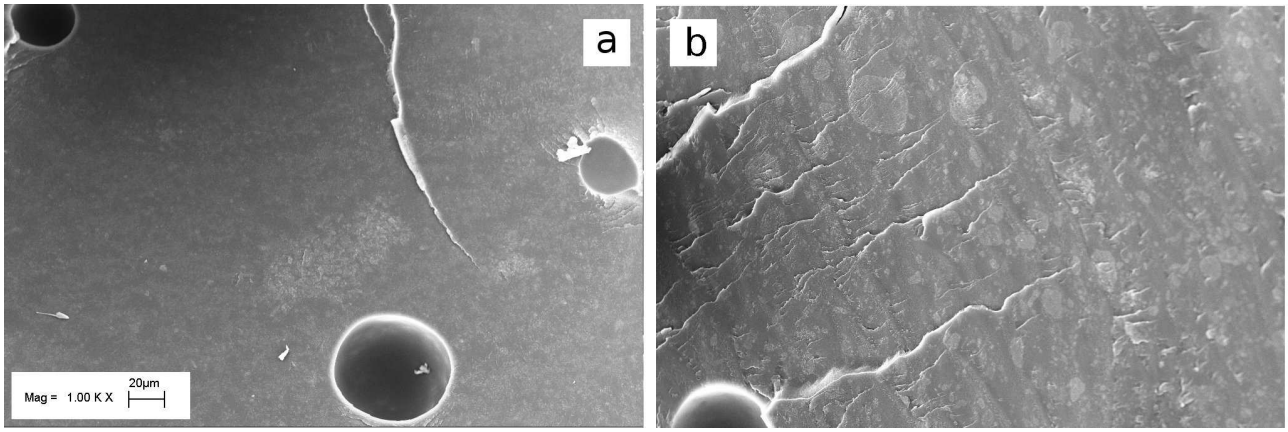


**Fig. 6-14 SEM micrograph of a) B70,75-S and b) B71-S**

## 6.3 Conclusions

In this chapter the effect of surfactant on the dispersion and resulting properties of CNT filled composites were studied. Of the three surfactants used BYK2150 was found to greatly help dispersion, BYK9076 and BYK 9077 instead don't improve the dispersion in a significant way, at least for low percents of filler loading. It was also found that the effect of dispersion on the dielectric properties of a composite has a threshold, it was clearly shown comparing SU and NT that the better dispersed samples have higher values of real permittivity but lower values of imaginary permittivity. A link between this phenomenon with the microstructure is then made. Less dispersed samples don't reach this threshold and follow the usual path described in the previous chapter where better dispersion leads to higher values of real and imaginary permittivity.

## 6.4 References

[1] Jou W-S, Cheng H-Z, Hsu C-F. The electromagnetic shielding effectiveness of carbon nanotubes polymer composites. Journal of Alloys and Compounds. 2007;434-435(SPEC ISS):641-5.
[2] Li J, Ma PC, Chow WS, To CK, Tang BZ, Kim J-K. Correlations between percolation threshold, dispersion state, and aspect ratio of carbon nanotubes. Advanced Functional Materials. 2007;17(16):3207-15.
[3] Thostenson ET, Ren Z, Chou TW. Advances in the science and technology of carbon nanotubes and their. Composites Science and Technology. 2001;61(13):1899-912.
[4] Gorrasi G, Sarno M, Di Bartolomeo A, Sannino D, Ciambelli P, Vittoria V. Incorporation of carbon nanotubes into polyethylene by high energy ball milling: Morphology and physical properties. Journal of Polymer Science, Part B: Polymer Physics. 2007;45(5):597-606.
[5] Sandler J, Shaffer MSP, Prasse T, Bauhofer W, Schulte K, Windle AH. Development of a dispersion process for carbon nanotubes in an epoxy matrix and the resulting electrical properties. Polymer. 1999;40(21):5967-71.
[6] Song YS, Youn JR. Influence of dispersion states of carbon nanotubes on physical properties of epoxy nanocomposites. Carbon. 2005;43(7):1378-85.
[7] Chun K-Y, Choi SK, Kang HJ, Park CY, Lee CJ. Highly dispersed multi-walled carbon nanotubes in ethanol using potassium doping. Carbon. 2006;44(8):1491-5.
[8] Du F, Fischer JE, Winey KI. Coagulation method for preparing single-walled carbon nanotube/poly(methyl methacrylate) composites and their modulus, electrical conductivity,

and thermal stability. Journal of Polymer Science, Part B: Polymer Physics. 2003;41(24):3333-8.
[9] Musumeci AW, Silva GG, Liu J-W, Martens WN, Waclawik ER. Structure and conductivity of multi-walled carbon nanotube/poly(3-hexylthiophene) composite films. Polymer. 2007;48(6):1667-78.
[10] Zhao L, Gao L. Stability of multi-walled carbon nanotubes dispersion with copolymer in ethanol. Colloids and Surfaces A: Physicochemical and Engineering Aspects. 2003;224(1-3):127-34.
[11] Li Q, Zaiser M, Koutsos V. Carbon nanotube/epoxy resin composites using a block copolymer as a dispersing agent. Physica Status Solidi (A) Applied Research. 2004;201(13):89-91.
[12] Sluzarenko N, Heurtefeu B, Maugey M, Zakri C, Poulin P, Lecommandoux S. Diblock copolymer stabilization of multi-wall carbon nanotubes in organic solvents and their use in composites. Carbon. 2006;44(15):3207-12.
[13] Martin CA, Sandler JKW, Shaffer MSP, Schwarz MK, Bauhofer W, Schulte K, et al. Formation of percolating networks in multi-wall carbon-nanotube-epoxy composites. Composites Science and Technology. 2004;64(15):2309-16.
[14] Nanni F, Travaglia P, Valentini M. Effect of carbon nanofibres dispersion on the microwave absorbing properties of CNF/epoxy composites. Composites Science and Technology.In Press, Corrected Proof.
[15] Juan-Farfan RS, Hernandez-Lopez S, Martinez-Barrera G, Camacho-Lopez MA, Vigueras-Santiago E. Electrical characterization of polystyrene-carbon black composites. Physica Status Solidi C. 2005(10):3762-5.
[16] Nakamura S, Ito A, Kitagawa K, Sawa G. Resistor and dielectric properties of carbon black-epoxy resin composites. Transactions of the Institute of Electronics, Information and Communication Engineers C-II. 1991;J74C-II(11):749-54.
[17] Nakamura S, Kitagawa K, Sawa G. Dielectric properties of carbon black-epoxy resin composites in high frequency range. 1992; Sestri Levante, Italy: IEEE; 1992. p. 97-101.
[18] Gojny FH, Wichmann MHG, Fiedler B, Kinloch IA, Bauhofer W, Windle AH, et al. Evaluation and identification of electrical and thermal conduction mechanisms in carbon nanotube/epoxy composites. Polymer. 2006;47(6):2036-45.

# 7 CB CNF CNT comparison

CB is the most common filler, it is cheap and easy to incorporate into the matrix, but its aspect ratio is low. On the other hand CNT aspect ratio is very high as are its electrical properties but it needs complicated processing before being included into the resin. CNF somehow lie in the middle, since they present electric properties close to CNT's ones, are also somewhat easier to disentangle but they are thicker.

In order to develop superior (i.e. thinner, cheaper) absorbing materials, a better understanding of the structure-property relationship is needed, here we compare CB, CNF and CNT filled epoxy with the aim of linking the dielectric and thus EM properties attained by the different composites with their microstructure.

Fig. 7-1 and Fig. 7-2 report ε' and ε'' for samples loaded with different nanofiller type and amount, that present similar ε'. Table 7-1 reassumes the major characteristics of the samples, while Table 7-2 report the resistivity of the different filler.

**Table 7-1 Summary of samples produced, name filler type, filler contemt**

| Name | Filler type | Filler content %w |
|---|---|---|
| XE-5S | Degussa XE2-B (CB) | 5 |
| SP3-S | Super-P (CB) | 3 |
| NF1-SM | Pyrograf III (CNF) | 1 |
| SU0,5-S | Nanocyl 3150 (CNT) | 0,5 |

**Table 7-2 Electric resistivity of the various fillers employed**

| | XE2-B | Super-P (Super-P datasheet) | CNF [1] | MWCNT [1] |
|---|---|---|---|---|
| Electric resistivity $(\Omega \cdot cm)$ | Not published | $0{,}11 - 0{,}2$ | $1 \times 10^{-4}$ | $2 \times 10^{-3} - 1 \times 10^{-4}$ |

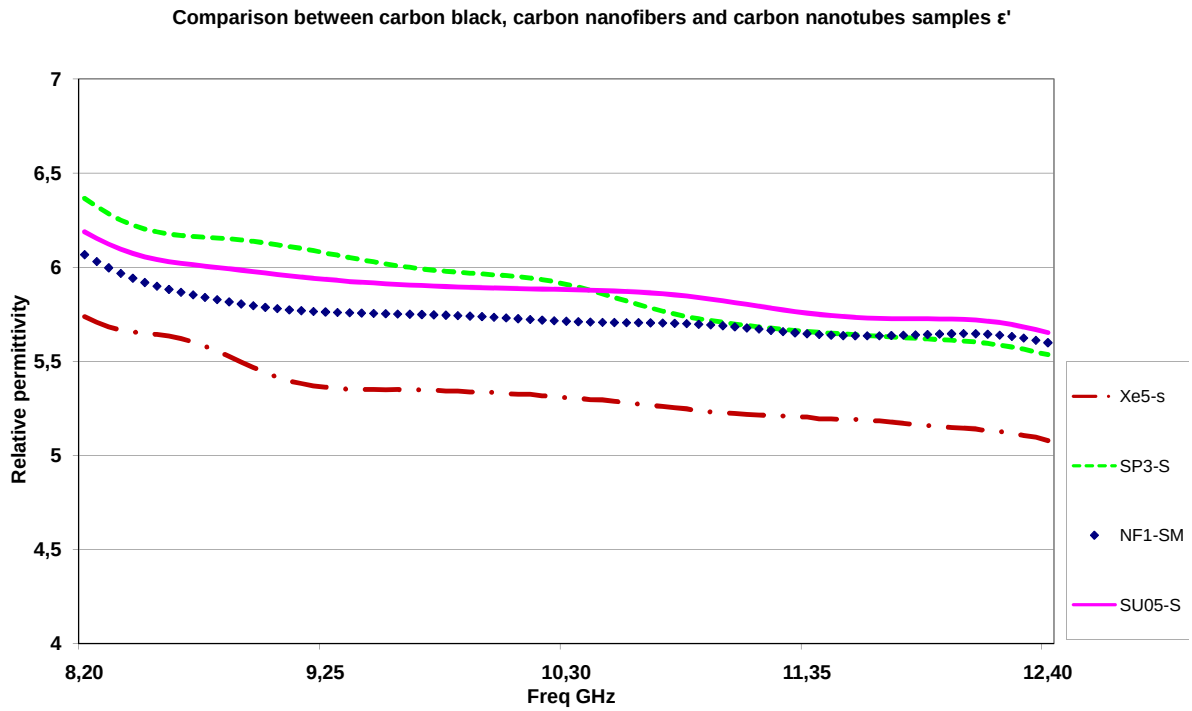


**Fig. 7-1 Real permittivity of the different samples in X-band**

The ε' data highlight that to attain similar values of real permittivity very different amount of the diverse nanofillers need to be employed: 0,5%w of well dispersed CNT ,1%w CNF with the same quality of dispersion, 5%w of XE or 3% of Super-p CB are needed. This reflects the fact that CNT present the higher performance due to their superior aspect ratio.

**Table 7-3 Percent variance of real permittivity**

| | SU average | NF average | NF/SU Variance % | XE average | XE/SU variance % | SP average | SP/SU variance % |
|---|---|---|---|---|---|---|---|
| eq 0,5%w ε' | 5,87 | 5,73 | -2 | 5,33 | -9 | 5,25 | -10 |
| eq 0,5%w ε" | 0,93 | 0,27 | -71 | 2,93 | 215 | 0,99 | 6 |

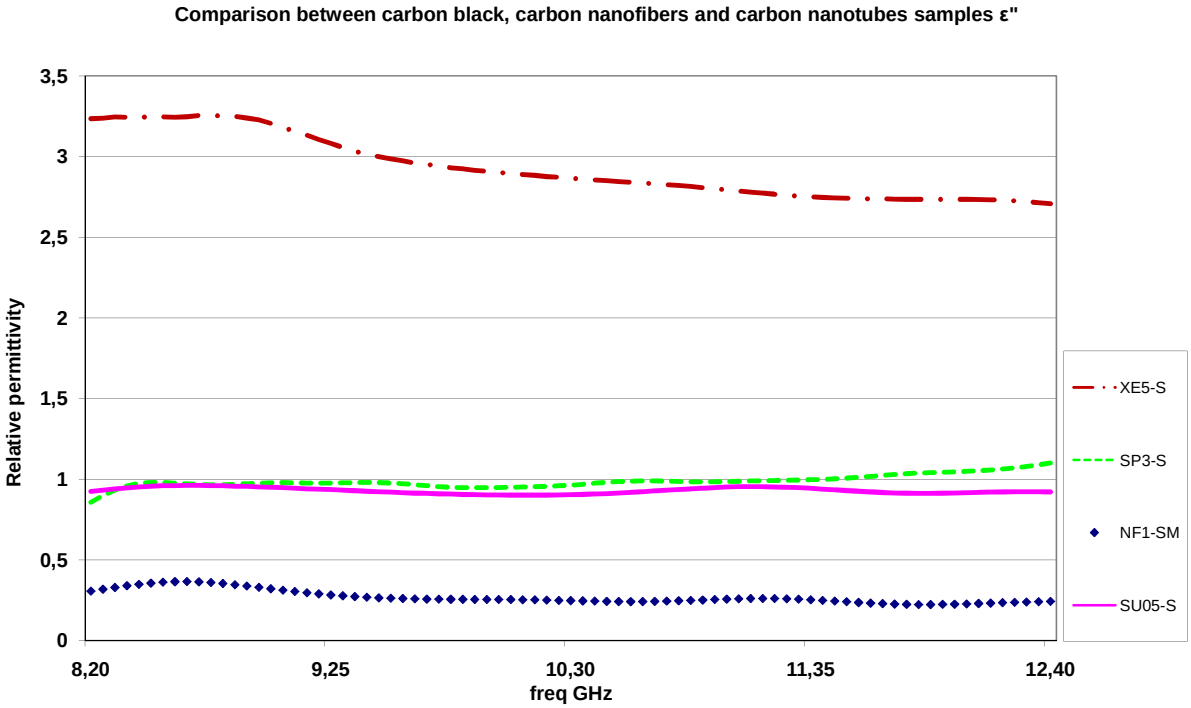


**Fig. 7-2 Imaginary permittivity of the different samples in X-band**

The values of the imaginary permittivity are not close banded around the value of SU0,5-S, and show how the different network patterns and intrinsic filler conductivity influence the dielectric properties of the composite. Samples now show a bigger dispersion in imaginary permittivity with a range of values that are 71% less or 215% more than the average value of SU0,5-S.

As noted above and demonstrated in Fig. 7-3 CNF are easier to disentangle than CNT, the 1 KX magnification micrograph show highly dispersed samples with just a very small aggregate in the upper right corner. Using the same tool, the equivalent circuit analogy, as used in the previous chapters, it is possible to relate the very low value of NF1-SM compared to SU0,5-S by the very good dispersion of fibres achieved, as it is possible to notice in Fig. 7-3 , as discussed in §6.2.2 there is a threshold after which the dispersion increases the value of real permittivity but decreases imaginary permittivity, other factors that shall be taken in consideration are

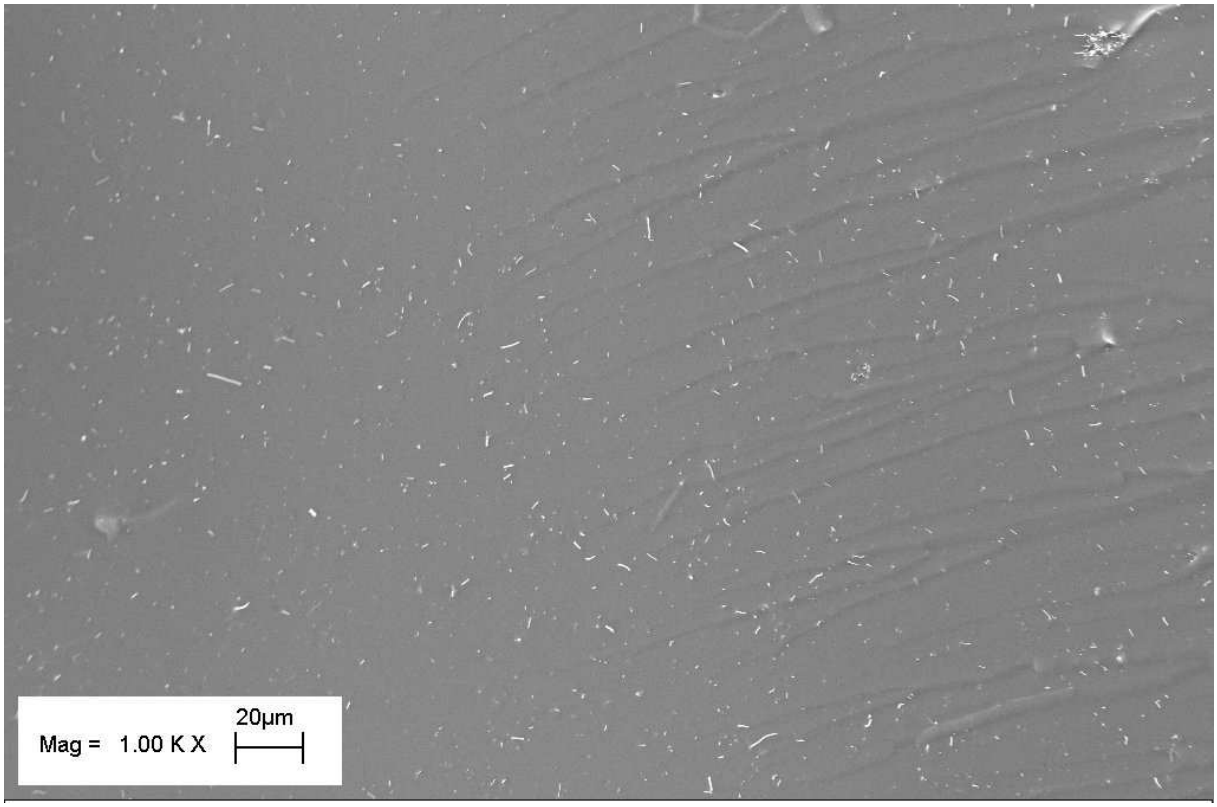


**Fig. 7-3 1 KX magnification of NF1-SM**

Electric conductivity of CNF is already close to that of CNT (cfr. Table 7-2 [1]), but is should be even closer, since they are thermal treated to increase their electric conductivity by removing the amorphous outer layer and obtain a fully graphitic structure (cfr. §5.1.1). Size shall be advantageous to the CNF since they are longer than CNT and so there should be more possibility of electrical contact between fibres, in Fig. 7-4 it is shown that the average length of CNF even after heavy cutting by sonication is still at least 4 times longer than the value of CNT length as stated on the datasheet.

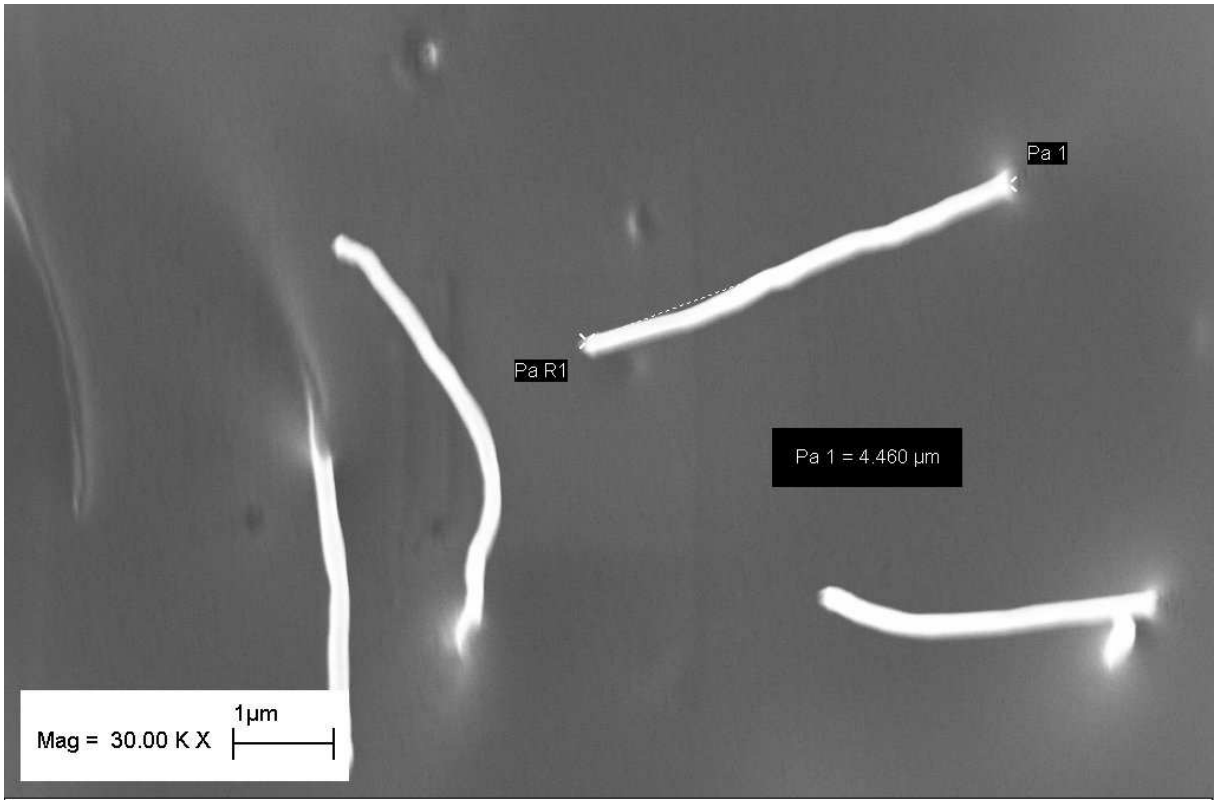


**Fig. 7-4 CNF length measurement**

Samples filled with CB show that in the case of Xe much higher conductivity was achieved that can be due to the high quantity of filler as well as to its internal microstructure that, as reported in the chapter devoted to CB, is formed by smaller and more numerous clusters that facilitate hopping and tunnelling conduction.

## *7.1 References*

[1] Al-Saleh MH, Sundararaj U. A review of vapor grown carbon nanofiber/polymer conductive composites. Carbon. 2009;47(1):2-22.

# 8 Conclusions

Samples loaded with different carbonaceous nanofillers (carbon black powders, nanofibres and nanotubes) were tested in X-band using the waveguide method in order to asses the dielectric properties, i.e. Complex permittivity, and the microwave absorbing performance of the realized materials. A link between permittivity and microstructure (assessed by FEG-SEM) was then attempted, using the equivalent circuit analogy. By means of this theory, the network of conductive paths inside the composite may be seen as a series of capacitors and resistors made by the nanofillers or their aggregates. The shape of the network, which is the dispersion of the filler, influences the number and efficiency of these capacitors and, as a consequence, the real permittivity. Imaginary part of permittivity, instead, takes into account conductivity and dissipations and is therefore directly related to the intrinsic conductivity of the filler, as well as once again to its dispersion in the resin that can facilitate electrical charges transportation.

Two different CB fillers were used, respectively with a very high specific surface area (XE) and small specific surface area (SP). Xe filled samples produced small short branched clusters, while sp microstructure was formed by long thick and meandering aggregates. In both cases the clusters are close to cylindrical shape and may be seen as parallel cylinders capacitors in the resin. If this approach is taken, then the difference in real permittivity can be explained since the sp meanders are longer and thicker offsetting the fact they are not as closely spaced as Xe. Xe samples have higher values of imaginary permittivity because, as noted above, they are closely spaced permitting the activation of hopping and tunnelling conduction modes. Cb samples show good performances as EM absorbers, reaching a peak of -38 dB using a sample 4 mm thick.

Fibrous fillers were then tested, starting with CNF. One crucial aspect of employing fibrous filler is disagglomeration to exploit their potential in forming a better network. To disagglomerate CNF three different methods were employed producing different level of disagglomearation, and different values of real and imaginary permittivity. This time the agglomerates and patters are more ovoid than cylindrical and what matters is the interface surface with the resin that causes polarization. Well dispersed samples expose more cnf surface to the resin and to other CNF and as a consequence present higher permittivity. Imaginary permittivity is higher on better dispersed samples because it causes more contacts between fibres. It has to be noted that, despite the use of many methodologies, the dispersion achieved with CNF in this work was not completely satisfying, limiting the EM results. Absorbing measurements, in fact, showed that the realized CNF samples did not offer interesting absorbing performance at reasonable thicknesses, and this is due to the poor dispersion of the filler in the matrix. CNT were then tried and dispersion was helped by the use of

three different surfactants and a more powerful sonicator. Samples produced without surfactant were employed as reference. It was found that one of the surfactants works very well, and the samples produced show a high dispersed pattern. In this case the relative permittivity is higher than the reference samples on a same percent content of filler basis, while the imaginary permittivity is lower. This results was explained considering that if a too good dispersion is reached, to the limit of single CNT in the resin, a high number of equivalent capacitors is produced resulting in high e'. Nevertheless, in this case, most of the CNT are covered by a layer of resin and the number of shortcuts between nanotubes is limited, restricting the dissipation that happens the most through joule effect. This result induce to think that there is an optimum level of nanofiller dispersion, above which the dielectric properties, at least ε", decrease. This result was confirmed in a CNF sample produced with the aid of surfactant in which, the perfect dispersion brought to achieve much higher real permittivity and much lower imaginary permittivity than those obtained in the former not well dispersed other CNF samples.

With CNT a peak of -34 dB is reached with a thickness of 2,5 mm , it has almost 2 GHz of band where the attenuation is more than 10 db.

# Acknowledgment

I would like to thank Prof. G. Simon and the material engineering staff at Clayton campus of Monash University for hosting and guidance during my stay in Australia.

Special thanks are due to CEMIN s.r.l. via della farnesina 363 00194 Rome, for technical support in EM measurers.

Also I would like to thank all the Material science and technology group for the advices and company during these 3 last years.

One special thank goes to my family and friend , especially Federica.